

ABSTRACT

Title of Document: ON THE SUMMER TIME DEVELOPMENT
OF THE NORTH PACIFIC SEA-LEVEL
PRESSURE ANTICYCLONE

Steven Carl Chan, Doctor of Philosophy, 2008

Directed By: Professor Sumant Nigam
Department of Atmospheric and Oceanic Science

With the exception of the North Indian Ocean, subtropical ocean basins are dominated by climatological planetary-scale sea-level pressure (SLP) anticyclones. The seasonal variability of the North Pacific subtropical SLP anticyclone is examined here. The largest ERA-40 and linear diagnostic modeled Northern Hemisphere SLP seasonal variabilities are found in the mid-latitudes with relatively less change in the subtropics; this leads to the poleward boreal summer development of the North Pacific and Atlantic subtropical SLP high. Unlike the Northern Hemisphere, the Southern Hemisphere subtropical SLP highs develop equatorward. The zonal-mean Northern Hemisphere subtropical SLP and ω seasonal variabilities are dominated by continental seasonality – a uniform boreal winter descent changing to a zonally asymmetric continental monsoon ascent and heat lows with relatively little change over the oceans. A linear diagnostic model is used to examine the forcing of the SLP seasonal cycle. The modeled North Pacific SLP seasonal variability is forced mainly

by winter stormtracks, extra-tropical North Pacific diabatic cooling, and boreal winter ITCZ. Asian monsoon forces a SLP ridge downstream, but the monsoon response is cancelled significantly by East Pacific diabatic heating and transients. North American diabatic heating and transients are also found to have a limited upstream effect. Boreal summer ITCZ forcing has limited North Pacific SLP response, and that is possibly linked to the prescribed tropical zonal-mean easterlies.

ERA-40 and TRMM CSH diabatic heating is inter-compared with other independent measures of diabatic and latent heating. Zonal-mean ERA-40 ITCZ diabatic heating is nearly twice that of NCEP and ERA-15 reanalyses, which indicates a much stronger ERA-40 Hadley Circulation. The ERA-40 Walker Circulation is also stronger than of NCEP Reanalysis, which is consistent with excessive Maritime Continent diabatic heating. Largest differences are also found in the Tropical East Pacific and Atlantic. Vertically integrated TRMM CSH heating is too weak even compare with other TRMM products. However, TRMM CSH mid-tropospheric tropical heating compares well with other datasets. The largest differences appear in the upper and lower troposphere, which implies CSH limitations in handling shallow convection (a known issue) and stratiform precipitation in deep convection.

ON THE SUMMERTIME DEVELOPMENT OF THE NORTH PACIFIC SEA-
LEVEL PRESSURE ANTICYCLONE

By

Steven Carl Chan

Dissertation submitted to the Faculty of the Graduate School of the
University of Maryland, College Park, in partial fulfillment
of the requirements for the degree of
Doctor of Philosophy
2008

Advisory Committee:
Professor Sumant Nigam, Chair
Professor James Carton
Professor Robert Hudson
Professor Daniel Kirk-Davidoff
Professor James Farquhar, Dean's Representative

© Copyright by
Steven C. Chan
2008

Dedication

To my grandparents, my parents, and my sister.

To my pre-university education teachers.

Acknowledgements

I would like to thank Dr. Harlen Spence (Boston University), Dr. Theodore Fritz (Boston University), Dr. Jenni Evans (Pennsylvania State University), Dr. Robert Hart (Florida State University), Dr. Brian Etherton (University of North Carolina), and Dr. William Frank (Pennsylvania State University) for their assistance to my university education prior of the University of Maryland.

I would also like to thank my doctoral committee – Dr. Sumant Nigam, Dr. Philip Arkin, Dr. Daniel Kirk-Davidoff, Dr. James Carton, Dr. Robert Hudson, and Dr. Ruth DeFries – for their time spent. Current and former members of Dr. Sumant Nigam research group have also played a big role for my completion of my doctoral degree. Key former members that have played important contributions are Dr. Renu Joseph and Dr. Scott Weaver.

Table of Contents

<u>Dedication</u>	ii
<u>Acknowledgements</u>	iii
<u>Table of Contents</u>	iv
<u>List of Tables</u>	vi
<u>List of Figures</u>	vii
<u>List of Abbreviations</u>	xiv
<u>Chapter 1: Introduction</u>	1
<u>1.1 The subtropical anticyclones in a historical context</u>	1
<u>1.2 Current hypotheses for Pacific High’s seasonality</u>	4
<u>1.3 Key unanswered questions</u>	10
<u>Chapter 2: On the summertime strengthening of the Northern Hemisphere Pacific sea-level pressure anticyclone</u>	19
<u>2.1 Introduction</u>	19
<u>2.2 Data sets</u>	24
<u>2.3 Seasonal variability of Pacific sea-level pressure</u>	24
<u>2.4 The Hadley Cell descent</u>	29
<u>2.5 Monsoon influence on Pacific basin descent</u>	32
<u>2.6 Evolution of sea-level pressure over the Atlantic</u>	35
<u>2.7 Evolution of sea-level pressure in the Southern Hemisphere</u>	37
<u>2.8 Concluding remarks</u>	40

<u>Chapter 3: The linear diagnostic modeling of North Pacific SLP seasonality</u>	56
<u>3.1 Introduction</u>	56
<u>3.2 Forcing data and the linear model</u>	60
<u>3.3 Modeled JJA and annual cycle</u>	62
<u>3.4 Diagnosing the boreal summer and winter North Pacific SLP</u>	65
<u>3.5 DJF to JJA SLP change – changes to forcing regimes</u>	68
<u>3.6 Discussion and conclusions</u>	75
<u>Chapter 4: Residue diagnosis of diabatic heating from ERA-40 and NCEP reanalyses: intercomparison with TRMM</u>	89
<u>4.1 Introduction</u>	89
<u>4.2 Data sets</u>	93
<u>4.3 Residue diagnosis of diabatic heating</u>	98
<u>4.4 Heating intercomparisons</u>	99
<u>4.5 Tropical heating diagnosis: inference from precipitation</u>	103
<u>4.6 Heating vertical structure: intercomparison with TRMM profiles</u>	105
<u>4.7 Concluding remarks</u>	111
<u>Chapter 5: Conclusions</u>	126
<u>5.1 Key Findings</u>	127
<u>5.2 Final Words</u>	132
<u>Bibliography</u>	133

List of Tables

Table 3.1: The above table shows the definition of the boxes that forcings are prescribed. All forcings are from 1979-1998 ERA-40 climatologies, and both diabatic heating and transients within the boxes are used.....88

Table 4.1: Estimated Precipitation in four geographical regions. Estimates (mm/day) are obtained from (a) the vertical integral of diagnosed heating profiles, (b) cloud-ensemble simulations and global model forecasts, (c) satellite observations, and (d) station data. The smallest estimate for each region is indicated in red.....125

List of Figures

- Figure 1.1:** Shown above is the 1907-1913, 1925-1937 “climatological” P39 (July 10 - July 14) Northern Hemisphere SLP from Lahey et al. (1958).....14
- Figure 1.2:** Shown above is an early schematic by Bjerknes (1937) to explain the existence of the subtropical SLP highs. According to Bjerknes (1937), zonal pressure belts and “helical” flow (tropical surface northeasterly/upper level southeasterly, mid-latitude surface southwesterly/upper level northwesterly) are expected by zonal mean dynamics, but are not consistent with observed wind patterns. Separate SLP high centers that are separated by “cols” are needed to explain the observed wind patterns. Such “cols” are “theoretically” transient disturbances, but they winded up anchored in certain areas due to land-sea contrasts.....15
- Figure 1.3:** Shown in the above two panels are the ERA-40 1979-1993 climatological zonal mean Q (contours and shadings) and $v-\omega$ (vectors) for (a) July and (b) January. Contours are drawn for $\pm 0.25, \pm 0.75, \pm 1.5, \pm 2, \text{ and } \pm 3 \text{ K dy}^{-1}$. Units for zonal mean v and ω are m s^{-1} and $-\text{Pa min}^{-1}$ respectively.....16
- Figure 1.4:** The ERA-40 1979-2001 climatological monthly seasonal cycles of (a) the Pacific longitudes $25^{\circ}\text{N} - 45^{\circ}\text{N}$ averaged and (b) zonal mean $25^{\circ}\text{N} - 45^{\circ}\text{N}$ averaged SLP are shown above. The SLPs above 1016 hPa and below 1012 hPa are shaded with red and blue color respectively. The contour interval is 1 hPa.....17
- Figure 1.5:** Shown above is the Pacific High – American monsoon Q schematic by Hoskins (1996). Central American Q forces tropospheric descent to the west and north of the heat source when the precipitation moves poleward during boreal summer. The descent leads to vortex compression; vorticity balance requires low level equatorward flow below the maximum descent. Such equatorward flow leads to a wind stress that forces coastal upwelling.....18

Figure 2.1: Cold-to-warm season evolution of sea-level pressure (contoured) and precipitation (shaded) in the 1979-2001 period monthly climatology. SLP is from ERA-40 and precipitation from CMAP-2: (a) January, (b) March, (c) May, and (d) July. SLP is contoured every 3.0 hPa, and precipitation shaded at 4.0 mm/day intervals, beginning at 4.0 mm/day, as indicated by the color bar. Major SLP centers – Pacific High and the Aleutian Low – are marked. The Tropic of Cancer (drawn) provides positional reference during seasonal evolution.....45

Figure 2.2: Monthly evolution of the Pacific High – the sea-level pressure anticyclone in the Northern Hemisphere. The 1020 hPa isobar in the climatological (1979-2001) SLP field is tracked at two-month intervals, beginning January. Isobars are labeled by the calendar month number; for example, January is ‘1’ and November ‘11’. The cold-to-warm season development essentially consists of a westward and northward expansion of the anticyclone.....46

Figure 2.3: Sea-level pressure *development*: The two-month change in climatological SLP. (a) January to March, (b) March to May, (c) May to July, and (d) July to September. The SLP change is contoured at 1.0 hPa interval, with solid (dashed) contours indicating positive (negative) development. The Tropic of Cancer is again shown for positional reference.....47

Figure 2.4: Annual-mean and annual-cycle of sea-level pressure in the Pacific basin, based on ERA-40 monthly climatology (1979-2001). Annual-mean SLP is contoured at 2.0 hPa intervals, with values above (below) 1018 (1010) hPa shaded. The annual variability is displayed using vectors, with the length denoting amplitude, and the direction, the phase; as indicated above. A *locally* northward pointing vector, for example, indicates maximum (minimum) SLP in July (January). Vectors are not drawn when the variability amplitude is less than 0.5 hPa.48

Figure 2.5: Monthly evolution of sea-level pressure and 300 hPa vertical velocity ($-\omega_{300}$) in the NH subtropics (15°N-25°N), i.e., in the Hadley Cell descent latitudes; based on ERA-40 climatology (1979-2001). Longitudinal distribution is shown in the left panels while evolution of the corresponding zonal-means is displayed in the right ones. SLP (upper panel) is contoured at 3.0 hPa intervals, with values above (below) 1017 (1011) hPa shaded. Vertical velocity (lower panel) is contoured with a 0.5 hPa/hour interval, with the zero-contour omitted.....49

Figure 2.6: Mean meridional streamfunction (mass weighted) in December-February (upper panel) and June-August (lower panel) months, from the ERA-40 Atlas (Kållberg et al. 2005); based on the 1979-2002 climatology. Contour interval is 5.0×10^9 Kg/sec and shading is as indicated.....50

Figure 2.7: Divergent circulation in the upper troposphere in June-August (upper panel) and December-February (lower panel), based on ERA-40 climatology (1979-2001). The 200 hPa divergence is contoured at 10^{-6} s^{-1} intervals and the divergent wind vector is displayed using the indicated scale. Solid (dashed) contours indicate positive (negative) divergence, and the zero-contour is omitted.....51

Figure 2.8: Annual-mean and annual-cycle of sea-level pressure in the Atlantic basin, based on ERA-40 monthly climatology (1979-2001). Rest as in Figure 2.4.....52

Figure 2.9: Monthly evolution of sea-level pressure in the Pacific and Atlantic subtropics (20°N-30°N), based on ERA-40 climatology (top panel). The annual and semi-annual components are shown in the middle and bottom panels, respectively. The full field (top) is contoured at 2.0 hPa intervals, with values above (below) 1018 (1012) hPa shaded. The components are contoured at 0.5 hPa intervals, with solid (dashed) contours indicating positive (negative) values; and the zero-contour omitted.....53

Figure 2.10: Annual-mean and annual-cycle of sea-level pressure in the global Southern Hemisphere, based on ERA-40 monthly climatology (1979-2001). A *locally* northward pointing vector, for example, indicates maximum SLP in July, as before. Rest as in Figure 2.4.....54

Figure 2.11: Annual component of sea-level pressure and 850 hPa temperature variability in the Southern Hemisphere subtropics (20°S-30°S), based on ERA-40 monthly climatology (1979-2001). Temperature is shaded at 1.0K intervals beginning at $\pm 0.5K$ (see color bar), while SLP is contoured at 0.5 hPa intervals, with the zero-contour omitted.....55

Figure 3.1: Shown above are the ERA-40 DJF (panel a) and JJA (panel b) 1979-1998 climatological monthly 850-hPa sub-monthly eddy meridional wind variance $\langle v_{850}^{\prime 2} \rangle$. $\langle v_{850}^{\prime 2} \rangle$ is contoured every $10 \text{ m}^2\text{s}^{-2}$78

Figure 3.2: Shown above are the modeled (panels *a* and *c*) and ERA-40 (panels *b* and *d*) JJA stationary wave SLP (SLP^*) (upper two panels) and 200-hPa stationary wave stream function (Ψ_{200}^*) (lower circumpolar panels). SLP^* and Ψ_{200}^* are contoured every 1 hPa and $4 \times 10^6 \text{ m}^2\text{s}^{-1}$ respectively.....79

Figure 3.3: Same as in Figure 3.2, but it is for DJF.....80

Figure 3.4: The modeled and ERA-40 1979-1998 climatological annual SLP mean (contours and shades) and harmonic (vectors) are shown above in panels *a* and *c*. The amplitudes of the modeled and ERA-40 annual harmonic (with the annual mean shaded the same way as in *a* and *c*) are contoured in panels *b* and *d*. The annual harmonic is defined that arrows pointing up and right correspond to a July and October annual maximum. The contour intervals for annual SLP means and harmonic amplitudes are 2 and 1 hPa respectively. Unlike Figures 3.2 and 3.3, the zonal mean is retained here.....81

Figure 3.5: Different JJA regional (as indicated by the boxed area) diabatic heating and transients forced SLP* under a JJA basic state are superposed in increasing complexity. Panel *a* show the Asian box forced solution only, *b*: Asian + WPac, *c*: Asian + WPac + EPac, and *d*: Asian + WPac + EPac + NEPac. Contours are every 1 hPa.....82

Figure 3.6: Same as in Figure 3.4, but it is for DJF basic state. The full atmospheric forced solution is shown in panel *a*. The regionally forced SLP* from the Stormtrack and Pac ITCZ box is shown in panel *b-d*. Contour intervals are 1 hPa.....83

Figure 3.7: The above four panels are the JJA minus DJF in *a*: 1979-1998 ERA40 SLP* climatology, *b*: modeled SLP* difference due to atmospheric and surface forcings, *c*: atmospheric forcing forced JJA-DJF SLP* differences, and *d*: SLP difference due to surface forcing and prescribed zonal mean. Contour intervals are 2 hPa.....84

Figure 3.8: Similar to Figure 3.7, but the above panels are for modeled JJA-DJF differences that are forced by the atmospheric forcing within the boxed areas. Contour intervals are 1 hPa.....85

Figure 3.9: Similar to Figure 3.8, but different boxes are used. The boxes are *a*: box Pac ITCZ, *b*: extratropical Pacific (box WPac plus NEPac, 20°N-60°N only), *c*: same as in *b* but with only transient fluxes, and *d*: box American. Contour intervals are 1 hPa.....86

Figure 3.10: The vertical profile of 1979-1998 ERA-40 climatological JJA minus DJF zonal wind difference is shown above. Contour intervals are every 2 ms⁻¹.....87

Figure 4.1: Zonally and vertically averaged ERA-40 diabatic heating in January (top) and July (bottom) in the 1979-1993 period climatology. Heating is residually diagnosed and the surface-to-125 hPa vertical average is mass-weighted. ERA-40's departure from the NCEP (red) and ERA-15 (green) diagnosed heating is also shown.....116

Figure 4.2: Vertically-averaged ERA-40 diabatic heating in January in the 1979-1993 period climatology (top panel). Heating is residually diagnosed and the surface-to-125 hPa vertical average is mass-weighted. ERA-40's departure from the NCEP and ERA-15 diagnosed heating are shown in the middle and bottom panels, respectively. The ERA-40 heating (top panel) is shown using the ± 0.5 , ± 1.0 , ± 2.0 , ± 3.0 , and ± 4.0 K/day contours, while its *departure* is contoured at *half* these levels. Red (blue) color indicates the diabatic heating (cooling) region. The zero-contour is omitted in all panels.....117

Figure 4.3: As in Figure 4.2, but for July.....118

Figure 4.4: Zonally-averaged diabatic heating and the Hadley Circulation in the ERA-40 reanalysis in January (panel *a*) and July (panel *c*), based on the 1979-1993 period climatology. The ERA-40 departures from the corresponding NCEP fields are shown in the right panels. Residual diabatic heating is contoured and shaded at the ± 0.25 , ± 0.75 , ± 1.5 , ± 2.0 , and ± 3.0 K/day levels. Red (blue) color indicates the heating (cooling) region. The Hadley Circulation [zonal-mean v (m/s) and $-\omega$ (Pa/min)] is displayed using vectors with the indicated scale; vectors smaller than 10% of the scale are not plotted. Note, vector-scale for departures is half that of the full fields.....119

Figure 4.5: Diabatic heating and the Walker Circulation in the ERA-40 reanalysis in October, based on the 1979-1993 period climatology. The 5S-5N latitudinal average is plotted in the calendar month of heightened zonal SST-contrast, i.e., when the SST cold-tongue is fully fledged. ERA-40 departures from the corresponding NCEP fields are shown in the bottom panel. Residual diabatic heating is contoured and shaded at the for ± 0.5 , ± 1.5 , ± 2.5 , ± 3.5 , and ± 4.5 K/day levels. Red (blue) color indicates the heating (cooling) region, as before. The Walker Circulation [divergent zonal wind (m/s) and $-\omega$ (Pa/min)] is displayed using vectors with the indicated scale; vectors smaller than 20% of the scale are not plotted.....120

Figure 4.6: Seasonal evolution of diabatic heating and precipitation in the Indian subcontinent sector (80E-100E), in the 1979-2002 climatology: Heating is residually diagnosed from global reanalyses and the mass-weighted surface-to-125 hPa vertical average is shown in panels (a) ERA-40, and (b) NCEP. Panel c displays CMAP-2 precipitation, after its conversion into latent heating units. The contour interval and shading threshold is 0.5 K/day and the zero-contour is omitted in all panels. Note, negative contours are present in upper panels as radiative (and sensible) heating is included there, on account of residual estimation.....121

Figure 4.7: As in Figure 4.6 but for the eastern Pacific sector (140W-120W).....122

Figure 4.8: Heating vertical structure in the Inter-Tropical Convergence Zone, based on 3-year climatology (1999-2001); the overlapping data period. The EQ-5N latitudinal average in January is displayed, with latent heating in the left panels and total diabatic heating in the right ones: (a) TRMM-CSH latent heating, (b) ERA-40 diabatic heating (diagnosed), (c) NCEP-model latent heating, (d) NCEP-model total diabatic heating. Heating is contoured and shaded at ± 0.25 , ± 0.75 , ± 1.5 , ± 2.0 , and ± 3.0 K/day levels, with the zero-contour omitted, as before. Red (blue) color indicates the heating (cooling) region.....124

Figure 4.9: Diabatic heating profiles in selected region, marked in figures 2-3: (a) Indian summer monsoon (July, land box); (b) Maritime Continent (January, land box); (c) South American continent (January, land box); and (d) Pacific winter storm tracks (January, oceanic box). Five profiles are shown in each case: Diagnosed ERA-40 (thick black) and NCEP (thick green) heating; NCEP-model latent (thin red dashed) and total diabatic (thin green dashed) heating; and the TRMM-CSH latent heating profile (thick red).....125

List of Abbreviations

AL – Aleutian Low

PH – Pacific High

BH – Bermuda/Azores High

GCM – General Circulation Model

LPEM – Linear Primitive (Diagnostic) Equation Model

MSC – Marine Stratus Cloud

NWP – Numerical Weather Prediction

PBL – Planetary Boundary Layer

SLP – Sea Level Pressure

Chapter 1: Introduction

1.1 The subtropical anticyclones in a historical context

Mare Pacificum is the name that Ferdinand Magellan gave to the Pacific Ocean, charmed by its relative calm. The contrast in sea state must be striking as Magellan crossed the stormy Atlantic and entered *Mare del Zur* (the South Sea, as the Pacific was referred to prior to Magellan's voyage) through the narrow tempestuous channels of the Tierra del Fuego archipelago. The sea-state contrast that Magellan encountered, which led to the naming of *Mare del Zur* as Pacific Ocean, resulted, in part, from the presence of a majestic sea-level pressure anticyclone (to be shown) in the southern (and northern) subtropical Pacific basin. The one in the northern basin is the focus of this dissertation.

Magellan entered the South Pacific on November 28, 1521 and sailed northwestward across the basin in his quest to find a westward route to the Spice Islands.¹ Interestingly, Magellan's entry into the South Pacific was at a time when regional sea-level pressure (SLP) would be at its seasonal peak (see Figure 2.10 in the following chapter). Since high SLP is synonymous with fair weather, Magellan found calm seas in the initial leg of his Pacific voyage which must have included a significant section across the expansive subtropical anticyclone of the southeastern basin. Not only that, Magellan's earlier transit through the southwestern Atlantic was at a time when SLP would be seasonally weak (if not the weakest) there (cf., Figure

¹ Magellan had earlier visited India in 1505 under Portuguese command taking the eastward route through the Cape of Good Hope; and then again in 1508, taking part in battles along the Malabar Coast, which ultimately led to Portuguese supremacy over the Indian Ocean.

2.10); that is, during period of potentially adverse weather. The seasonal timing and track of Magellan's pioneering voyage to the East Indies was thus influential in arriving at the *Pacificum* name.²

In the subtropical northeastern Pacific basin that Magellan never visited, a high surface-pressure belt also suppresses “stormy” weather. During boreal summer, this high pressure belt spans much of the Pacific, and is one of the most prominent climatological features of the near surface circulation. This high pressure feature is commonly referred as the Pacific High (PH). A similar sea-level feature exists in the North Atlantic, and goes by the Azores or Bermuda High name.

When was the Pacific High “discovered?” One supposes that this general circulation feature was recognized well after the invention of the barometer in the 17th century by Evangelista Torricelli (1608-1647), as it would follow collection and analysis of surface pressure measurements over the open ocean, obtained from ships of opportunity. Routine measurements of surface air pressure began in Europe in the mid-18th century (Lamb and Johnson 1959; Maugeri et al. 2004). Lamb and Johnson (1959) display a global climatological SLP map – the oldest the author has encountered – showing that documentation of the North Pacific sea-level pressure distribution began in the late 19th Century; that is, nearly a century after similar documentation of the Azores / Bermuda High (Lamb and Johnson 1959). Such delay is, of course, not surprising given the delayed European settlement of the North

² Although Magellan did cross the Inter-Tropical Convergence Zone on his way to the East Indies, he was obviously unaware of the other face of the Pacific that is prominently manifest in the middle and high latitudes of each hemisphere: where the stormtracks rule. One wonders what this basin would be named had Magellan known (and survived) the stormtracks.

American West Coast. Shown in Figure 1.1 is the distribution of climatological SLP in the pentad-39 period (July 10-15), constructed from 1907-13 and 1925-37 period data (Lahey et al. 1958). Similar maps are presented in Lamb and Johnson (1959) but their poor quality precludes reproduction here. The map clearly shows the presence of notable SLP anticyclones in the subtropical Pacific and Atlantic basins. .

The Pacific High is a robust, planetary-scale feature of the near-surface atmospheric circulation. The high is positioned in between the trade winds of the Tropics and the westerlies in midlatitudes. Existence of the surface high-pressure belt in the subtropics has generally been attributed to the descent in the poleward branch of the meridionally overturning Hadley Cell. That this belt should consist of separate anticyclones and intervening cols (a relatively low pressure region), rather than uniform high pressure, was first emphasized by Bergeron (1930) in context of air mass and frontal development. Bjerknes (1935) argued for such a belt structure from “stability considerations,” and discussed the organization of the subtropical anticyclones, including continentally anchored cols (Figure 1.2).

Bjerknes however sought no explanation for the pronounced seasonal variability of the Pacific High. The recent surge of interest in this aspect of atmospheric general circulation was triggered by a seminal paper of Sir Brian Hoskins in 1996 (Hoskins 1996), which links the robust summertime Pacific High to development of continental monsoons to the east of this High; that is to American monsoon development.

The key question addressed in this thesis concerns the seeming contradiction between Pacific High development and the Hadley Cell evolution. The canonical attribution of the subtropical SLP-Highs to Hadley Cell descent provides backdrop for the contradiction. If the *zonal-mean* Hadley Cell structure/evolution is indeed the reason for the occurrence of subtropical anticyclones, the high would be strongest during the boreal winter when the northern Hadley Cell is the strongest; this is not the case in observations, as the northern anticyclones are strongest in the boreal summer. It is thus likely that this counterintuitive seasonality of the anticyclones is related to some zonally-varying, rather than zonal-mean, aspect of the general circulation.

The expansive subtropical anticyclones, especially in summer, are not just a reflection of midlatitude westerlies and the tropical trade winds, but of great consequence for regional climate and global radiative balance. The Pacific High, for instance, leads to northerly flow along the US West Coast in summer, leading to coastal upwelling, and colder waters. The related low-level vorticity advection leads to large-scale subsidence, leading to California's summertime 'Mediterranean climate'. More globally, the expansive Pacific High cools Earth through longwave radiative emissions from the low-level cloud (stratus/stratocumulus) tops – the so called atmospheric “radiator fins” (Pierrehumbert 1994).

Why does the Pacific High exist? How is its seasonality generated? Why is Hadley Cell's seasonality seemingly irrelevant in accounting for the seasonal waxing and waning of the northern subtropical anticyclones? It is hoped that the ensuing analysis will answer some of these questions.

1.2 Current hypotheses for Pacific High's seasonality

The seasonal evolution of the Pacific sea-level pressure is seemingly at odds with the evolution of the zonal-mean meridional overturning circulation in the Tropics and sub-Tropics, as noted before. The thermally direct Hadley Cell consists of ascent in the deep Tropics (a radiation surplus region) and descent in the winter subtropics, with the Northern Hemisphere Cell exhibiting pronounced seasonality (Oort and Yienger 1996); the winter cell is much stronger than the summer cell. Shown in Figure 1.3 is the meridionally divergent circulation (zonal-mean v and ω) from the 1979-1993 retrospective analyses (ERA-40, Uppala et al. 2005) produced by the European Centre for Medium-Range Weather Forecasts (ECMWF) for both January and July. Ascent occurs in the summer hemisphere's tropics (15°N - 15°S) and descent in the winter hemisphere subtropics in the 10° - 30° latitude band. The considerably weaker Ferrel Cells in the winter extratropics in the 30° - 60° latitude band are also evident in the figures.

The disconnect between the seasonal evolution of the Hadley Cell and the North Pacific SLP is illustrated in Figure 1.4, which shows the climatological monthly evolution of the Pacific SLP in the 25N - 45N band (the PH latitudes) in the 1979-2001 ERA-40 reanalysis. The Pacific High covers much of the central and eastern Pacific during the boreal summer. In the boreal winter, high SLP is confined to the coastal regions, reflecting oceanic extensions of the continentally rooted winter high pressure features. The seasonal evolution of subtropical (25N - 45N) sea-level

pressure – zonally averaged across the entire Northern Hemisphere (and not just the Pacific longitudes) – is displayed in the right panel. The panel is vividly conveying the above noted disconnect between zonal-mean and zonally-varying features of the general circulation.

The zonal-mean subtropical SLP is lowest (~ 1014 hPa) during June and July, and highest (~ 1019 hPa) during December. Regional SLP in the northern subtropical Pacific is however highest in July (1023 hPa near 150W), which is more than 8 hPa higher than the contemporaneous zonal mean SLP. That is also more than 10 hPa higher than the regional January SLP.

The discordance between the zonal-mean and the Pacific basin SLP evolution suggests that the former is influenced by other longitudes, including somewhere SLP evolution runs counter to that in the Pacific basin. The SLP evolution thus exhibits considerable longitudinal dependence, indicating the significant contribution of stationary waves to the zonal-mean SLP evolution. The Pacific High is itself a stationary wave feature since not all of the subtropics is a high SLP region: For instance, when Pacific High is strongest in summer, a deep monsoon low can be found over the warm Asian Continent to the west.

Viewing the Pacific High as a stationary wave feature facilitates the investigation of its seasonality, given the well developed framework for theoretical and numerical modeling of seasonal stationary waves (Hoskins and Karoly 1981, Nigam 1983, Valdes and Hoskins 1989, Ting 1994, and others). The large-scale stationary Rossby waves can be forced locally or remotely by orography, diabatic

heating, and convergence of vorticity and thermal transient fluxes. Diagnostic modeling indicates the latter two to be quite influential, especially, in summer; making seasonal variation of these forcings prime candidates for explaining Pacific High's seasonality.

Linear dynamical models have been quite successful in explaining key features of the winter and summer circulation (e.g., Valdes and Hoskins 1989). The suitability of the linearity assumption in stationary wave modeling allows one to consider the role of each forcing independently, greatly facilitating the proposed diagnosis of the causes of the counterintuitive Pacific High seasonality.

1.2.1 Remote diabatic heating

The Pacific High is strongest during boreal summer when the North Pacific storm tracks (and related transient fluxes) are weakest. Investigations of the boreal summer Pacific High have thus focused on the role of orography and diabatic heating.

An influential analysis of Pacific High's seasonality is by Sir Brian Hoskins (1996). Hoskins tried to explain PH development in the context of American diabatic heating, following the paradigm laid out in Rodwell and Hoskins (1996), where dry summers in Eastern Mediterranean, Eastern Sahara, and Asia Minor are linked to the Indian summer monsoon induced Rossby wave descent. For deep diabatic heating sufficiently far away from the equator (such as the Indian monsoon heating), descent occurs north and west of the deep heating induced upper-troposphere outflow.

Descending isentropic surfaces and equatorward planetary vorticity advection (west of the upper-troposphere ridge) leads to large-scale descent, and suppressed precipitation.

Hoskins (1996) applies the same principle to Central and North America, and a schematic of his hypothesis is shown in Figure 1.5. He argues that the American heating moves poleward during the boreal summer, and causes large-scale descent to its northwest, over the Northeast Pacific. Near the surface, the descent driven vortex squeezing can only be balanced by equatorward planetary vorticity advection (i.e. the Sverdrup Balance), and hence there is northerly flow along the North American West Coast. This low-level northerly maintains the PH's eastern flank.

Rodwell and Hoskins reexamine the American heating hypothesis with additional diabatic heating forcings and orography in their 2001 paper (Rodwell and Hoskins 2001). They evaluate the response of different regional heating and orography from initial-value integrations of a non-linear primitive equation model; the model starts off with a realistic zonal-mean climatology. Their analysis shows orography, the Pacific ITCZ, and the Asian monsoon to be important in PH development. They argue that American heating is important; it contributes up to 40% of the descent over the North Pacific. In addition, they find the Asian monsoon to force the low-level poleward flow over the West Pacific that forms the Pacific High's western flank.

Unlike Rodwell and Hoskins (2001), Chen et al. (2001) focus on the “downstream” effect from the Asian monsoon. They argue that the Asian Monsoon is

the primary PH forcing mechanism, and downplay the importance of the American heat source. The role of Asian and tropical West Pacific heating in forcing boreal summer stationary waves is actually examined in an earlier paper (Ting 1994).

Ting (1994) does not address, directly, the question of Pacific High evolution. Using a steady linear primitive equation model and the diabatic heating distribution from the GFDL GCM, Ting shows that Asian and West Pacific latent heating forces a low-level anticyclone over the North Pacific. She also shows (again without reference to the PH evolution) that Central American and East Pacific latent heating forces a low-level trough over the Northeast Pacific – a result found by Chen et al. (2001) as well. Despite some disagreements on the relative roles of different regional heatings, all of the proposed hypotheses involve the influence of remote convective latent heating on the North Pacific basin.

1.2.2 Local feedbacks and land-sea contrast

Low-level equatorward flow along the eastern flank of the Pacific High leads to notable cold air advection, especially, in the boreal summer. Diagnosis of diabatic heating from the ERA-40 reanalysis (chapter 4) shows this eastern sector to be a region of net diabatic cooling. The thermodynamic budget for the region indicates that the descent-induced adiabatic warming balances both advective and diabatic cooling. The northerly flow along the High's eastern flank not only generates cold air advection, but also coastal upwelling along the North American West Coast, which further strengthens the cold advection.

The aforementioned diabatic cooling arises from longwave emission to space from the stratus cloud tops, which blanket the region. The clouds, themselves arise underneath the large-scale descending regions of the free troposphere. Cold advection along the eastern flank of the Pacific High and the cloud top diabatic cooling destabilize the planetary boundary layer, leading to vigorous mixing below the inversion, and marine stratus cloud (MSC) formation (Schubert et al. 1979, Klein 1997). The inversion suppresses deep convection and precipitation.

Norris et al. (1998) have shown a significant statistical relationship between sea surface temperatures (SST), marine stratus cloud cover, and the North Pacific SLP. Using SVD analyses, Norris et al. (1998) link the strengthening (weakening) of the Pacific High with increased (decreased) MSC cover along the California coast and trade wind regions in the East Pacific. Figure 7 in Norris et al. (1998) shows that reduced (increased) subtropical SST to the east (west) of 140°W is associated with positive (negative) SLP anomalies in the extratropical East Pacific.

Seager et al. (2003) also relate SST with Pacific SLP. They argue that the east-west SST asymmetry across the extra-tropical Pacific basin, which is influenced by the Pacific High development, is in turn, influential on SLP. The Pacific High's influence is realized through stratus shading of the sea-surface and through coastal upwelling along the North American coast, both of which lead to local SST-cooling, and greater SST asymmetry across the basin. The greater SST asymmetry, Seager et al. argue, leads to the modulation of the heating distribution, with impact on extratropical Pacific SLP.

More recently, two papers (Liu et al. 2004, Miyasaka and Nakamura 2005) have argued that sensible heating of the American continent and continent-ocean temperature contrast contribute to Pacific High development. The argument posits that near-surface sensible heating is balanced by a low-level anticyclone positioned west of the sensible heat source. This corollaries to the extra-tropical deep convective latent heating with maximum heating in the middle troposphere with an upper troposphere anticyclone to the west of the deep latent heat source.

1.3 Key unanswered questions

Despite the analysis and modeling advances pertaining to Pacific High development, two major questions remain unanswered:

1) Why is the Pacific High weakest during boreal winter when the zonal-mean SLP is highest in the northern subtropics at that time? Which longitudinal sectors are particularly influential in determining the seasonal evolution of the zonal-mean component?

2) Most atmospheric scientists will link the subtropical SLP field seasonal variability with the meridionally overturning Hadley Circulation. The role of extratropical diabatic cooling and stormtrack is not clearly addressed in terms of the seasonal cycle. Descent (and its associated tropospheric radiative cooling) is a passive and remotely forced process. The diabatic cooling itself forces its own planetary waves as a feedback from the remotely forced stationary wave and large-

scale descent. Stormtrack influence in boreal winter climate is relative well known (Hoskins and Valdes 1990). What is the stormtrack's contribution to the Pacific annual mean and seasonal cycle?

Observational analysis can often reveal important clues to the underlying dynamics. Chapter Two critically examines the “observed” ERA-40 subtropical/mid-latitude SLP seasonality. The observational analysis shows the concept of zonally symmetric tropical heating in explaining in Hadley Circulation to be inconsistent with observations. The analysis also shows the Northern Hemisphere subtropical high and continental monsoon seasonal variabilities are inconsistent with the monsoon forced subtropical high mechanism.

Both questions raise questions about the relationship between the Hadley overturning circulation and Northern Hemisphere subtropical high seasonal variabilities. The seasonal cycle forcing to the Pacific High is examined using a diagnostic model analysis in Chapter Three. Different regional forcings are prescribed in a linear diagnostic model to diagnose not only the mature JJA Pacific High features, but also diagnose the change from DJF to JJA. The results of Chapters Two and Three are currently also submitted to journal peer review (see Nigam and Chan 2008).

The ERA-40 diabatic heating is not available from ECMWF. The three dimensional diabatic heating in reanalyses and GCMs are fundamental quality controls of their assimilated/modeled general circulations. The same diabatic heating is also needed to perform the model diagnosis in Chapter Three. Estimates of atmospheric diabatic heating are controversial as it invokes issues in moist process

models and cloud/precipitation observations. As part of a side development of this thesis, the diagnoses of the ERA-40 diabatic heating is carried out. The ERA-40 diagnoses itself have generated some interesting results through intercomparison with other diabatic heating estimates. The results are also presented in this thesis in Chapter Four, and currently submitted for editorial review for the Journal of Climate (Chan and Nigam 2008).

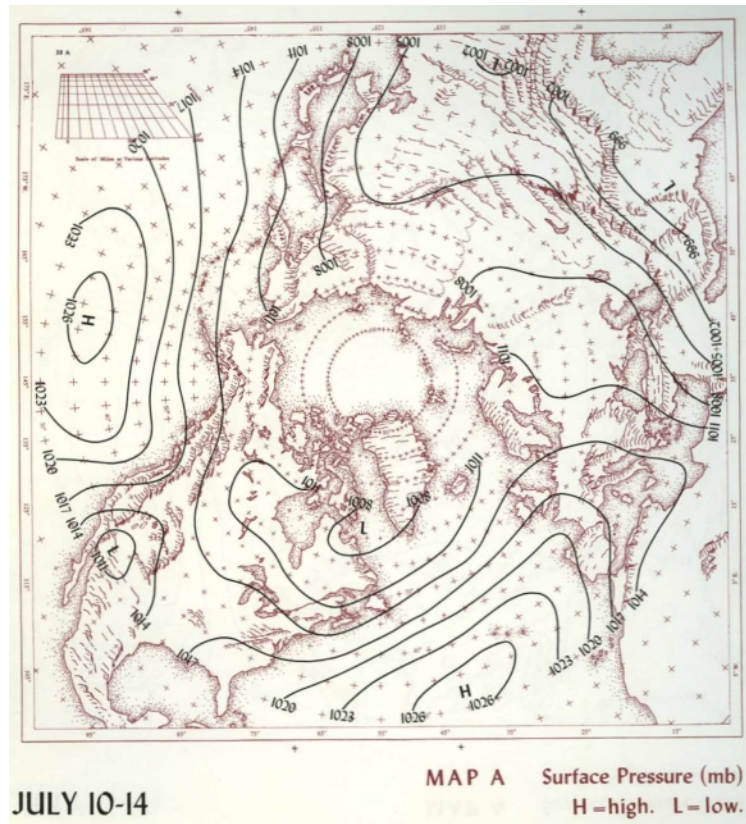
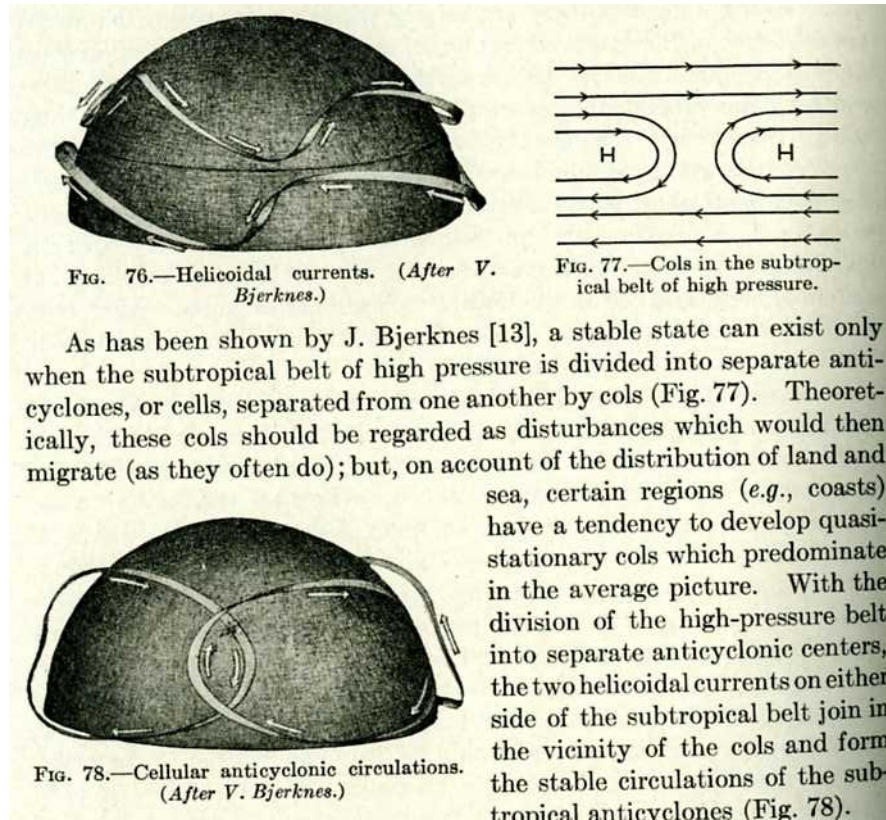


Figure 1.1: Shown above is the 1907-1913, 1925-1937 “climatological” P39 (July 10 - July 14) Northern Hemisphere SLP from Lahey et al. (1958).



As has been shown by J. Bjerknes [13], a stable state can exist only when the subtropical belt of high pressure is divided into separate anticyclones, or cells, separated from one another by cols (Fig. 77). Theoretically, these cols should be regarded as disturbances which would then migrate (as they often do); but, on account of the distribution of land and sea, certain regions (*e.g.*, coasts) have a tendency to develop quasi-stationary cols which predominate in the average picture. With the division of the high-pressure belt into separate anticyclonic centers, the two helicoidal currents on either side of the subtropical belt join in the vicinity of the cols and form the stable circulations of the subtropical anticyclones (Fig. 78).

Figure 1.2: Shown above is an early schematic by Bjerknes (1937) to explain the existence of the subtropical SLP highs. According to Bjerknes (1937), zonal pressure belts and “helicoidal” flow (tropical surface northeasterly/upper level southeasterly, mid-latitude surface southwesterly/upper level northwesterly) are expected by zonal mean dynamics, but are not consistent with observed wind patterns. Separate SLP high centers that are separated by “cols” are needed to explain the observed wind patterns. Such “cols” are “theoretically” transient disturbances, but they winded up anchored in certain areas due to land-sea contrasts.

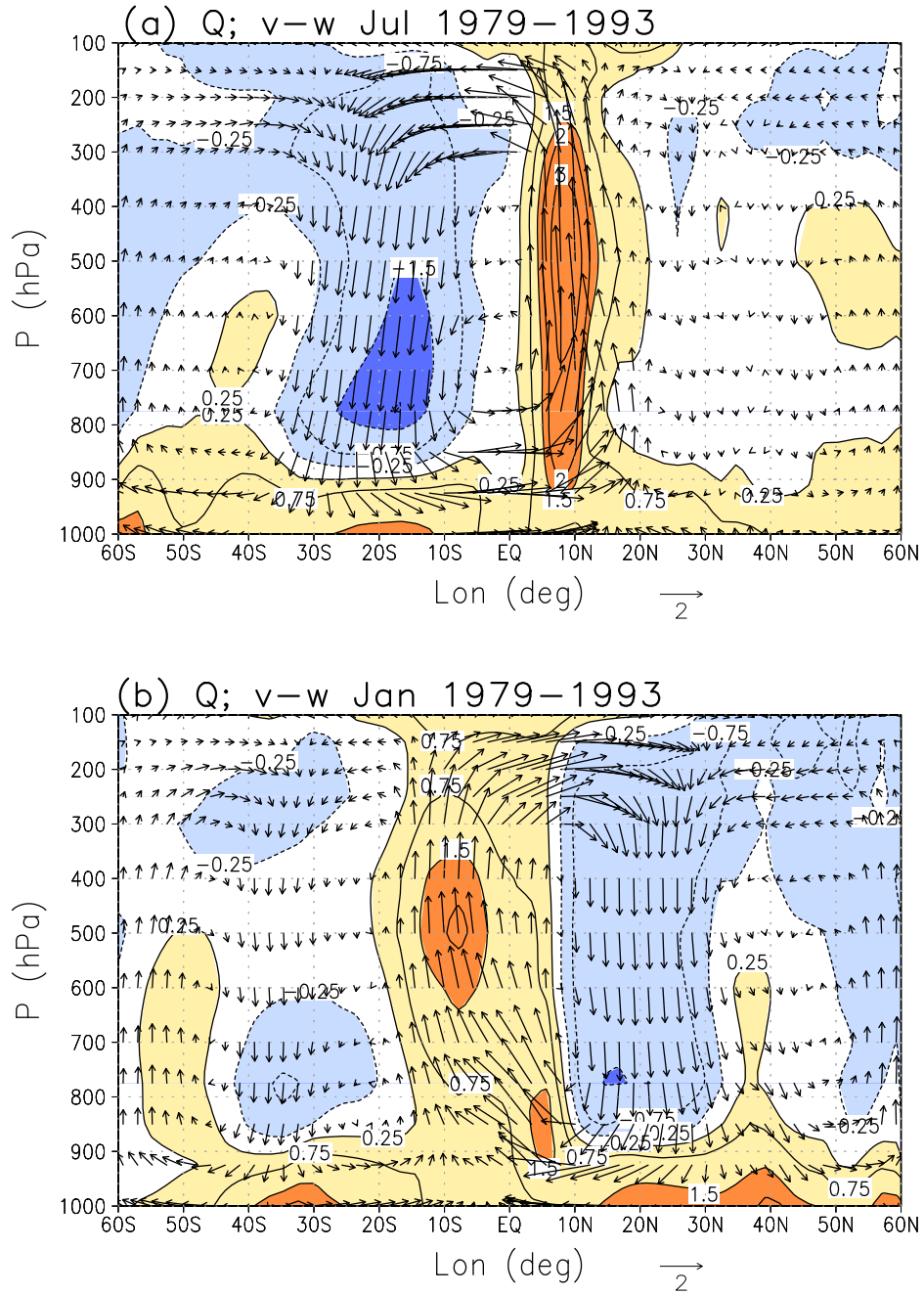


Figure 1.3: Shown in the above two panels are the ERA-40 1979-1993 climatological zonal mean Q (contours and shadings) and v- ω (vectors) for (a) July and (b) January. Contours are drawn for ± 0.25 , ± 0.75 , ± 1.5 , ± 2 , and ± 3 K dy^{-1} . Units for zonal mean v and ω are m s^{-1} and $-\text{Pa min}^{-1}$ respectively.

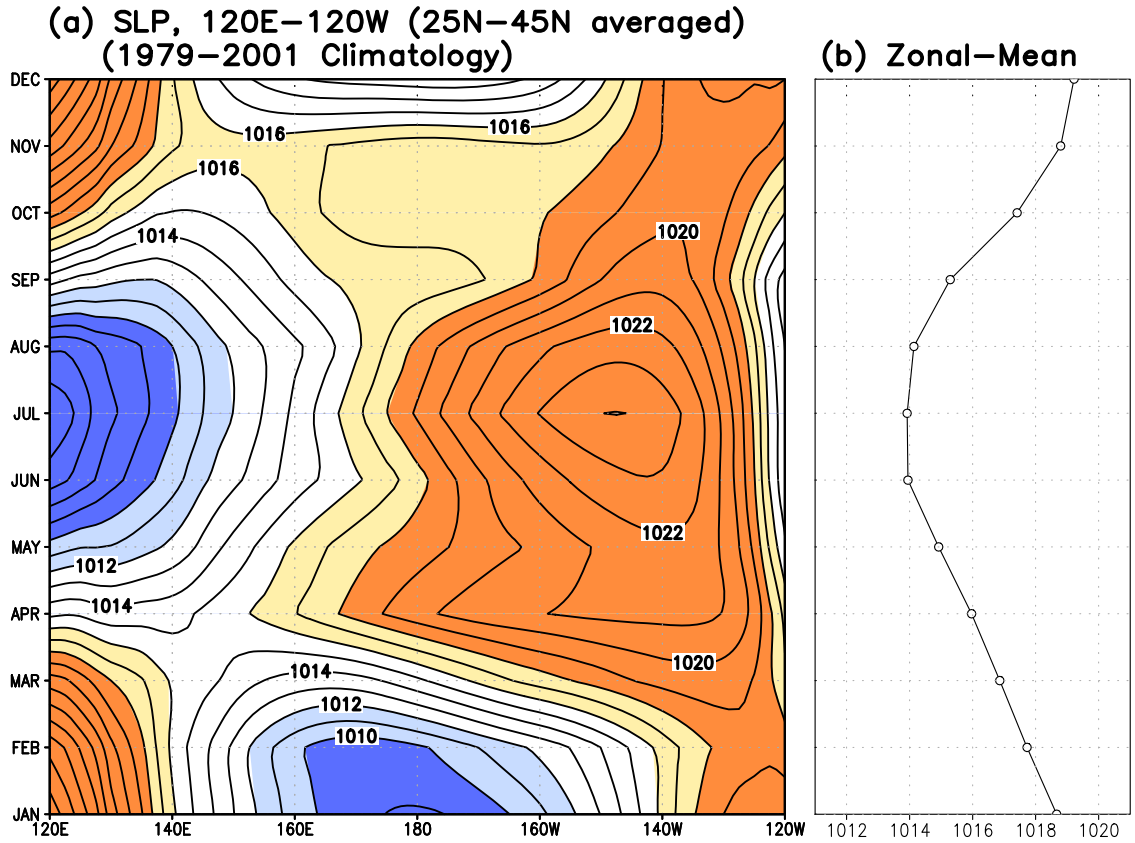


Figure 1.4: The ERA-40 1979-2001 climatological monthly seasonal cycles of (a) the Pacific longitudes 25°N - 45°N averaged and (b) zonal mean 25°N -45°N averaged SLP are shown above. The SLPs above 1016 hPa and below 1012 hPa are shaded with red and blue color respectively. The contour interval is 1 hPa.

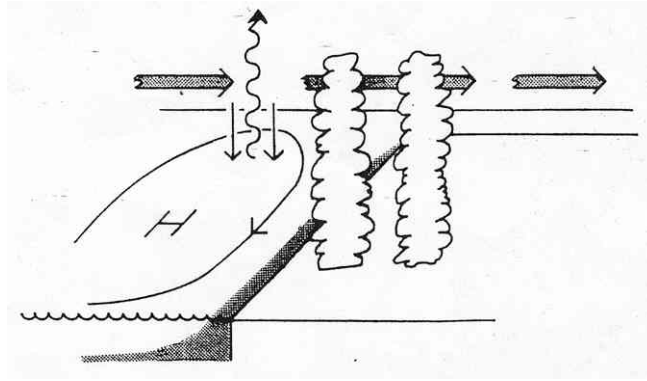


Figure 1.5: Shown above is the Pacific High – American monsoon Q schematic by Hoskins (1996). Central American Q forces tropospheric descent to the west and north of the heat source when the precipitation moves poleward during boreal summer. The descent leads to vortex compression; vorticity balance requires low level equatorward flow below the maximum descent. Such equatorward flow leads to a wind stress that forces coastal upwelling.

Chapter 2:

On the summertime strengthening of the Northern Hemisphere

Pacific sea-level pressure anticyclone

2.1 Introduction

The subtropical sea-level pressure anticyclones – majestic semi-permanent features over the ocean basins – are an integral element of the atmospheric general circulation: Their clockwise (in the Northern Hemisphere) near-surface flow connects the Tropical trade wind regime with the mid-latitude westerly belt, influencing both. Thermodynamically, the anticyclones reside between the intense convection zones in the deep tropics and the mid-latitude stormtracks which extend from the eastern coasts of the continents to the mid basins, especially in winter. The Northern Hemisphere anticyclones extend well into the mid-latitudes in summer, when they occupy close to 50% of the Western Hemisphere surface.³

The canonical explanation for the existence of the subtropical anticyclones, or at least of the surface high-pressure belt in the subtropics, is the descent in the poleward branch of the meridionally overturning Hadley Cell. That this belt should consist of separate anticyclones and intervening cols (a relative low pressure region), rather than uniform high pressure, was first emphasized by Bergeron (1930) in context of air mass and frontal development. Bjerknes (1935) argued for such a belt

³ The ‘subtropical’ reference of the anticyclones is at some odds with respect to their summer structure, which exhibits robust amplitude in the mid-latitudes.

structure from “stability considerations,” and discussed the organization of ascending and descending regions.⁴ The subtropical descent is, of course, associated with deserts, both continental and oceanic, and provides unique and critical pathways for radiative cooling of the tropics (“radiator fins”, Pierrehumbert 1994).

The subtropical anticyclones interact with the underlying oceans as well, and not just by suppressing precipitation along their eastern/southeastern flanks (i.e., through salinity impacts): The clockwise circulation over the northern Pacific, for instance, influences the gyre-scale circulation through the wind stress curl, and SSTs along the California Coast from coastal upwelling. The colder SSTs and resulting near-surface coolness coupled with the warming of the lower troposphere from adiabatic descent leads to static stability enhancement (e.g., trade inversion), and in turn, extensive low-level cloudiness with significant radiative impacts in the very regions of suppressed precipitation!

Following Bjerknes’ analysis, several hypotheses have been put forward to account for the subtropical anticyclones, including monsoon heating to the east and the west of the anticyclones. The role of eastward heating was noted in a seminal paper by Hoskins (1996; the 1995 Bernhard Haurwitz Memorial Lecture of the American Meteorological Society), who discussed the forcing of anticyclones in context of large seasonal fluctuations in their strength and expanse. Hoskins argued that latent heat released over the neighboring land masses to the east during the advance of the continental monsoon into the subtropics generates a Rossby wave

⁴ See Chapter III (*Production and Transformation of Air Masses*) in Petterssen’s 1940 book titled *Weather Analysis and Forecasting* for a brief English language discussion of these papers.

response to the northwest of monsoon heating, with the related descent contributing to anticyclone development.

A strong case for both eastward and westward monsoon heating in forcing the NH summer anticyclones, especially, the one in the Pacific, was made by Rodwell and Hoskins (2001) from modeling the response of observationally constrained diabatic heating (diagnosed residually from ERA-15 reanalysis) through initial-value integrations of a nonlinear, primitive equation model. Ting (1994) had recognized the importance of both heatings, especially, the Indian monsoon heating in anticyclone forcing earlier (see her Fig. 13), albeit in the more general context of diagnostic modeling of the summertime circulation.⁵ The importance of westward heating was also shown by Chen et al. (2001), from quasi-geostrophic modeling analysis. Seager et al. (2003) suggested that the summer strength of the Pacific anticyclone is, secondarily, due to local air-sea interaction at the far ends of the basin, which lead to zonal SST variations, and, in turn, modulation of the heating distribution; which is consequential.

The influence of local diabatic heating on the summer anticyclone was also assessed by Rodwell and Hoskins (2001), who found low-level diabatic cooling in the northeastern Pacific to be influential. Since this cooling is, in part, due to the longwave emission from stratus/stratocumulus cloud tops, it depends on the large-

⁵ Ting analyzed the summertime circulation generated by the Geophysical Fluid Dynamics Laboratory's (GFDL) GCM, using a steady-state, linear, primitive equation model. The assessment of the influence of various monsoon heatings is insightful, but some caution is in order given the significantly stronger summertime stationary waves in this GCM; by a factor of ~2 in the lower troposphere (see Figs. 1b and 2b in Ting's paper). This is consistent with the stronger diabatic heating in the GCM; for example, heating in the Indian and western Pacific sector is larger by a factor of 1.5-2.0 vis-à-vis the observationally constrained heating estimate (cf. Fig. 2 in Rodwell and Hoskins 2001).

scale adiabatic descent over the anticyclone's eastern/southeastern flank for sustenance. As such, its influence, while considerable, is of a feedback rather than causative nature.⁶

It is noteworthy that the above cited studies focus on modeling the summer circulation; not circulation development, the pertinent modeling target in context of the summer peaking of anticyclone's strength and expanse. The origin of the spring-to-summer change in circulation features, for instance, depends as much on the spring forcing as the summer one, especially, in case of gradual development. Modeling either circulation should, nonetheless, provide some insights into the origin of circulation evolution, as the above cited studies seek to do from modeling of the summertime flow.

The monsoon heating – intrinsically seasonal – could well account for the summer vigor of the anticyclones. The continental heating to the east and west of the Pacific anticyclone, for example, is undoubtedly influential in the above modeling studies. The modeled monsoon influence (especially, Asian monsoon's) however extends over large parts of the tropical and subtropical basin where annual sea-level pressure variability is weak in nature (a section 3 finding); indicating that monsoons may not be the sole significant influence in the region.⁷ Observational analysis, described in section 3, moreover shows the largest winter-to-summer Pacific sea-level

⁶ A similar feedback role for the low-level diabatic cooling from stratus cloud tops in fostering the annual warm-to-cold SST transition in the eastern tropical Pacific was indicated by the modeling analysis of Nigam (1997), who argued that the dynamic feedback of cloud-top longwave cooling in coastal upwelling regions is more rapid than the thermodynamic feedback due to stratus shading.

⁷ Modeling and observational analyses can be reconciled if the monsoon heating response replaces another which abates from winter-to-summer (e.g., Hadley Cell descent in the northern subtropics); a possibility, investigated in the follow-up modeling analysis of circulation development.

pressure change to occur in the middle and high latitude basin.⁸ Together, these observational features suggest that the reasons for the summer robustness of the NH anticyclone may not all be known.

This observationally rooted study revisits the question posed by Hoskins (1996) on why the NH anticyclones are strongest and maximally extended in summer when the Hadley Cell descent in northern latitudes is the weakest. It begins with the examination of seasonal sea-level pressure (SLP) development over the Pacific basin. It will be shown that the annual variability is dominated by the gradual build-up of the anticyclone during spring and summer months, which is inconsistent with our current “understanding” of the anticyclone. Therefore, it is necessary to revisit of the anticyclone development question.

The study seeks to critique the mechanisms advanced for the impressive waxing and waning of the NH anticyclones, especially, the Pacific one from observational analysis alone. A modeling analysis is presented after the criticisms. Intercomparisons of SLP evolution in the Pacific and Atlantic basins, and the Northern and Southern Hemispheres contribute to the assessment. The seasonal variability of Pacific SLP is discussed in section 3, while that of Hadley descent in the NH subtropics in section 4. The Asian monsoon’s influence on descent over the Pacific is examined in section 5 from analysis of the upper-level divergent circulation. The evolution of SLP over the Atlantic basin and in the Southern Hemisphere is

⁸ Eastern Hemisphere monsoons are found influential in this region too in the cited modeling studies but the influence was generated from an overly extended diabatic heat source in most cases: up to 150°E-170°W to the east, and 60°N; making separation of local and remote effects difficult.

analyzed for insights into anticyclone development in sections 6 and 7, respectively. Concluding remarks follow in section 8.

2.2 Data sets

The European Centre for Medium-Range Weather Forecasts (ECMWF) global reanalysis data provides the necessary atmospheric variables for the present analysis. The ECMWF 40-year global reanalysis (ERA-40; Uppala et al 2005) spans September 1957-August 2002 and is locally available on a 2.5° grid and 23 levels in the vertical. The seasonal evolution is analyzed using the calendar month climatology for the satellite era (1979-2001).

Monthly precipitation data came from the Climate Prediction Center (CPC) Merged Analysis of Precipitation (CMAP; Xie and Arkin 1997). The CMAP precipitation is also available on a 2.5° grid, and the observation-only CMAP product (CMAP-2) was used.

2.3 Seasonal variability of Pacific sea-level pressure

The monthly distribution of climatological SLP and precipitation is shown in Fig. 2.1 for the first half of the calendar year. The most remarkable SLP change is the winter-to-summer abatement and northward retreat of the AL and its replacement by high pressure, especially in the central and eastern basin; resulting in a majestic

anticyclone in July. The synchronicity of these changes is noteworthy. At its peak, the anticyclone is centered in the 35°-40°N band and extends over most of the extratropical basin. In contrast, the anticyclone is quite weak in January when it is confined to the far eastern basin. The January-to-July change in core pressure is ~ 6 hPa, but substantially larger SLP changes occur in the northern basin (as shown later).

The concurrent seasonal changes in precipitation, which reflect vertically averaged latent heating, are depicted on the same panels for context. Winter precipitation occurs along the southern flank of the AL which forms the axis of the jet and winter storm tracks, and along its eastern/southeastern flank where the large-scale vorticity balance – the Sverdrup balance – leads to low-level convergence, and thus ascending motion and rainfall: the winter rainy season in the Pacific Northwest (see Nigam and Ruiz-Barradas 2006 for more discussion, including relative contribution of the transient moisture fluxes to winter rainfall). The Aleutian Low is, of course, itself forced in good measure by the stormtrack diabatic heating and transients (cf. Fig. 9b, Hoskins and Valdes 1990). With the onset of spring and summer, the AL retreats northward and related precipitation impacts diminish, vanishing altogether by July when the US West Coast is under the influence of descending motions associated with the eastern flank of the anticyclone; California's "Mediterranean" summer climate. Further equatorward, the Asian and American monsoons and the Inter-Tropical Convergence Zone (ITCZ) are fully developed by July; note the double ITCZ in March.

The location and spatial extent of the SLP anticyclone is tracked in Fig. 2.2 by monitoring the movement of the 1020 hPa SLP contour in alternate months, beginning with January ('1'). The tracking of curves labeled 1 through 7 indicates that anticyclone development during spring and summer primarily involves northward advance of the high pressure region; the westward advance occurring earlier (late winter). The most striking feature however is the little change in the subtropical basin, as evident from the overlap of the March-to-July (3, 5, and 7) isobars.

The case for the absence of significant seasonal SLP-change in the tropical and subtropical basin is more directly made in Fig. 2.3, which displays the SLP change over two month periods; along with the Tropic of Cancer for positional reference. The largest two-month change (~ 8 hPa) is between January and March (top panel) when SLP increases over the extratropical Pacific in the Aleutian Low longitudes (i.e., the central basin; cf. Fig. 2.1a). Meridionally, this SLP change is in quadrature with the AL, so that the Low is confined to the northern basin in March. It is noteworthy that the largest seasonal increase in SLP in the tropics/subtropics (e.g., the 15° - 30° N belt) – up to 4 hPa – occurs in this period. The subsequent March-May change (upper middle panel) is focused in the mid-latitudes but with some preference for the western basin. The following May-July SLP change is more like the January-March change in the mid-latitudes but with the Tropics and subtropics exhibiting 1-2 hPa reduction in SLP! The reduction is moreover concentrated in the western and eastern basin, adjacent to the warm continents; and consistent with the reach of the continental monsoons, especially, the Asian one to the west.

The May-to-July SLP reduction, albeit modest but occurring in the monsoon onset period, is seemingly at odds with the modeling analyses indicating a role for Asian monsoon heating in anticyclone development. These studies show that Asian monsoon heating leads to positive (and not negative) SLP development in the tropics and extratropics (Fig. 12b in Ting 1994; Fig. 9a in Chen et al. 2001)⁹. Ting's analysis (Fig. 12) also shows the low-level response over the Pacific to be both augmented and offset by heating in other sectors. The possibility that monsoon heating's influence over the Pacific is offset by other thermal and/or mechanical forcing in nature was raised in footnote 5.

The seasonal cycle of SLP over the full year is compactly shown in Fig. 2.4, where the annual harmonic is displayed atop the annual-mean SLP. The amplitude and phase of the annual cycle is denoted by the length and direction of the plotted arrows; arrows pointing due north (locally) indicate a summer maximum and a winter minimum. The annual-mean distribution consists of a High in the eastern subtropical basin and a Low in the northern basin, reflecting some persistence of the summer and winter features in these regions, respectively.

More striking though is the distribution of annual variability: Weaker than 1 hPa in amplitude (the vector plotting threshold) in the entire tropics and subtropics, excluding the far western and eastern coastal sectors where the influence of continental monsoons is manifest, with lower SLP in July. Robust annual SLP

⁹ Rodwell and Hoskins' (2001) modeling analysis does not show the low-level stream function (or SLP) forced by Asian monsoon heating alone. The closest is the display of the response of orography and Asian monsoon heating (Fig. 8b), which indicates positive SLP development in the Pacific tropics and extratropics in July. Their Asian heating box (10°S-60°N; 60° E-150°E) also seems too inclusive as the Western North Pacific monsoon is within the box.

variability is however found in the middle and high latitudes, with the amplitudes being particularly large northward of 35°N in the central and eastern basin. The structure of annual SLP variability over the Pacific basin raises interesting questions:

- Why is the seasonal SLP variability in the Pacific subtropics so weak despite the significant winter-to-summer variation of Hadley Cell descent in these latitudes? The question is similar to the one posed by Hoskins (1996), except that it is the lack of a seasonal SLP signal in the tropics/subtropics (deduced from observational analysis; cf. Figs. 1-4) rather than a counter-intuitive one in terms of the Hadley Cell seasonal variability.
- Monsoons are usually characterized by their abrupt onset and decline. How significant and extensive is the influence of abrupt continental monsoons on North Pacific SLP, which exhibits a more gradual development?
- How does the SLP anticyclone evolve in the Atlantic basin, which doesn't have an Asian monsoon equivalent to its west?
- What insights does anticyclone evolution in the Southern Hemisphere, where circulation is more zonal, stormtracks poleward, and monsoons weaker, provide on strengthening mechanisms? Do SH anticyclones peak in austral summer?

2.4 The Hadley Cell descent

Seasonal development of the Hadley Cell descent in the NH subtropics is examined in this section to unravel the paradox implicit in the first question. Before showing the descent structure, the monthly evolution of SLP in the global subtropics is displayed in a Hovmöller plot (Fig. 2.5a). The average SLP in the 15°–25°N belt – the core latitudes of Hadley descent in NH winter (e.g., [ERA-40 Atlas, Kallberg et al. 2005](#)) – is plotted across all longitudes, with the zonal-mean plotted in the adjacent right panel. The zonal-mean SLP distribution, with a maximum in January (~1016 hPa) and a minimum (~1011 hPa) in August, is in accord with the seasonal variation of the Hadley Cell (the zonal-mean meridional overturning circulation); with the vigorous winter cell, leading to stronger zonal-mean subsidence (and higher SLP) in the NH subtropics.

The underlying zonal distribution of SLP in the tropics/subtropics is displayed in the left panel. Immediately apparent is the large seasonal variability in the Asian longitudes and its considerable impact on the evolution of zonal-mean SLP, suggesting that the zonal-mean viewpoint (right panel) is descriptively inadequate, especially, since the Western Hemisphere subtropics exhibit substantially weaker seasonal variability, with a minimum later in the year. The hefty footprint of the Asian summer monsoon on the evolution of zonal-mean subtropical SLP also calls into question the usefulness of the zonally-symmetric dynamical perspective: The Asian monsoon related variability is clearly the reason for the zonal-mean SLP to be minimum in summer (right panel); not sensitivity of the zonal-mean dynamical response alone.

The surface view of the Hadley Cell descent is complemented by showing the descent structure in the upper troposphere (Fig. 2.5b); the negative of the 300 hPa pressure vertical velocity is displayed.¹⁰ The descent is strongest in winter across most longitudes, much as expected; with the zonal-mean description (right panel) being representative of the longitudinal distribution in this season. The weak variability of the descent between winter and spring seasons is however remarkable: The subtropical descent, evidently, continues unabated until late spring in some sectors (e.g., Sahara desert, and the western/central Pacific and mid-Atlantic basins); that is, during the period of Hadley Cell transformation, from a single-cell winter structure to a more evenly balanced two-cell equinoctial configuration. The zonal-mean descent, especially, its evolution, is clearly impacted by the development of the Asian and North American monsoons in late spring. The monsoon impact in summer is, of course, overwhelming, with strong, deep ascent manifest not only in the Asian and American longitudes but also in the zonal-mean, just as in case of SLP,¹¹ leading to northward extension of the rising branch (cf. ERA-40 Atlas), and thus, narrowing of the northern summer cell. Further to the north (e.g., 25°–30°N), the monsoon ascent leads to reduction in zonal-mean subsidence, i.e., to cell-weakening.

The analysis suggests that monsoons are integral to Hadley Cell's seasonality, in both strength and structure. Hitherto, this seasonality has been attributed, largely, to the sensitivity of the zonal-mean dynamical response to placement of zonal-mean

¹⁰ An upper rather than mid-troposphere level was chosen to avoid the below-ground interpolated values, given the presence of high mountains in the northern subtropics. The interpolation was, of course, unavoidable in the SLP plot.

¹¹ The monsoon's influence on upper-troposphere descent appears a little later than on SLP (cf. Fig. 5a). The upper-troposphere lag is consistent with basic notions of monsoon development in which the pre-onset phase involves heating of the land-surface (and thus SLP change).

heating with respect to the equator (e.g., Lindzen and Hou 1988); that is, without consideration of the influence of the subtropical continental monsoons on the zonal-mean meridional circulation!¹²

The surface and upper-tropospheric views of the Hadley descent in the NH subtropics, especially, spatio-temporal structure, indicate that:

- Seasonal evolution of the *zonal-mean* descent (i.e., of the Hadley Cell) is heavily influenced by the Asian summer monsoon.
- The notion of weaker summer descent across *most* longitudes in the NH tropics and subtropics – rooted in the anemic summer Hadley cell (and related models) – is unsound.
- Descent over the tropical/subtropical Pacific sector, in fact, exhibits far less seasonality than implied by the winter-to-summer Hadley Cell variation along with flawed notions of it being zonally representative; thus resolving the paradox implicit in first question (cf. section 3).
- The lack of consideration of the Asian summer monsoon – a planetary-scale circulation feature – in current descriptive and dynamical discussions of Hadley Cell’s seasonality is a significant omission, needing rectification.

The hypothesis for an integral role of the subtropical continental monsoons in seasonal evolution of the Hadley Cell suggests that cell-seasonality

¹² Hou and Plumb (1992) did examine the impact of subtropical thermal forcing (i.e., of an idealized continental monsoon) on the mean meridional circulation. However, the subtropical forcing was considered in isolation, and not in conjunction with tropical heating. This precluded an assessment of the dynamical model’s seasonal sensitivity under more realistic forcing conditions. Note, the model yields realistic seasonal sensitivity even without inclusion of subtropical thermal forcing, as noted above.

should be muted if the monsoons were weaker. An aqua-planet model would clearly be useful in investigating this hypothesis but a preliminary assessment can, perhaps, be obtained by examining the seasonality of the Hadley Cell in the Southern Hemisphere (SH), which has weaker monsoons. The austral summer (DJF) and winter (JJA) Hadley cells from the ERA-40 Atlas (2005) are shown in Fig. 2.6, using the mean meridional stream function. Immediately apparent is the considerably reduced seasonality of the SH cell, especially in strength; and even geometry. The seasonality manifest in the absence of significant monsoon interference, likely reflects the dynamical sensitivity of the Hadley circulation to tropical heating placements vis-à-vis the equator (Lindzen and Hou 1988), and other changes in tropical heating strength and structure. The contrast with the variability of the NH cell is striking, but not inconsistent with the alleged contribution of the Asian summer monsoon to its seasonality.

2.5 Monsoon's influence on Pacific basin descent

The influence of Asian monsoon on the far-field circulation is difficult to characterize from observational analysis, given the concurrent seasonal evolution of other climate features, e.g., ITCZ development in the central/eastern equatorial Pacific. The far-field influence consists of both rotational and divergent components, with identification of the former being particularly challenging, observationally, in view of Rossby wave propagation. The presence of multiple wave sources and refractive index variations (e.g., Karoly and Hoskins 1982, Nigam and Lindzen 1989)

can often be confounding. Not surprisingly, the monsoon influence is generally characterized using dynamical models (e.g., Ting 1994, Rodwell and Hoskins 2001).

The monsoon's influence on the divergent flow component, however, is somewhat easier to identify as the related flow originates in regions of strong diabatic heating; enabling tracking in the upper troposphere from regions of strong monsoon latent heating (or ascent). The monsoon's influence extends, at least, as far as the reach of the divergent flow, or the nearest descent regions. The upper-level descent is however not uniformly distributed with respect to the ascending region: Its organization is influenced by the rotational flow and other radiative and dynamical processes, not all of which are presently well understood.

The divergent wind and horizontal divergence (shaded) at the level of monsoonal outflow (e.g., 200 hPa) are shown in Fig. 2.7. Immediately apparent is the large summer divergent outflow from the Bay of Bengal – the region exhibiting strongest divergence in the Eastern Hemisphere – headed mostly northwestward, westward and southward. The organization of descent (and ascent) to the northwest bears imprints of Rossby wave propagation, which Rodwell and Hoskins (1996) emphasized in connecting the Asian summer monsoon with the aridity of western Afghanistan and eastern Iran (the first descent region), and the eastern Mediterranean (the second descent region to the northwest). The bulk of South Asian summer monsoon outflow is however directed southward, to the subtropical Southern Indian Ocean where it leads to the strengthening of the Mascarene High (Krishnamurti and

Bhalme 1976). This *regional* meridional overturning is the principal contributor to the austral winter's *zonal-mean* Hadley Cell.

The continental monsoon's influence to the east – the focus here in context of the summer strengthening of the Pacific anticyclone – is comparatively muted in the upper-level descent field, unless one also considers the Western North Pacific monsoon when this influence becomes more appreciable, but still modest. That this monsoon system can be assumed to be independent of the Pacific SLP anticyclone is however not clear for it can be argued that this monsoon owes its existence, in part, to the SLP anticyclone itself (Rodwell and Hoskins 2001). The synergism can contribute to anticyclone development but if the related upper-level descent in Fig. 2.7 provides any guidance, the Western North Pacific monsoon's influence is modest and confined largely to the tropics, except in the far eastern basin where the subtropics are also, to an extent, influenced.

Examination of the 200 hPa divergent circulation indicates the Asian monsoon's influence on upper-level descent over the Pacific to be modest. This, of course, is not a full measure of the monsoon's influence on the Pacific basin, as noted at the beginning of this section. Vorticity dynamics, in particular, vortex stretching in the monsoon latent-heat release regions, elicits a substantial rotational response with bearing on the SLP field – a response, difficult to isolate without the use of models.

A diagnostic modeling analysis of Pacific circulation and SLP, in particular, its seasonal evolution is presented in chapter 3. The analysis seeks to identify the forcing that leads to the development of key SLP features, including

anticyclone strengthening and expansion in the spring-to-summer months. The modeling analysis also discusses the forcing that offsets Asian summer monsoon's influence on Pacific SLP in the tropical and subtropical basin; leading to weak annual variability, in the net, there.

2.6 Evolution of sea-level pressure over the Atlantic

The seasonal evolution of SLP in a basin that does not have an Asian monsoon equivalent to its west is examined in this section to gain insight into the operative mechanisms. The annual cycle of Atlantic SLP is compactly displayed in Fig. 2.8 using vectors, just as in Fig. 2.4. The annual-mean field (contoured) consists of a basin-wide anticyclone, called the Azores High (or Bermuda High), which exhibits modest annual variability except near its northern flank. The annual variability is, evidently, largest in the northern basin, much as in the Pacific; and quite weak in the tropical and subtropical latitudes, as also in the Pacific.

As seasonal evolution can consist of more than just the annually varying signal, the full development of SLP in the 20°-30°N latitude band is shown in Fig. 2.9a,¹³ with a small contour interval (1 hPa) to bring out the subtle evolution features. The evolution is somewhat different in the two basins, with SLP attaining its maximum in the central/eastern Pacific earlier than in the Atlantic. The earlier (April)

¹³ The latitude band is 5° northward shifted with respect to the one in Fig. 5 in order to accommodate the evolution of Atlantic SLP variability (cf. Fig. 8), which is more northward focused than the Pacific's.

maximum in the Pacific is consistent with the previously shown build up of SLP in the Pacific subtropics (cf. Fig. 2.3), which is largest during January-March. The SLP range in the two mid-basins is quite similar (~ 2 hPa), though. The range is considerably larger near the coasts where the monsoon influence is manifest.

In the interest of closer intercomparisons, the annual and semi-annual components of SLP variability are also plotted in Fig. 2.9b and c. The annual signal consists of a summer low over/near the continents in both basins, reflecting the influence of the Western North Pacific (and Asian summer) monsoon, Mexican monsoon and heating of the Mexican highlands, and the Sahara desert heat-low. The correspondence of annual SLP variations in the two mid-basins is striking and remarkable considering that one of the basins has a powerful monsoon system to its west. The correspondence was not discernible in the full fields (top panel) because of the presence of semi-annual variability in the Atlantic sector.¹⁴ The amplitude and phase similarity of the annual signal in the two mid-basins suggests that either the monsoons to the west of the anticyclones are inconsequential, or else the global reach of the Asian summer monsoon.

2.7 Evolution of sea-level pressure in the Southern Hemisphere

¹⁴ The semi-annual component reflects the twice-yearly overhead position of the Sun at the Tropic of Cancer. The Atlantic sector (100°W-60°W) is more responsive to such Sun visits because of the presence of land in this sector (eastern Mexico, Florida and Cuba, among others); with the low SLP following the equinoxes within a month, at monthly resolution.

The seasonal variability of SLP in the hemisphere having significantly less landmass is examined in this section. Reduced landmass in the sub-polar Southern Hemisphere (SH) leads to weaker stationary waves, and thus, a more axisymmetric circulation. The stormtracks are more zonal as well, especially in the austral summer (e.g., Hoskins and Hodges 2005). The reduced continentality also leads to weaker monsoons. Such differences make SH attractive for testing understanding of the atmospheric general circulation.

The annual variability of SLP in the SH is displayed in Fig. 2.10. The annual-mean field (contoured) is quite zonal in the high latitudes, unlike the NH. A weak high in the Weddell Sea sector and a zonally diffuse low elsewhere is, nonetheless, discernible. The annual-mean SLP also contains three anticyclones in the SH subtropics, one in each ocean basin, with the Indian Ocean one (the Mascarene High) being the strongest (>1022 hPa).

The annual SLP variability in the SH is quite distinct from the NH, as evident from the distribution and orientation of the annual-harmonic vectors in Fig. 2.10. The annual variability is primarily focused in the tropical/subtropical latitudes; unlike NH, where high latitudes were the focus of seasonal development (cf. Fig. 2.4). This difference leads to strikingly different evolution: An equatorward strengthening / expansion of the SH anticyclones as opposed to poleward development of the NH ones. Phase differences, moreover, lead to different peak-phase timings: austral winter and boreal summer, respectively. What could cause such inter-hemispheric differences in SLP evolutions?

- *Stormtracks*: The SH storm tracks are located in the high latitudes, close to the Antarctic Circle.¹⁵ As such, they are well separated from the subtropical anticyclones, and perhaps, less influential. This is unlike the NH where storm tracks are mostly in the mid-latitudes (40°-50°N), i.e., in proximity to the SLP anticyclones.
- *Monsoons*: The SH monsoons are weaker; with the monsoon regions located somewhat equatorward. Even so, there is considerable rainfall development over the subtropical South American continent, including Amazonia, from winter (JJA) to summer (DJF). Assuming monsoon latent-heat release to be influential on downstream SLP development, as posited for the NH Pacific anticyclone (e.g., Rodwell and Hoskins 2001), one should expect a stronger anticyclone in the subtropical South Atlantic in austral summer (DJF).¹⁶ Observations however indicate this anticyclone to be stronger in austral winter, and not summer; as is also the one in the Indian Ocean.
- *Hadley Descent*: Meridional overturning in the Eastern Hemisphere is the principal contributor to the Hadley Cell, including its seasonality (cf. section 2.5). The descent in the SH tropics and subtropics is strongest in JJA, and focused in these longitudes, as it is related to the Asian/African summer monsoon outflow (cf. Fig. 2.7). Not surprisingly, this sector's SLP anticyclones are strongest in austral winter.

¹⁵ The poleward location (~60°S) of the SH storm tracks can be seen in the band-pass filtered variance of the mean SLP field. Compare, for instance, the NH winter (DJF) distribution (Fig. 3a in Hoskins and Hodges, 2002) with the SH winter (JJA) one (Fig. 3f in Hoskins and Hodges 2005).

¹⁶ A similar dynamical response (e.g., from Sverdrup vorticity balance) is expected in the SH, despite the negative Coriolis parameter; for it appears in both the vortex stretching term and the geostrophic relationship.

An additional contributor to SLP variability over the subtropical oceans is downstream thermal advection from the continents. A close inspection of vector orientations in Fig. 2.10 shows the arrows to turn clockwise as one moves eastward from the east coast of the continents, especially, in the subtropics. The eastward propagation of phase is manifest in the Hovmöller plot of annual SLP (and 850 hPa temperature) variability in the 20°-30°S band (Fig. 2.11). The mean wind in this latitude belt – weak westerly – advects continental temperature downstream, leading to a delayed temperature (and from hydrostatic approximation, SLP) signal over the oceans; both are shown, with the temperature shaded. The slope of SLP contours off the eastern coasts is $\sim 20^\circ$ longitudes per month, leading to a phase speed of ~ 1 m/s. The phase speed is small because the 20°-30°S belt contains both easterlies and westerlies, with the mean wind being a weak westerly.

The evolution of SLP anticyclones in the SH suggests

- Monsoons do not account for the seasonal strengthening of the anticyclones, which peak in austral winter.
- Stormtracks cannot be implicated either given their sub-polar, and thus distant, location relative to the subtropical anticyclones.
- Hadley Cell seasonality can apparently account for the waxing and waning of the SH anticyclones, in accordance with dynamical intuition; quite unlike the NH. Reduced interference from stormtracks is, perhaps, the reason for the manifestation of this intuitive link in the SH circulation.

2.8 Concluding remarks

The paper seeks to advance understanding of the causes of seasonal sea-level pressure variability over ocean basins in the Northern Hemisphere, in particular, the waxing and waning of the Pacific anticyclone; a majestic feature, occupying almost the entire extratropical basin in July. Because of its expanse, perhaps, the Pacific anticyclone has not acquired a different name, unlike its Atlantic counterpart, which is known as the Azores (or Bermuda) High. Sea-level pressure is, of course, one of the most analyzed meteorological variables (e.g., Walker and Bliss 1932) but its seasonal variability, as reflected in the strength and expanse of the NH anticyclones, has defied understanding; because of the timing, which is counterintuitive from the Hadley Cell perspective.

A number of studies have sought understanding of this counterintuitive evolution since the paradox was eloquently posed by Hoskins (1995, 1996). Given the summer vigor of the NH anticyclones, monsoons were implicated. Diagnostic modeling of the summer circulation (e.g., Ting 1994, Rodwell and Hoskins 2001) did show monsoon latent heating, both to the east and west of the anticyclone, to be important for the summer structure; in addition to local low-level diabatic cooling (of radiative origin), which is more feedback than causative in nature. Given these dynamical analyses, which are quite robust, one may well ask why the origin of anticyclone seasonality is being revisited in this paper.

The motivation to revisit the paradoxical evolution of the NH anticyclones came from analysis of seasonal SLP variability in the Pacific basin; in particular, the

structure and magnitude of SLP *change* over two-month periods, beginning January (Fig. 2.3). This straightforward analysis shows the

- Winter-to-summer SLP change to be *gradual*, and composed of three comparable 2-month changes. That is, the anticyclone build-up leading to the majestic summer structure is not confined to the monsoon-onset period (May-to-July, in the NH) alone. The waxing and waning of the Pacific anticyclone must thus be due to more than just the summer monsoons, the current hypothesis.
- In all three periods, positive SLP development over the Pacific is focused in the extratropical basin (northward of the Tropic of Cancer). The tropical and subtropical basin exhibits modest SLP-change, ~1-2 hPa; with the monsoon-onset period (May-to-July) change being, in fact, negative! This is the very region where modeling analyses show summer monsoon heating to have a significant positive SLP response.

The apparent contradiction between observational findings and related modeling results is however not because either is flawed, but because the two cannot be directly compared: The modeling studies target the summer circulation itself, not circulation development (cf. Fig. 2.3), the pertinent modeling target in context of the summer peaking of anticyclone's strength and expanse. Origin of the spring-to-summer change in circulation features can thus depend as much on spring forcing as the summer one, especially, in case of gradually evolving features such as the

anticyclones; that is, on both forcing onsets and abatements. This suggests that mechanisms for the summer robustness of the NH anticyclones need to be reaffirmed.

Tracking the Pacific anticyclone variation via the 1020 hPa isobar in the full monthly SLP field (more appealing, physically) confirms that SLP-change in the tropical and subtropical basin is quite modest, warranting restatement of the original paradox (Hoskins 1996): *The conundrum is, apparently, no longer why SLP is high in summer and low in winter in the NH subtropical basins (Hoskins 1996), but rather, why it doesn't vary much at all there.* The counterintuitive element remains seemingly intact, given the latitude belt and Hadley Cell's seasonality. The conundrum is resolved by analysis of the evolution of descent in the global subtropics, not just the zonal-mean descent. The investigation also yields interesting insight into the cause of Hadley Cell seasonality in the NH.

The seasonal evolution of the *zonal-mean* descent (i.e., of the Hadley Cell) is found to be heavily influenced by the Asian summer monsoon. The notion of weaker summer descent across *most* longitudes in the NH tropics and subtropics – rooted in the anemic summer Hadley cell (and related models) – is shown to be unsound. The descent over the tropical/subtropical Pacific sector, in fact, exhibits far less seasonality than implied by the winter-to-summer Hadley Cell variation along with flawed notions of it being zonally representative; thus resolving the paradox.

We find the lack of consideration of the Asian summer monsoon in current descriptive and dynamical discussions of Hadley Cell's seasonality a significant omission, needing rectification. Based on these findings, we believe that

observational evidence for the dynamical sensitivity of Hadley circulation models to tropical heating placements relative to the equator (Lindzen and Hou 1988) is better sought in seasonal variations of the Southern Hemisphere Hadley Cell, given weaker monsoonal interference there.

The influence of Asian summer monsoon *onset* on Pacific basin circulation is difficult to characterize without a modeling analysis. As such, we examined the evolution of other prominent anticyclones – Azores (Bermuda) High in the NH and the Mascarene High in the SH – with the hope that such intercomparisons may narrow the mechanism options.

The Azores High and Pacific anticyclone evolutions are similar, with both exhibiting peak amplitude/expanse in summer. Annual SLP variability in the Atlantic basin also exhibits largest amplitudes in the high latitudes and modest variability in the subtropics. The similarity, despite the absence of an Asian monsoon equivalent over the American continent, suggests that either the Asian monsoon-onset is not so consequential, or else of its considerable global reach; and/or the significant local influence of stormtrack abatement in each basin.

The Southern Hemisphere anticyclones are found to peak in austral winter, in contrast with the northern ones. The peak-phase timing rules out SH monsoons as a causative influence. However no deductions on the influence of NH monsoons are possible from this intercomparison because SH monsoons are much weaker to begin with. The winter peak-phase of the SH anticyclones rules out stormtracks as an influence as well; not surprising, given their sub-polar, distant location. The waxing

and waning of SH anticyclones, it turns out, can be accounted for by Hadley Cell seasonality, in accordance with dynamical intuition. The absence of interference from stormtracks (and monsoons) lends clarity to the linkage.

The intercomparisons, while interesting, provide limited deductive insight into the role of Asian summer monsoon in anticyclone growth. Diagnostic modeling of circulation development over the Pacific is discussed in chapter three to assess the influence of both forcing onsets and abatements.

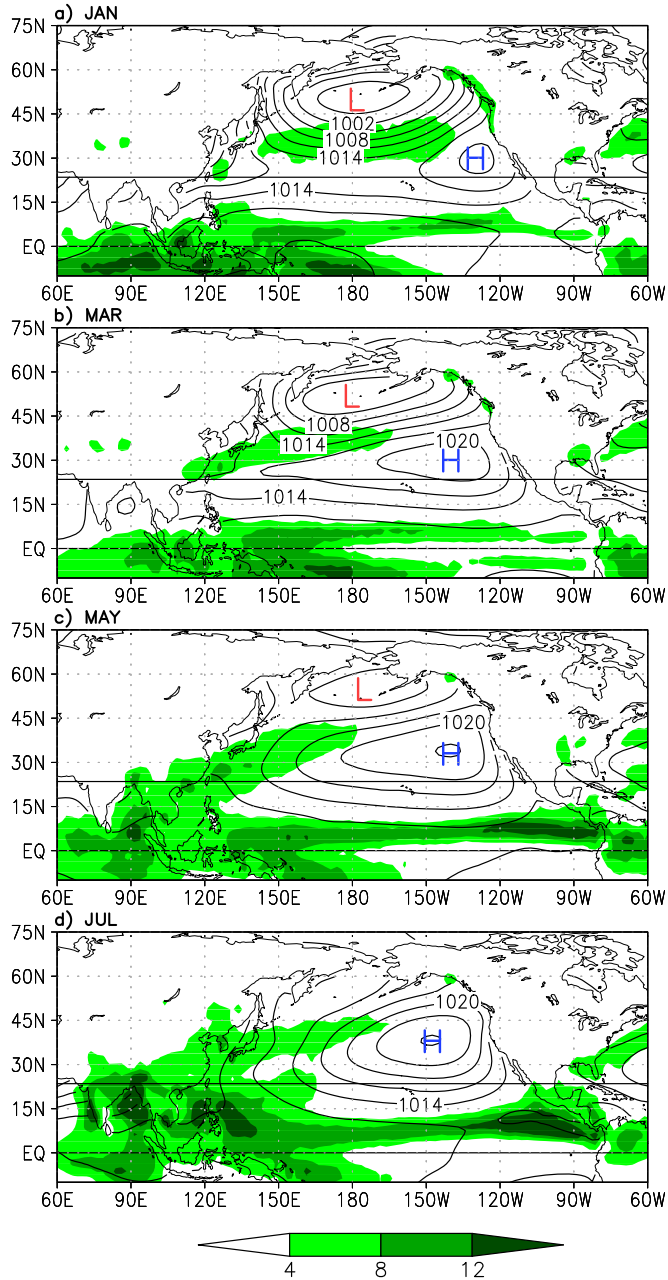


Figure 2.1: Cold-to-warm season evolution of sea-level pressure (contoured) and precipitation (shaded) in the 1979-2001 period monthly climatology. SLP is from ERA-40 and precipitation from CMAP-2: (a) January, (b) March, (c) May, and (d) July. SLP is contoured every 3.0 hPa, and precipitation shaded at 4.0 mm/day intervals, beginning at 4.0 mm/day, as indicated by the color bar. Major SLP centers – Pacific High and the Aleutian Low – are marked. The Tropic of Cancer (drawn) provides positional reference during seasonal evolution.

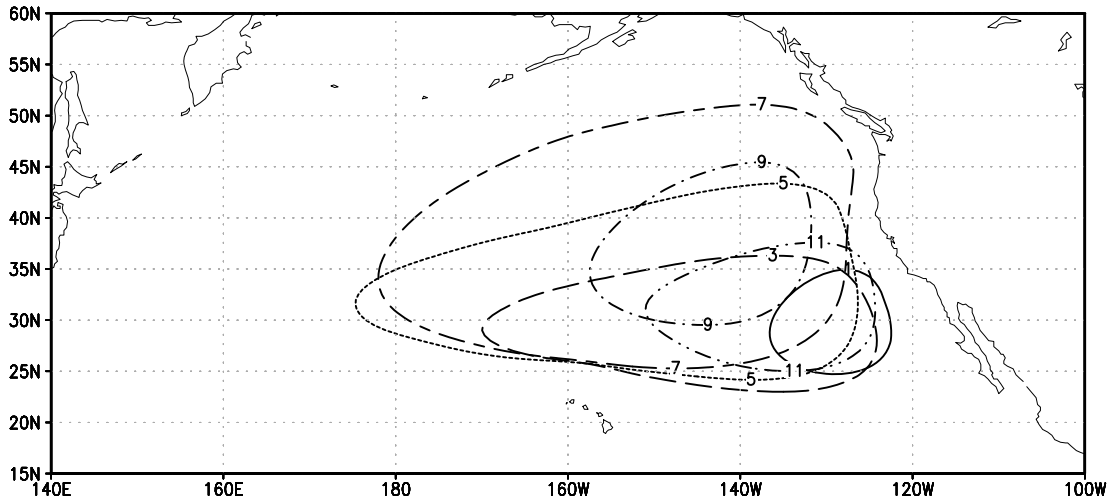


Figure 2.2: Monthly evolution of the Pacific High – the sea-level pressure anticyclone in the Northern Hemisphere. The 1020 hPa isobar in the climatological (1979-2001) SLP field is tracked at two-month intervals, beginning January. Isobars are labeled by the calendar month number; for example, January is ‘1’ and November ‘11’. The cold-to-warm season development essentially consists of a westward and northward expansion of the anticyclone.

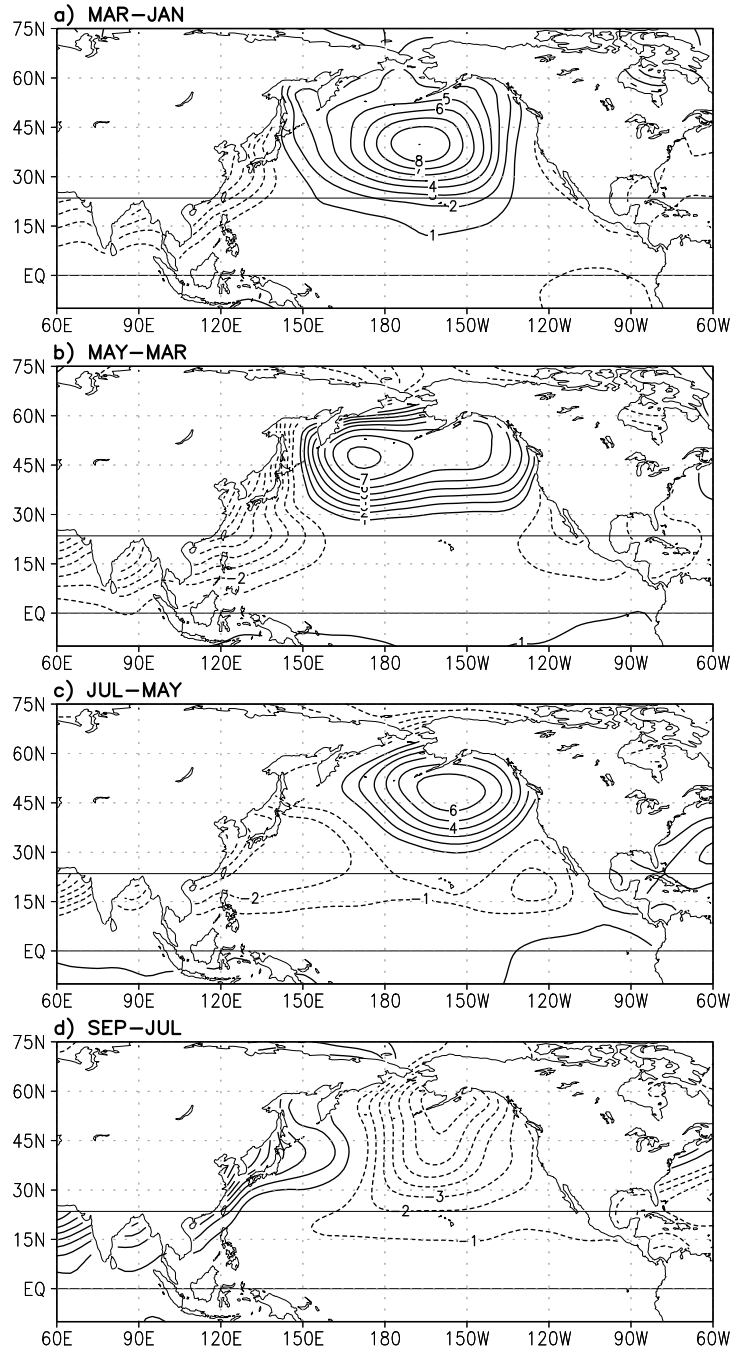


Figure 2.3: Sea-level pressure *development*: The two-month change in climatological SLP. (a) January to March, (b) March to May, (c) May to July, and (d) July to September. The SLP change is contoured at 1.0 hPa interval, with solid (dashed) contours indicating positive (negative) development. The Tropic of Cancer is again shown for positional reference.

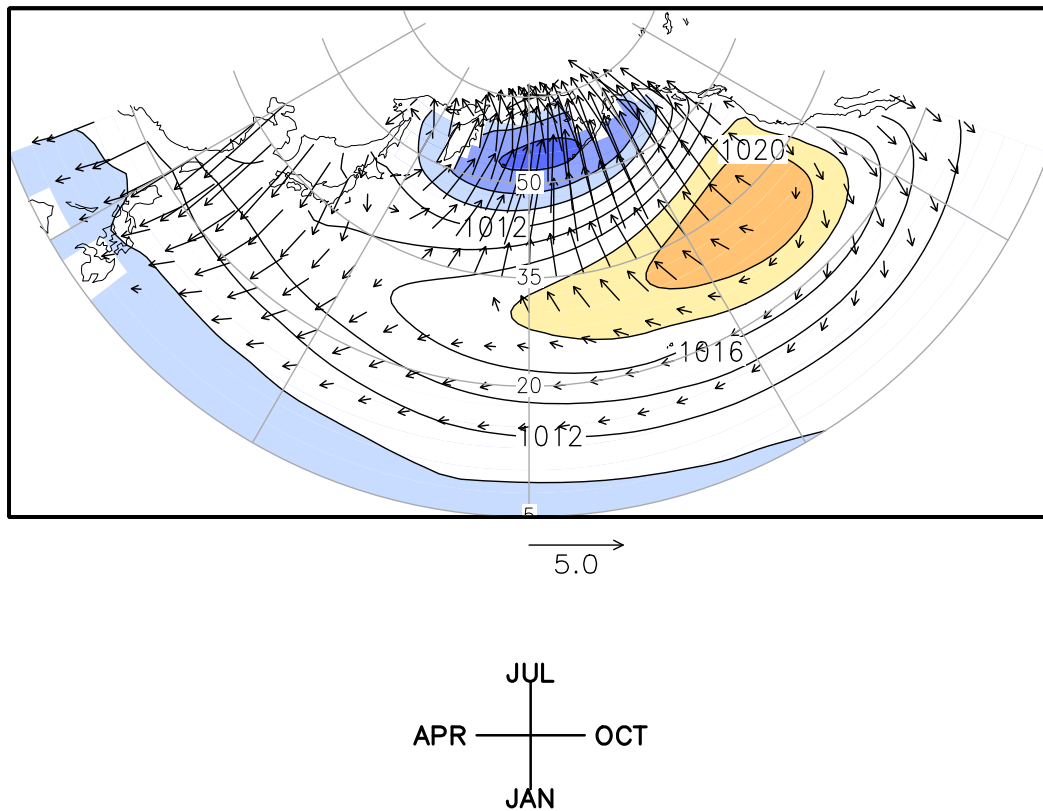


Figure 2.4: Annual-mean and annual-cycle of sea-level pressure in the Pacific basin, based on ERA-40 monthly climatology (1979-2001). Annual-mean SLP is contoured at 2.0 hPa intervals, with values above (below) 1018 (1010) hPa shaded. The annual variability is displayed using vectors, with the length denoting amplitude, and the direction, the phase; as indicated above. A *locally* northward pointing vector, for example, indicates maximum (minimum) SLP in July (January). Vectors are not drawn when the variability amplitude is less than 0.5 hPa.

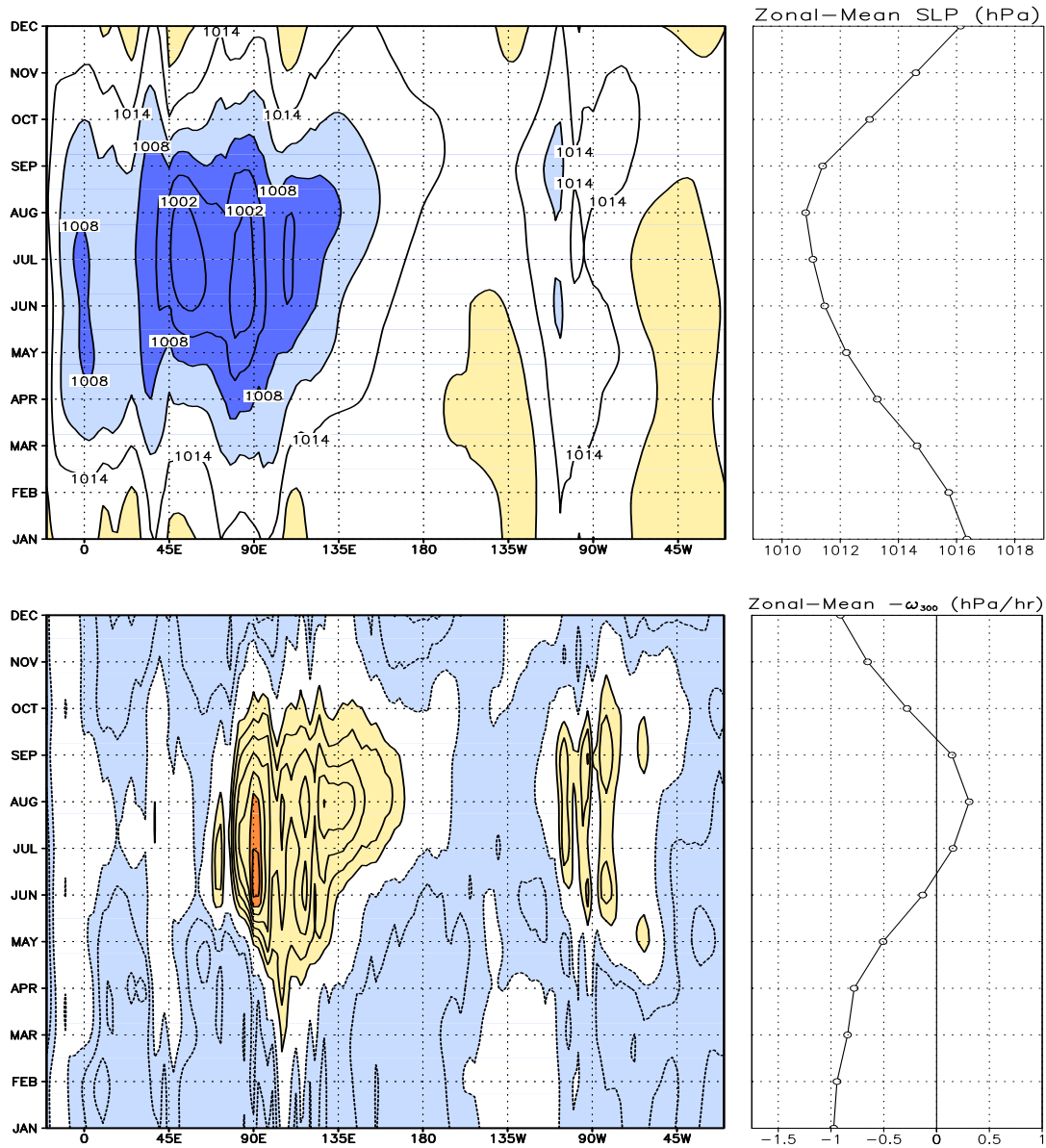


Figure 2.5: Monthly evolution of sea-level pressure and 300 hPa vertical velocity ($-\omega_{300}$) in the NH subtropics (15°N-25°N), i.e., in the Hadley Cell descent latitudes; based on ERA-40 climatology (1979-2001). Longitudinal distribution is shown in the left panels while evolution of the corresponding zonal-means is displayed in the right ones. SLP (upper panel) is contoured at 3.0 hPa intervals, with values above (below) 1017 (1011) hPa shaded. Vertical velocity (lower panel) is contoured with a 0.5 hPa/hour interval, with the zero-contour omitted.

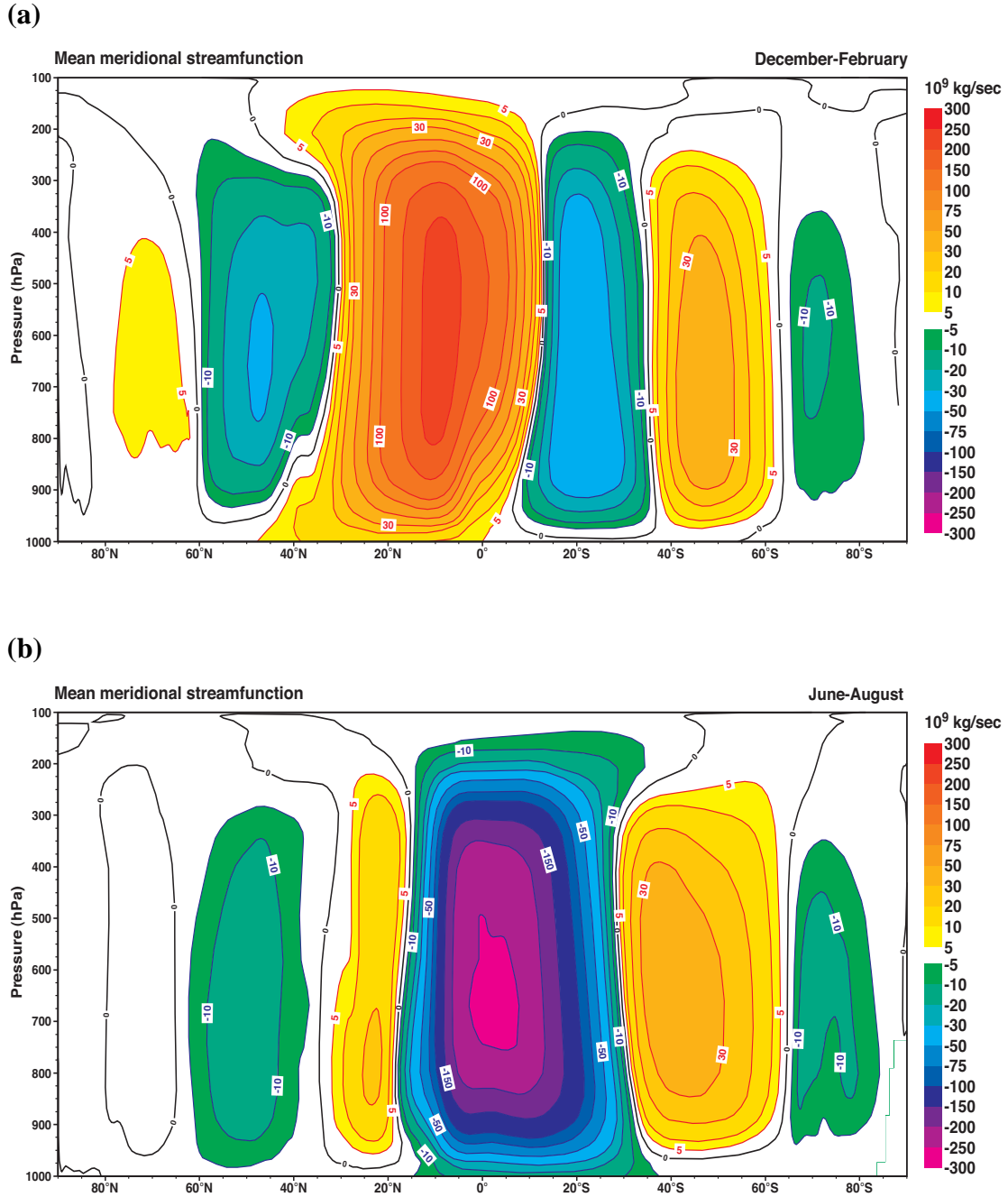


Figure 2.6: Mean meridional streamfunction (mass weighted) in December-February (upper panel) and June-August (lower panel) months, from the ERA-40 Atlas (Källberg et al. 2005); based on the 1979-2002 climatology. Contour interval is $5.0 \times 10^9 \text{ Kg/sec}$ and shading is as indicated.

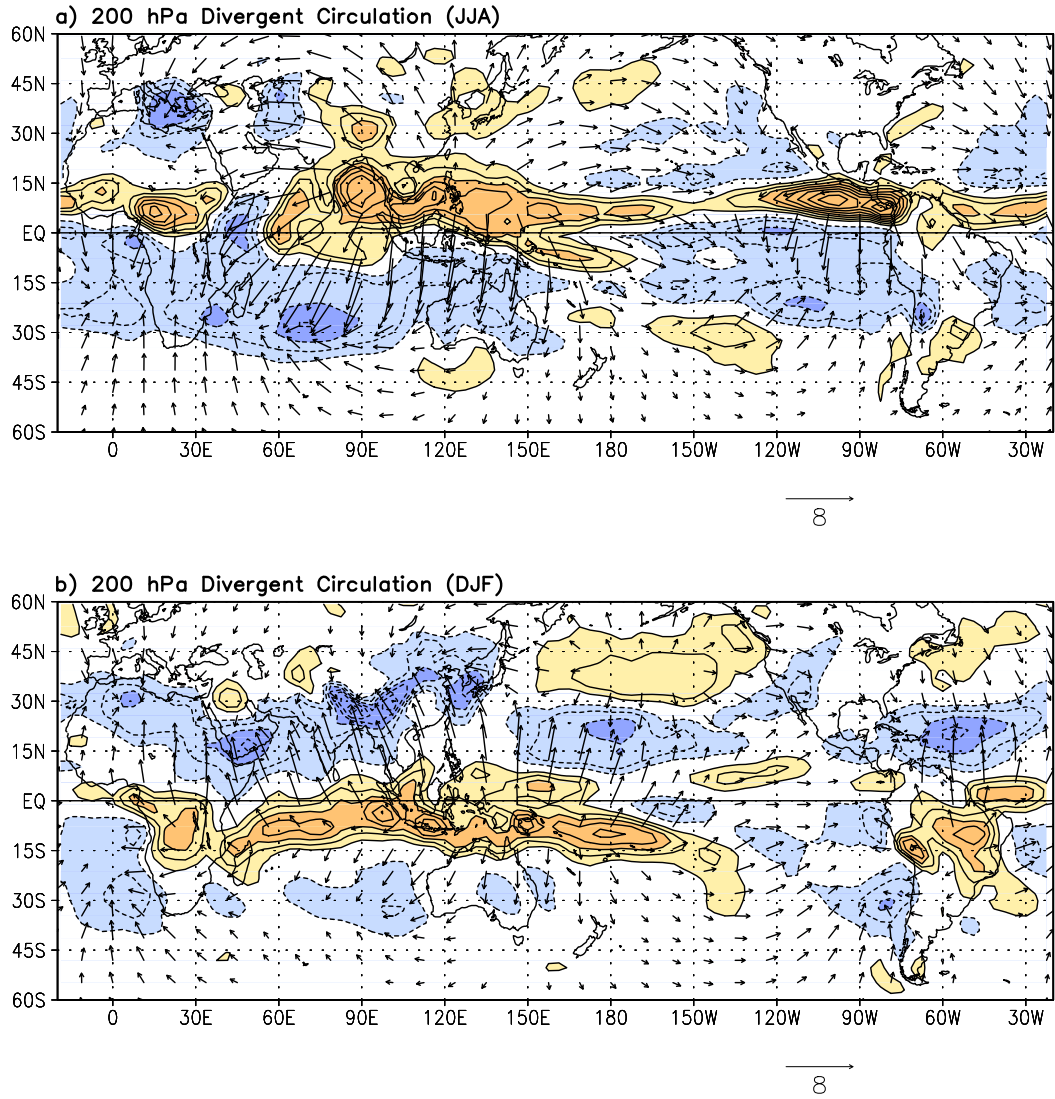


Figure 2.7: Divergent circulation in the upper troposphere in June-August (upper panel) and December-February (lower panel), based on ERA-40 climatology (1979-2001). The 200 hPa divergence is contoured at 10^{-6} s^{-1} intervals and the divergent wind vector is displayed using the indicated scale. Solid (dashed) contours indicate positive (negative) divergence, and the zero-contour is omitted.

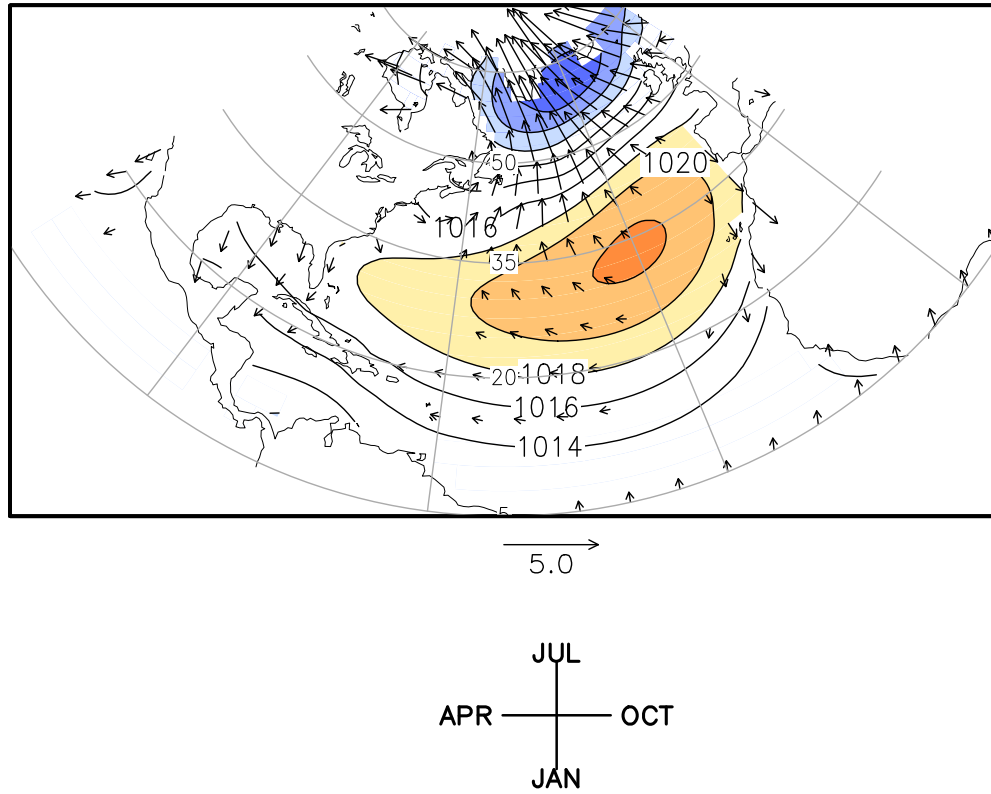


Figure 2.8: Annual-mean and annual-cycle of sea-level pressure in the Atlantic basin, based on ERA-40 monthly climatology (1979-2001). Rest as in Figure 2.4.

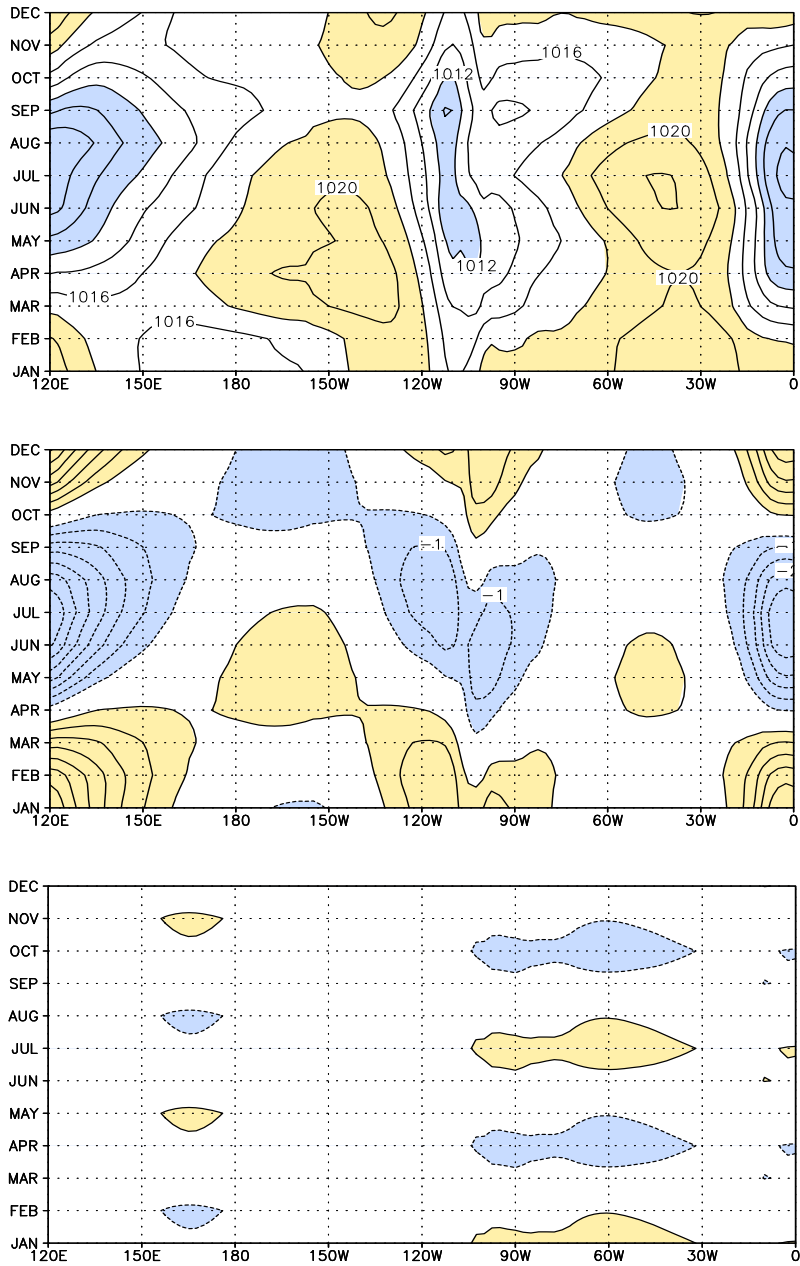


Figure 2.9: Monthly evolution of sea-level pressure in the Pacific and Atlantic subtropics (20°N-30°N), based on ERA-40 climatology (top panel). The annual and semi-annual components are shown in the middle and bottom panels, respectively. The full field (top) is contoured at 2.0 hPa intervals, with values above (below) 1018 (1012) hPa shaded. The components are contoured at 0.5 hPa intervals, with solid (dashed) contours indicating positive (negative) values; and the zero-contour omitted.

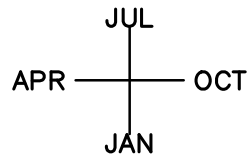
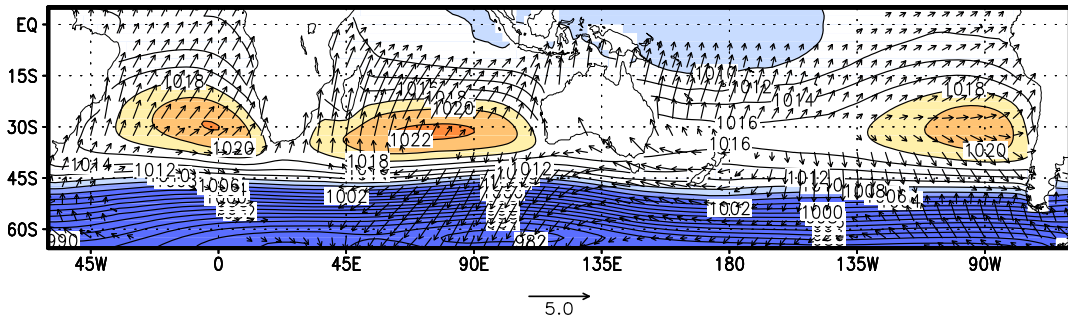


Figure 2.10: Annual-mean and annual-cycle of sea-level pressure in the global Southern Hemisphere, based on ERA-40 monthly climatology (1979-2001). A *locally* northward pointing vector, for example, indicates maximum SLP in July, as before. Rest as in Figure 2.4.

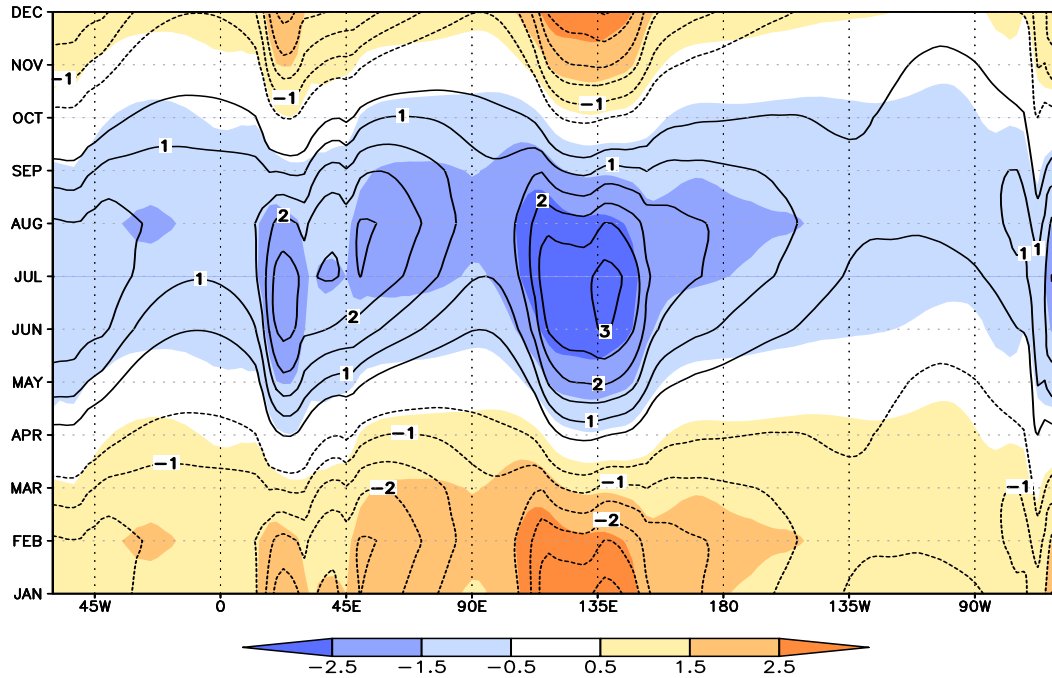


Figure 2.11: Annual component of sea-level pressure and 850 hPa temperature variability in the Southern Hemisphere subtropics (20°S-30°S), based on ERA-40 monthly climatology (1979-2001). Temperature is shaded at 1.0K intervals beginning at ± 0.5 K (see color bar), while SLP is contoured at 0.5 hPa intervals, with the zero-contour omitted.

Chapter 3:

The linear diagnostic modeling of North Pacific SLP seasonality

3.1 Introduction

This chapter is the modeling continuation of the observational seasonal SLP development analysis in the extratropical basin reported in Chapter 2. The focus here is more than the modeling of the “mature” seasonal SLP features (e.g., the boreal summer subtropical anticyclones over the oceanic basins and the boreal winter sub-polar lows), which is a common theme of many modeling papers (e.g., Hoskins and Valdes 1990, and Rodwell and Hoskins 2001). Our interest here is on the seasonal *development* of SLP, i.e., on the winter-to-summer SLP *change*, and how it is forced.

As discussed in chapter two, the largest observed Northern Hemisphere SLP seasonality is in the mid-latitudes. The ERA-40 North Pacific SLP seasonality is closely associated with the rise and demise of the sub-polar surface low pressure – the Aleutian Low (AL). When AL weakens during the boreal spring, the Pacific High (PH) expands poleward into the mid-latitudes. The relative storminess of the mid-latitudes is replaced by calmer weather: decreased transient activity and increased large scale diabatic cooling. Further equatorward, seasonal SLP variability in the northern subtropical (15°N-25°N) basins is relatively weak, notwithstanding the striking seasonality of the Northern Hadley Cell. Analysis, in fact, shows that this zonal-mean cell’s seasonality reflects the development of the continental monsoons, rather than seasonal changes in SLP and tropospheric descent over the oceanic sectors

(see also Dima and Wallace 2003). In contrast, the winter Hadley Cell is fairly representative of divergent circulation occurring in most longitudinal sectors. The winter-to-summer development of SLP and large-scale descent is thus quite modest over the subtropical ocean basins; this is in contrast with the situation in middle and higher latitudes.

It is difficult to diagnose the mechanisms for seasonal SLP variability from observational analysis, although the latter can suggest hypotheses (as in chapter two). The testing of such hypotheses however requires models where the circulation forcing (e.g., diabatic heating) can be controlled. A steady, linearized general circulation model is used to analyze the mechanisms for seasonal development here. A linear modeling analysis can be potentially insightful as linear solutions can be superposed, thus allowing estimation of the influence of various regional forcings. Of course, a linear model must simulate the NH stationary waves reasonably well in order to be a useful analysis tool; and it does, as discussed later.

Stationary wave modeling has a rich history. Two of the earliest papers on the topic are those of Charney and Eliassen (1949) and Smagorinsky (1953), which investigated the role of orography and diabatic heating, respectively. Hoskins and Karoly (1981) examine the response to orographic forcing and idealized diabatic heating distributions using a primitive equation model on a sphere. Nigam et al. (1988) assess the role of orography, diabatic heating, and transient heat and vorticity fluxes in generating the winter stationary waves in the GFDL general circulation model. Valdes and Hoskins (1989) provided a comprehensive and definitive

assessment of the role of various forcings in generation of wintertime stationary waves in nature. There are three main stationary wave forcing mechanisms:

- Diabatic heating creates local temperature perturbations that are compensated / balanced by adiabatic warming/cooling and horizontal temperature advection. The diabatic heating forced vertical motions also act as Rossby wave sources due to the associated divergences.
- Orography acts as a barrier by forcing the large-scale flow to either go around or above the barrier. Vortex stretching occurs near the barrier, and conservation of potential vorticity leads to flow deflection during vortex stretching.
- Barotropic and baroclinic instabilities lead to development of “transient eddies” from the conversion of available potential energy into eddy kinetic energy (as part of the well-known Lorenz energy cycle). An important forcing of extratropical stationary waves is thus from the convergence of transient momentum and heat fluxes.

Current modeling analyses attribute the expansion and intensification of the Pacific High in boreal summer to four mechanisms: Asian/West Pacific monsoon latent heating (Ting 1994, Chen et al. 2001, Rodwell and Hoskins 2001), American/East Pacific latent heating (Hoskins 1996, Rodwell and Hoskins 2001), Northeast Pacific radiative diabatic cooling (Rodwell and Hoskins 2001), and the North American sensible heating (Liu et al. 2004, Miyasaka and Nakamura 2005). The first two mechanisms are related to convection related latent heating, while the third one is related to longwave radiative cooling from stratus/stratocumulus cloud

tops in regions where the middle and upper troposphere is cleared of clouds due to local and/or remotely forced subsidence.

The North Pacific (and North Atlantic) winter stationary waves, in contrast, are forced mainly by stormtrack transients and diabatic heating (Hoskins and Valdes 1990). It is noteworthy that the PH is also present at this time (see chapter two), albeit with weaker amplitude and extent; that is, in the absence of any northern monsoon forcing. It is thus quite likely that both winter and summer mechanisms are responsible for the winter-to-summer SLP development in the extratropical North Pacific. The PH is after all present in both DJF and JJA periods, and could not possibly be forced by the Northern Hemisphere continental monsoons during the former.

This chapter is divided into six sections. Section two describes the linear diagnostic primitive equation model and the data that are used to force the model. Section three compares the modeled seasonal climatologies and the SLP annual-cycle with the ERA-40 representations of the same. Section four diagnoses the forcing of the boreal summer and winter extratropical Pacific SLP, individually. Section five discusses the difference between the modeled DJF and JJA SLP, and diagnoses the mechanisms responsible for the winter-to-summer development. Discussion and conclusions are presented in section six.

3.2 Forcing datasets and the linear model

3.2.1 The linear diagnostic model

The analysis of mechanisms is conducted using a linear, semi-spectral, diagnostic (time-independent) primitive equation model (Nigam 1983). The model is linearized about a zonally-symmetric circulation state, and is forced by climatological diabatic heating and transient fluxes derived from the ERA-40 reanalysis, with the objective of simulating the zonally-varying circulation component, i.e., the climatological stationary waves. Horizontally, the model has 15 zonal wave numbers, and a meridional resolution of 2.5° latitude. Vertically, it has 18 sigma-pressure (p/p_s) levels from $\sigma=0.95$ to $\sigma=0.025$. The lower boundary condition uses the ERA-40 orography and the two-meter temperature. The model is linearized about the zonal-mean ERA-40 U , V , T , and $\ln P_s$ and forced by the zonally-asymmetric ERA-40 transient fluxes and diabatic heating. The zonal-mean basic state is also used in the simulations of Rodwell and Hoskins (2001). Linearization of the model about a zonal-mean state is quite appropriate for simulation of the climatological stationary waves, as it is only in the simulation of seasonal anomalies that one prefers linearization about the zonally-varying climatological flow, which allows for more realistic propagation of the excited Rossby waves.

Linear damping and diffusion processes are represented in the model. The original model version (Nigam 1983, Held et al. 1989) does not have vertical diffusion, and the diffusion physics in the present version follows the treatment in

Nigam (1994) but with differing diffusion and drag coefficients. The coefficients are, to an extent, determined by tuning the model response.

The linear Newtonian temperature damping (α), vertical momentum diffusion (ν_m), and vertical temperature diffusion coefficients are vertically dependent (ν_T):

$$\alpha = \begin{cases} (15dy)^{-1}, \sigma < 0.5 \\ ([15 + 2(\sigma - 0.5)(5 - 15)]dy)^{-1}, \sigma \geq 0.5 \end{cases} \quad (1)$$

$$\nu_M = \nu_T = 30.0\{1 + \tanh[10\pi(\sigma - 0.850)]\} \quad (2)$$

The vertical diffusion dissipation requires extra boundary conditions at both the uppermost and lowest sigma levels (as described in Nigam (1994)). Parameters such as the vertical lapse rate also need to be specified; a 6 K/Km temperature lapse rate is used. The surface momentum and heat flux specifications are based on a common drag coefficient (10^{-3}) and a 10 m/s horizontal wind speed. A second-order ∇^2 horizontal diffusion is also included in the model's momentum and thermodynamic equations, with a $5 \times 10^5 \text{ m}^2 \text{ s}^{-1}$ diffusion coefficient.

3.2.2 ERA-40 basic state and forcing fields

The 1979-1998 ERA-40 zonal-mean monthly climatology is used as the model basic state. The same period's climatological transient fluxes and diabatic heating are used as model forcing. The ERA-40 diabatic heating is diagnosed as a residue from the thermodynamic equation; the diagnoses are discussed in detail in

Chapter 4. Intercomparisons of the diagnosed ERA-40 diabatic heating with other independent estimates are also presented in that chapter.

Since the ERA-40 data archive does not contain the monthly momentum and thermal transient fluxes needed for model forcing, the fluxes are diagnosed from the 6-hourly reanalysis. An overview of the ERA-40 DJF and JJA Northern Hemisphere transient activity is shown in Figure 3.1 using the 850 hPa meridional wind variance ($\langle v_{850}^2 \rangle$) as a metric. Maximum DJF $\langle v_{850}^2 \rangle$ tends to concentrate in Central North Pacific and Atlantic with stormtrack diabatic heating concentrated to the west of the wind variance maximum (see Figure 4.2). The summer stormtracks are weaker and located poleward as evident from the northward location of the summer wind variance maximum. Poleward of 25°S, JJA $\langle v_{850}^2 \rangle$ strengthens from DJF to JJA reflecting increased austral winter stormtrack activity.

3.3 Modeled JJA circulation and annual sea-level pressure variability

3.3.1 Model's simulation of JJA and DJF circulations

The linear model's performance is examined by comparing the model solutions to ERA-40's climatological (1979-98) stationary waves (i.e., the zonally-asymmetric circulation component). Because of model's linearization about the ERA-40 zonal-mean climatology, the latter is common to the solution and target fields, and as such is excluded in the ensuing comparisons. Shown in four panels of Figure 3.2 are the modeled and ERA-40 JJA stationary wave SLP (SLP^*) and 200 hPa stream function (Ψ_{200}^*); the asterisk denotes the zonally-asymmetric component. The

simulated JJA PH is about 2 hPa stronger and located $\sim 5^\circ$ northward. The simulated PH is centered along the coast (for reasons discussed later), whereas this feature is positioned substantially off-shore in ERA-40. The model captures the near coastal SLP low near Baja California reasonably well. The simulated Bermuda High is about 3 hPa weaker, but has a realistic overall structure. The upper tropospheric simulation is even more remarkable. The Ψ_{200}^* is well simulated, particularly, the Tibetan anticyclone, which is a bit stronger in the simulation. The upper-level troughs located above the subtropical SLP anticyclones are however marginally weaker in the simulation. Over all, the linear model simulation is quite realistic, allowing dynamical diagnosis of the forcing of the Pacific High.

The DJF counterpart of Figure 3.2 is shown in Figure 3.3. The overall model features compare well with ERA-40. The modeled AL is located further west and weaker. A similar westward shift of extra-tropical North Pacific Ψ_{200}^* is also noted, with both Northeast Asian trough and Pacific Northwest Ridge shifted to the west. The model captures the SLP ridge to the east/southeast of the AL. The two simulated Pacific subtropical Ψ_{200}^* centers (in the east and west subtropical Pacific) are more far apart from each other than observed.

3.3.2 Simulation of seasonal sea-level pressure variability

The SLP seasonal cycle is simulated from the modeling of each calendar month's stationary circulation, using the 1979-1998 ERA-40 zonal-mean monthly circulation and zonal-asymmetric forcing climatology. The annual component of modeled SLP variability is extracted from Fourier decomposition of the twelve

monthly values at each grid point. The annual-mean and the first harmonic are displayed in Figure 3.4, both in model simulation (top two panels) and ERA-40 reanalysis (bottom two panels). In all panels, the annual-mean is contoured and shaded. The annual harmonic is shown as vectors in panels *a* and *c*, with the vector's length denoting amplitude and its direction, the phase; all using the indicated scale and orientation convention. The annual-cycle magnitude is also depicted using contours in panels *b* and *d* in view of the overlap of vectors in the North Pacific.

The annual-mean SLP in model simulation and ERA-40 reanalysis is broadly similar, except for the coastal proximity of the maximum and some weakness of the North Pacific trough in the simulation. The annual-cycle variability is however simulated quite realistically, with largest amplitudes (3-4 hPa) in the North Pacific where arrows point northward indicating a summer maximum in SLP. Comparison of the annual-cycle amplitude (panels *b* and *d*) attests to the realism of the simulation, except for the coastal focus; much as in the annual-mean component.

Oppositely directed arrows are present in the subtropical western and eastern basin in both simulation and ERA-40 reanalysis. The vector direction indicates that SLP in these regions is a minimum in summer. The coastally trapped structure, moreover, suggests that this variability arises from the extension of the warm-season continental lows to adjacent oceanic regions. The modeled variability amplitude in the western subtropical basin is however significantly weaker than in ERA-40. In between the two east and west subtropical variability zones, ERA-40 shows weak variability with peak SLP in boreal spring (as evident in Figure 2.9). The simulation

also contains this SLP variability feature, but with weaker amplitude; it is below the vector-plotting threshold, and does not show up in panel *a*.

The reasonable similarity of modeled and observed annual SLP variability suggests that linear model is an adequate tool for investigating the origin of the observed seasonal SLP variability. The remainder of the chapter is devoted to further analysis of annual SLP variability, with a focus on the DJF and JJA differences, for SLP in the extratropical Pacific is highest during summer and lowest during winter.

3.4 Origin of the boreal summer and winter North Pacific SLP features

The boreal summer and winter circulation and SLP simulation is compared with the ERA-40 counterparts in Figure 3.2 and 3.3. The model is successful in simulating both the summertime and wintertime stationary waves. This is encouraging as the boreal summer and winter forcings in the extratropical Pacific are clearly not the same – winter stormtrack transients and heating vs. monsoon and Pacific Warm Pool latent heating. It is, perhaps, misleading to call monsoon and the Pacific Warm Pool heating as “tropical” features, as they extend beyond the Tropic of Cancer. The objective of the section is to investigate the origin of the key features in Figure 3.2 and 3.3 through diagnostic modeling, i.e., from the computation of the response of various regional forcings. Hoskins and Valdes (1990) and Rodwell and Hoskins (2001) show that the North Pacific stationary waves are forced from around the Pacific basin. With this cue, we construct various regional forcings in and around

the North Pacific basin. Due to model's linearity, the regionally forced responses can be superposed, which serves as the basis for diagnostic analysis.

The regional forcings are based on latitude-longitude domains used by previous investigators (e.g., Ting 1994; Hoskins and Valdes 1990; and Rodwell and Hoskins 2001). The domains of various regional boxes used in the analysis are stated in Table 3.1. Figure 3.5 (3.6) depict the JJA (DJF) SLP responses forced by the heating and transients within the different regional boxes.

3.4.1 Boreal Summer Diagnosis (Figure 3.5)

The importance of Asian Monsoon in forcing the robust Pacific High in summer is emphasized by Chen et al. (2001). Diabatic heating and transients in the Asian Monsoon box (box "Asian") do force high SLP to the east of the box, as shown in panel *a*. The high SLP response is centered at 25°N and confined to the subtropics; in contrast with the full linear model response (cf. Figure 3.2), which is focused in the mid-latitudes. Augmented forcing from addition of the West Pacific box heating and transients further strengthens the SLP ridge, centering it to the east of the Dateline. However, the ridge is still located in the subtropics, and is not in the mid-latitudes.

The SLP response of heating and transients in the eastern tropical Pacific and Central American region is similar to that shown in Ting (1994), where the eastern Pacific latent heating forces an 850 hPa trough over the subtropical Northeast Pacific. Here, inclusion of this additional East Pacific/Central American forcing, equivalently, weakens the Asian + WPac forced SLP ridge by 1-2 hPa (panels *b-c*). Further

augmentation of the forcings through inclusion of heating and transients in the Northeastern Pacific box leads to substantial enhancement of the response, by up to 5 hPa, and its northward focus. The North Pacific SLP ridge almost doubles in strength, and its position is now in accord with that in the fully forced linear response (Figure 3.2). The modeling diagnosis indicates that the robust boreal summer Pacific High is forced, in good measure, by extratropical forcing, and that Asian monsoon forcing is secondary.

3.4.2 Boreal Winter Diagnosis (Figure 3.6)

The prominent heating and transient forcing in the boreal winter are the stormtrack transient fluxes and diabatic heating from stormtrack precipitation. The latter is vertically distributed quite differently in comparison with deep convective latent heating in the Tropics. Stormtrack heating, including its maximum, is confined to the lower troposphere. The vorticity and thermal transient fluxes and diabatic heating, all rooted in ERA-40 reanalyses, are prescribed as model forcing in two key regions: The Pacific storm tracks in the midlatitudes, and the tropical Pacific where the rising branch of the robust winter Hadley Cell (i.e., ITCZ) is located. The latter forcing is of some interest because of related descent in the subtropics, potentially impacting SLP, which is a field of interest here. The responses forced by the Pacific stormtrack and ITCZ boxes are shown in Figure 3.6, after first showing the fully forced linear solution in panel *a* (i.e. Figure 3.3*a*).

The most prominent SLP feature in the extratropics in winter is the Aleutian Low in the North Pacific, centered off the tip of the Aleutian Island chain (see Fig.

3.6a). As anticipated from the modeling analysis of Hoskins and Valdes (1990), this feature is forced to a large extent by local stormtrack heating and transients; as confirmed by the linear model's response here (panel *b*), which show ~6 hPa trough in the North Pacific. There is significant cancellation between the response of momentum and thermal transients in the upper troposphere, but diabatic heating and transient fluxes all tend to force a SLP trough in the North Pacific, as indicated by the robust signal there. The related 2 hPa ridge near 25°N is linked to subtropical cooling within the box (not shown). This calls into question whether the “Stormtrack” box extends too far equatorward, especially, as transient fluxes (and convergences) are significant also in the subtropics (not shown). The stormtrack box definition is thus not as straightforward as it may seem. To avoid controversy, the box definition here is identical to the definition in Hoskins and Valdes (1990).

The SLP response of heating and transients in the Pacific ITCZ box is displayed in Figure 3.6c. In the northern midlatitudes, an east-west dipole – a 3-5 hPa high in the Northeast Pacific (and even higher over the Bering Straits) and a 6 hPa SLP low near Japan – is present. In the extratropical Northeast Pacific, the tropical forced ridge is ~3 hPa weaker than the stormtrack forced trough; only south of 35°N is the Pac ITCZ forced ridge stronger than the stormtrack forced trough.

The cumulative effects of the Pacific stormtracks and tropical forcing are a ~9 hPa low over the Northwest Pacific and a ~5 hPa high near Baja California. The AL in Figure 3.6c is shifted westward from the 3.6b center as a consequence of the “Pac

ITCZ” response. The westward shifted AL (w.r.t. observations) is evidently in line with the fully forced DJF solution (panel *a*).

3.5 Winter-to-Summer SLP change

The DJF-to-JJA simulation difference arises from changes in the prescribed zonal-mean basic state and zonally-asymmetric atmospheric and land-surface forcing. The goal of this section is to analyze the origin of seasonal SLP development (cf. Figure 3.4) in the extratropical basin, where annual changes are most pronounced. Among others, we seek to determine if seasonal development can be attributed to changes in zonal-mean basic state, surface forcing changes manifest through the surface temperature lower boundary condition, or to atmospheric forcing developments in key regions. The SLP change resulting from seasonal changes in orographic forcing (different basic state winds blowing over orography) and surface temperature are easily diagnosed by running the linear model with zero atmospheric forcing (i.e. the “Topo” run in Table 3.1). This component of seasonal SLP change is factored out prior to evaluation of various regional influences/contributions, all facilitated by the linearity of the diagnostic model.

The winter-to-summer SLP change due to seasonal development of atmospheric forcing (global or regional) is thus computed as the difference of the fully forced DJF and JJA model solutions, from which the difference of model

solutions to surface forcing (orography and surface temperature) are further subtracted.

3.5.1 Simulation of Winter-to-Summer SLP Development

The difference of the fully forced boreal winter and summer SLP simulations is shown in Figure 3.7*b* and compared to the ERA-40 difference depicted in panel *a*; only the zonally-asymmetric component is displayed in these panels. The SLP development is simulated reasonably well except for the weaker amplitude. As before, the simulated development has a coastal focus, in variance with observations. Interestingly, SLP development over the Pacific is under simulated while that over the Atlantic over simulated. Overall, the linear simulation is notable for its feature-to-feature correspondence with the observed structure.

The contribution of seasonal change in atmospheric forcing to SLP development is ascertained in panel *c*, which shows the winter-to-summer development attributable to diabatic heating and transient flux variations alone. The development is pronounced in the extratropical basins (~ 8 hPa), with the longitudinal position of the Pacific maximum more in line with observations (panel *a*). The atmospheric forcing evidently accounts for almost the entire zonally-asymmetric component of seasonal SLP change in both extratropical basins. It is noteworthy that atmosphere forced SLP development in the northern subtropics (15-25N) is modest relative to that in the middle and higher latitudes, especially in the Pacific basin.

3.5.2 Dynamical diagnosis of Winter-to-Summer SLP Development

Figure 3.7 indicates that atmospheric diabatic heating and transient fluxes provide the principal forcing for winter-to-summer SLP development in the extratropical Pacific basin. This section seeks to identify the geographical regions that most influence this seasonal development, from diagnostic modeling; with the model's linearity as the basis for the analysis.

The contribution of key regions to the winter-to-summer SLP development over the Pacific basin is shown in Figure 3.8. The forcing change over the Asian continent, dominated by development of the summer monsoon, enhances SLP over the subtropical Pacific (and Atlantic) basins, as seen in panel *a*. Not surprisingly, this response is very similar to that forced just by the summertime heating and transients (Figure 3.5a), except for the marginally stronger amplitude. The Asian continent influenced Pacific SLP change is nonetheless modest given the 2-3 hPa amplitudes, and cannot account for the ~ 8 hPa development in the full linear simulation (Figure 3.7c) which is focused in more northern latitudes. The larger magnitude in Figure 3.8a vis-à-vis 3.5a shows that winter forcing from the Asian continent box also contributes some (~ 1 hPa) to the seasonal SLP change over the Pacific.

The West Pacific region is considered next, following the longitude range in Ting (1994) demarcation of the West Pacific latent heating. Although relevant in boreal summer, the box may be unsuitable in winter when it would include both deep convection over the Pacific's SH warm pool as well as a significant portion of the Pacific stormtracks in the northern midlatitudes. [For this reason, an alternate

delineation of regions is considered in Figure 3.9.] When forcing changes in the West Pacific box are additionally included, the SLP response over the subtropical Pacific and Atlantic is enhanced by 1-2 hPa. More interesting however is the modulation of the response in the midlatitudes, off Japan, where ~ 5 hPa SLP increase is in evidence. This SLP development is not generated from local forcing, as shown in Figure 3.9.

The seasonal forcing changes over the tropical Pacific that are not included in the West Pacific box are considered next. The accumulated response, displayed in panel *c*, shows significant changes in the extratropical eastern Pacific, vis-à-vis panel *b*; attesting to some cancellation between the response of earlier (Asian+WPac) and new (EPac) forcings. The inclusion of the EPac forcing moves the SLP development focus to the western basin. Finally, the seasonal heating plus transient changes in the NEPac box, which include winter stormtrack development as well as summertime diabatic cooling from stratus cloud tops, are considered. The accumulated response, shown in panel *d*, depicts largest SLP changes in the mid-latitudes, extending across the North Pacific. The mid-latitude SLP change is ~ 8 hPa, that is close to that in the full linear simulation (Figure 3.7c).

Although insightful, the modeling diagnosis of seasonal Pacific SLP development (Figure 3.7) did not clearly reveal the role of deep tropical and extratropical regions, in part, because of the extensive latitudinal span of the West Pacific box. As noted earlier, this large box is useful in boreal summer, but of questionable relevance in modeling the winter-to-summer development. The WPac box encapsulates the boreal summer West Pacific Warm Pool and the East Asian

summer monsoon's extension over oceanic mid-latitudes (see Figure 4.3). The monsoon's northward extension results from the large-scale low-level southerly flow related to Asian monsoon heat low (to the west) and the Pacific High (to the east). The WPac box thus needs to reach well into the midlatitudes in summer. This northward reach however compromises the box in winter when it includes both the Pacific Warm Pool region and the midlatitude storm tracks.

Difficulties associated with the inclusion of both tropical and midlatitude phenomena in the WPac box are circumvented through more traditional domain choices in Figure 3.9, which shows SLP development from the seasonal heating plus transient changes in the Pacific Tropics and the extratropics. The tropical Pacific forced SLP development (Figure 3.9a) is very similar to the winter response (Figure 3.6c) except for the sign; indicating strong influence of the winter tropical forcing, especially, its dissipation, on the winter-to-summer SLP development in the Pacific extratropics; or the lack of tropical summer heating's influence on extratropical SLP development in the Pacific. The latter thus results from the disappearance of DJF features rather than onset of the summer ones. The tropical Pacific forced component however provides an incomplete account of SLP development for it includes low pressure along and in the vicinity of the North American coast, where SLP is highest in summer, with the majestic Pacific High.

The SLP development arising from heating and transient changes in the Pacific extratropics is shown in Figure 3.9b. Stormtrack heating and transients in winter and the low-level diabatic cooling in summer are principal contributors to the

winter-to-summer forcing change in the extratropical box. The response to extratropical forcing change is larger than the one from tropical change. Like the latter, it is broadly similar to the wintertime response forced from the extratropics (Figure 3.6a) except for the sign. Figure 3.9b is however more fleshed out in the subtropics and midlatitudes with an eastern basin focus. These differences from the extratropics-forced winter response (Figure 3.6a) indicate a significant role for also summertime diabatic cooling in seasonal SLP development over the Pacific.

Regardless of the precise apportioning of the role of winter stormtrack abatement and summer radiative cooling, changes in extratropical forcing can account for much of the modeled SLP development (Figure 3.6c) in the central/eastern basins, including the build-up of the Pacific High.

The response of the changes in transient forcing alone in the extratropical box (which can be attributed more to the abatement of winter stormtracks) is shown in Figure 3.9c. Note heating changes in the same box cannot be attributed to one season, given contributions from both winter stormtrack latent heating and summer longwave cooling. Figure 3.9c resembles Figure 3.6a more closely than it does Figure 3.9b, indicating a role for also summertime radiative cooling (from cloud tops over the central/northeastern basin) in local SLP development.

We finally ascertain the role of heating over the North American continent in Pacific SLP development. Hoskins (1996), Rodwell and Hoskins (2001) Liu et al. (2004), and Miyasaka and Nakamura (2005) have argued that North American heating is important for the boreal summer development of the Pacific High. The

winter-to-summer change in heating and transients over the North American continent generates, at best, a tepid response over the extratropical Pacific basin (Figure 3.9*d*), with no indication for a significant role of this forcing in the summertime development of the Pacific High. More equatorward, though, this forcing is of consequence along the Baja Coast, where it produces low SLP pressure.

3.6 Discussion and Conclusion

3.6.1 Uncertainties and limitations of the diagnostic modeling experiments

The model's linearization about a prescribed zonal-mean basic state makes the equatorially forced response sensitive to both the sign and structure of the zonal-mean zonal winds. Easterly winds in the upper troposphere Tropics, as in summer (Figure 3.10), can effectively shield the extratropics from tropical influences (e.g., Webster and Holton 1982). This explains, in part, the noted ineffectiveness of summer tropical heating and transients in impacting SLP development in the Pacific extratropics. It may be of some interest to diagnose seasonal SLP variability with a model linearized about an annual-mean, zonally-varying climatological basic state. The presence of a westerly duct in the zonal wind field over the central/eastern Pacific in this basic state could lead to greater tropical-extratropical connectivity, but the impact is likely be modest given the reasonable agreement obtained here between simulated and observed winter-to-summer SLP development (Figures 3.6*a* and *c*).

Regardless of the precise role of the tropical Pacific, extratropical SLP development results from the abatement of Pacific winter stormtracks related latent heating and transient forcing, and summertime longwave cooling over the Pacific basin. The development is only secondarily forced from the influence of Asian summer monsoon latent heating.

The role of summertime radiative cooling in SLP development merits some discussion as its origin is likely related to the existence of the Pacific High itself. Note, more than half of the modeled Pacific High results from diabatic cooling and transient forcing from the Northeast Pacific box (Figures 3.5 *c-d*). The cooling results from longwave emissions from the marine stratocumulus cloud tops. Such diabatic cooling generally occurs in large-scale subsidence zones. There is some evidence that divergent outflow from the Asian and West Pacific summer monsoon systems descends in the Northeast Pacific (Figure 2.7), creating a conducive environment for stratus and stratocumulus clouds, and thus diabatic cooling. The cooling should lead to intensification of subsidence. This mechanism cannot be investigated from diagnostic modeling. A time dependent model that generates its own diabatic heating, i.e., a general circulation model, would be needed for this purpose.

3.6.2 Conclusions

A model linearized about the climatological ERA-40 zonal-mean circulation, and forced by thermal and vorticity transients, and diabatic heating is used to understand the causes of winter-to-summer SLP development in the Pacific extratropics. We find extratropical forcing to be the major contributor to both the

climatological summer SLP distribution and the winter-to-summer SLP change. Northern extratropical forcing changes from boreal winter stormtrack heating and transients to large-scale diabatic cooling in the boreal summer; the former forces low SLP in the northern basin (the Aleutian Low), while the latter a SLP-high (the Pacific High). The net change is a profound winter-to-summer increase in SLP in the extratropics.

The tropical Pacific diabatic heating and the Asian and North American summer monsoon heating are not found to be particularly influential on SLP development in the extratropical basin. Hoskins (1996), Rodwell and Hoskins (2001) and Chen et al. (2000) also found the tropical Pacific heating to be inconsequential, but these authors find monsoon heating on both sides of the Pacific basin to be influential for Pacific High development; in contrast with our findings. They reach different conclusions because they focus on the analysis of summertime SLP distribution, rather than on the winter-to-summer SLP development; the more appropriate target, in context of seasonal variability.

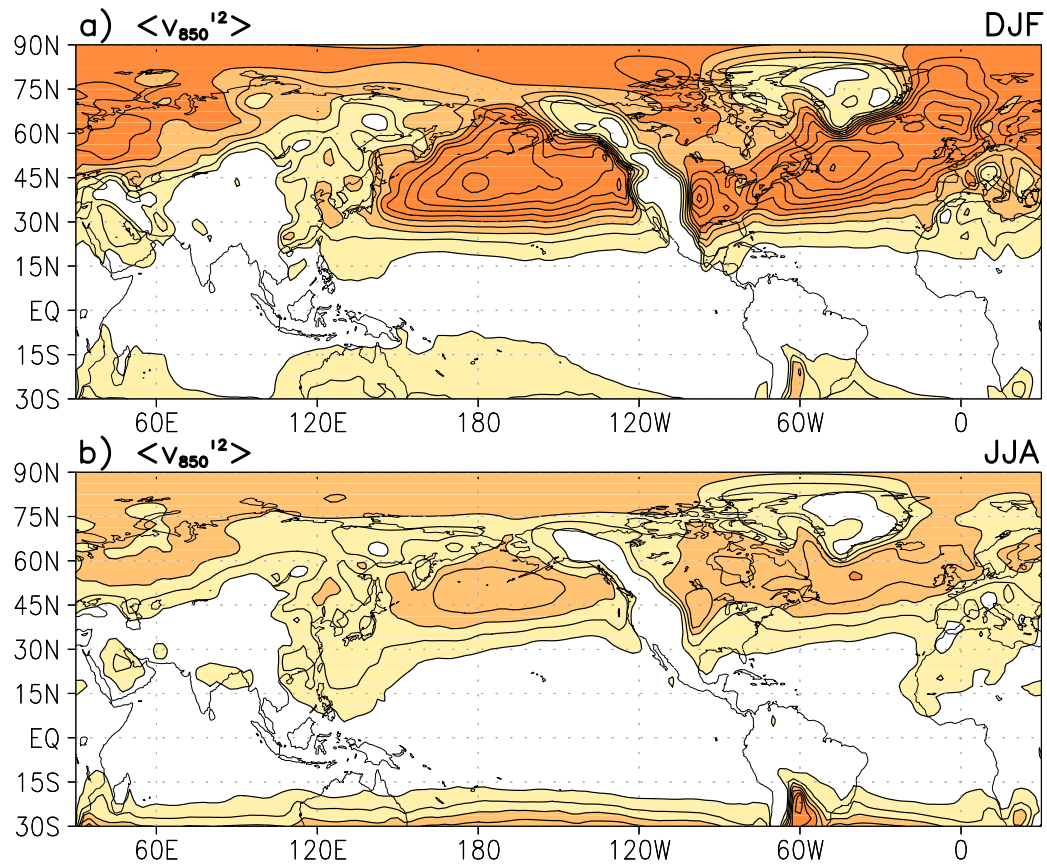


Figure 3.1: Shown above are the ERA-40 DJF (panel a) and JJA (panel b) 1979-1998 climatological monthly 850-hPa sub-monthly eddy meridional wind variance $\langle v_{850}^{\prime 2} \rangle$. $\langle v_{850}^{\prime 2} \rangle$ is contoured every $10 \text{ m}^2 \text{ s}^{-2}$.

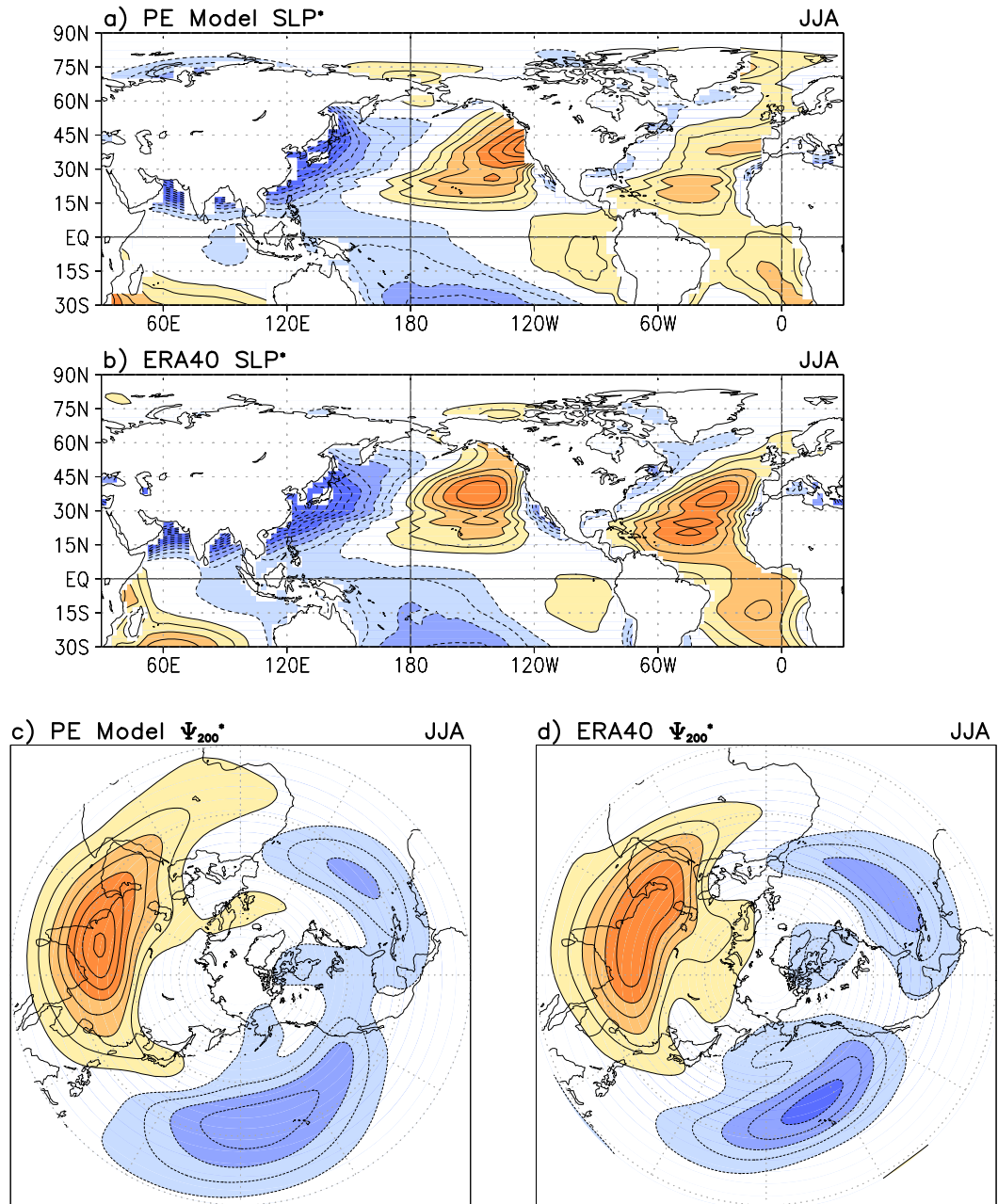


Figure 3.2: Shown above are the modeled (panels a and c) and ERA-40 (panels b and d) JJA stationary wave SLP (SLP^*) (upper two panels) and 200-hPa stationary wave stream function (Ψ_{200}^*) (lower circumpolar panels). SLP^* and Ψ_{200}^* are contoured every 1 hPa and $4 \times 10^6 \text{ m}^2 \text{ s}^{-1}$ respectively.

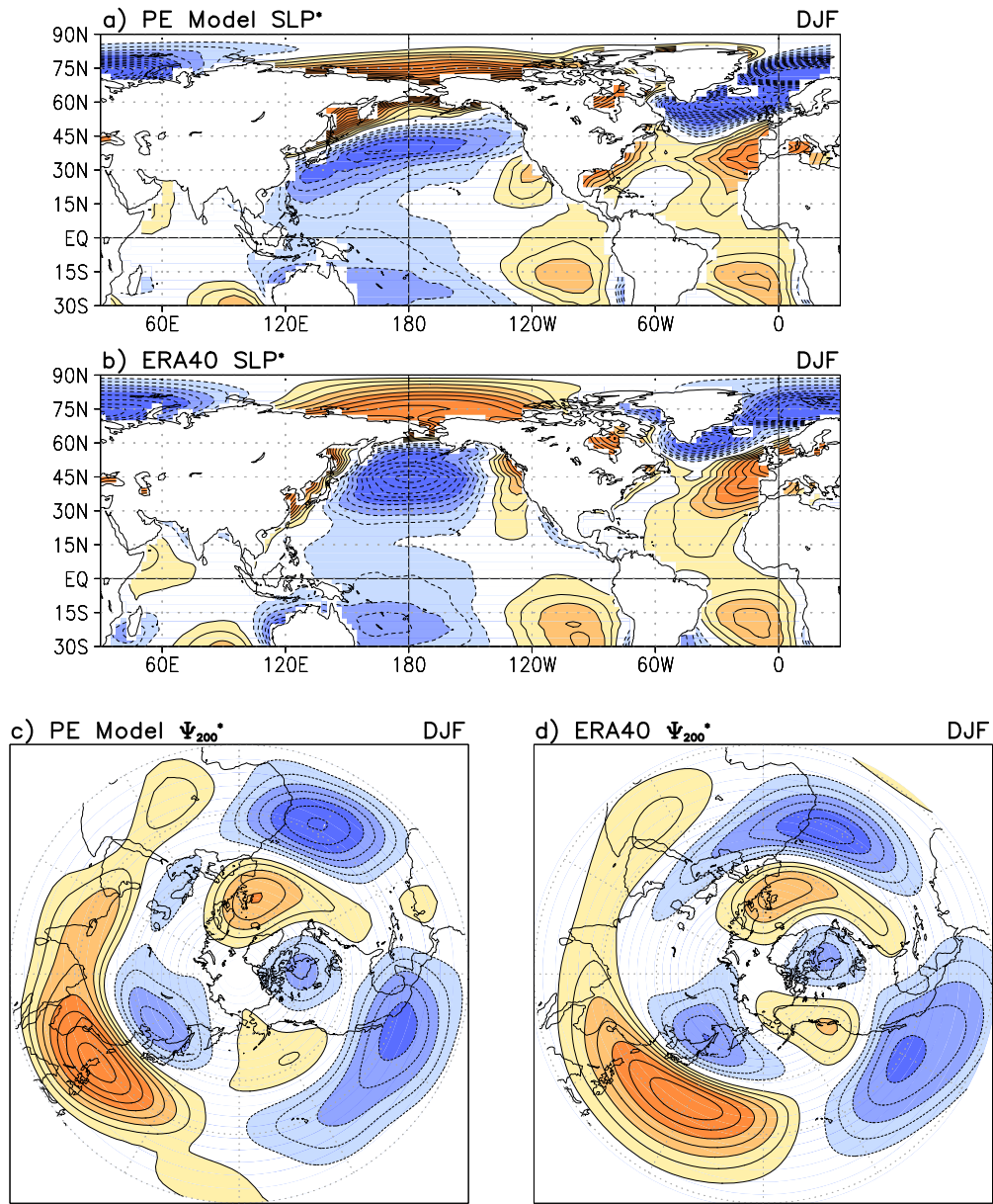


Figure 3.3: Same as in Figure 3.2, but it is for DJF.

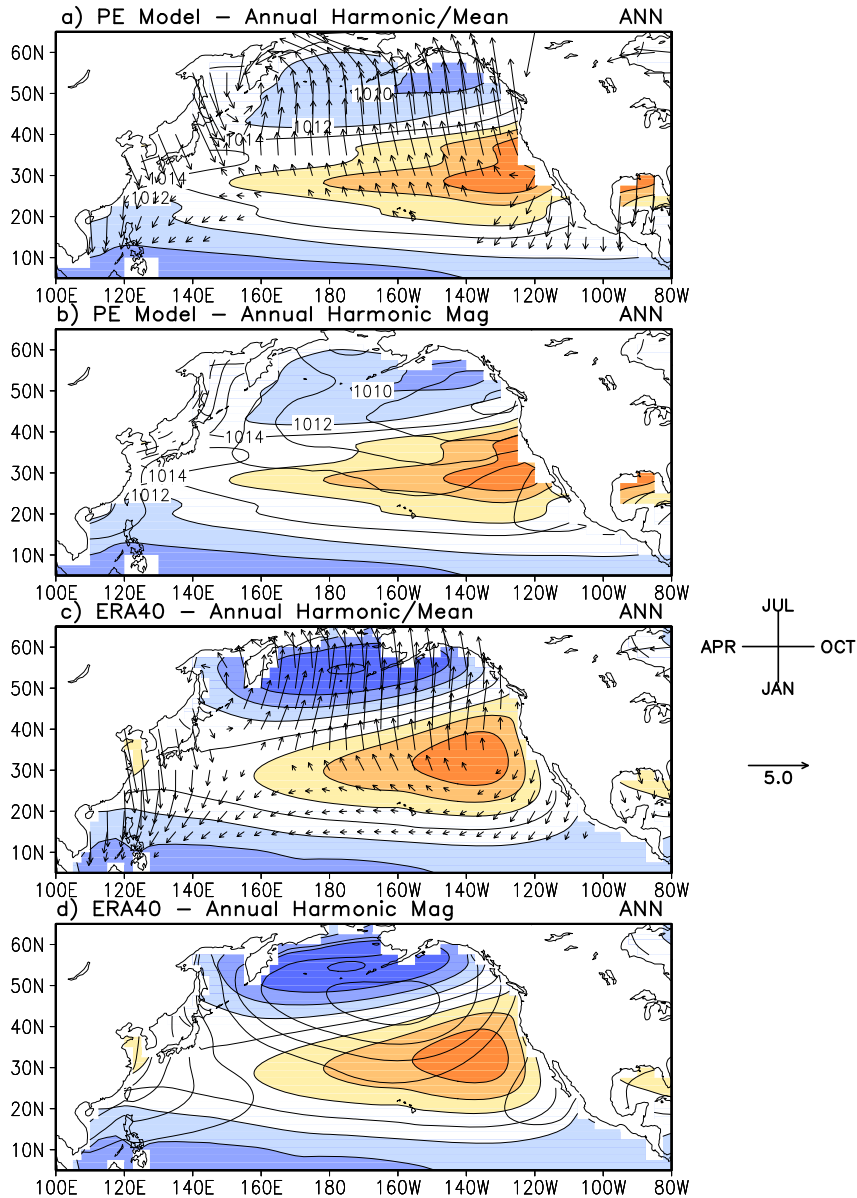


Figure 3.4: The modeled and ERA-40 1979-1998 climatological annual SLP mean (contours and shades) and harmonic (vectors) are shown above in panels *a* and *c*. The amplitudes of the modeled and ERA-40 annual harmonic (with the annual mean shaded the same way as in *a* and *c*) are contoured in panels *b* and *d*. The annual harmonic is defined that arrows pointing up and right correspond to a July and October annual maximum. The contour intervals for annual SLP means and harmonic amplitudes are 2 and 1 hPa respectively. Unlike Figures 3.2 and 3.3, the zonal mean is retained here.

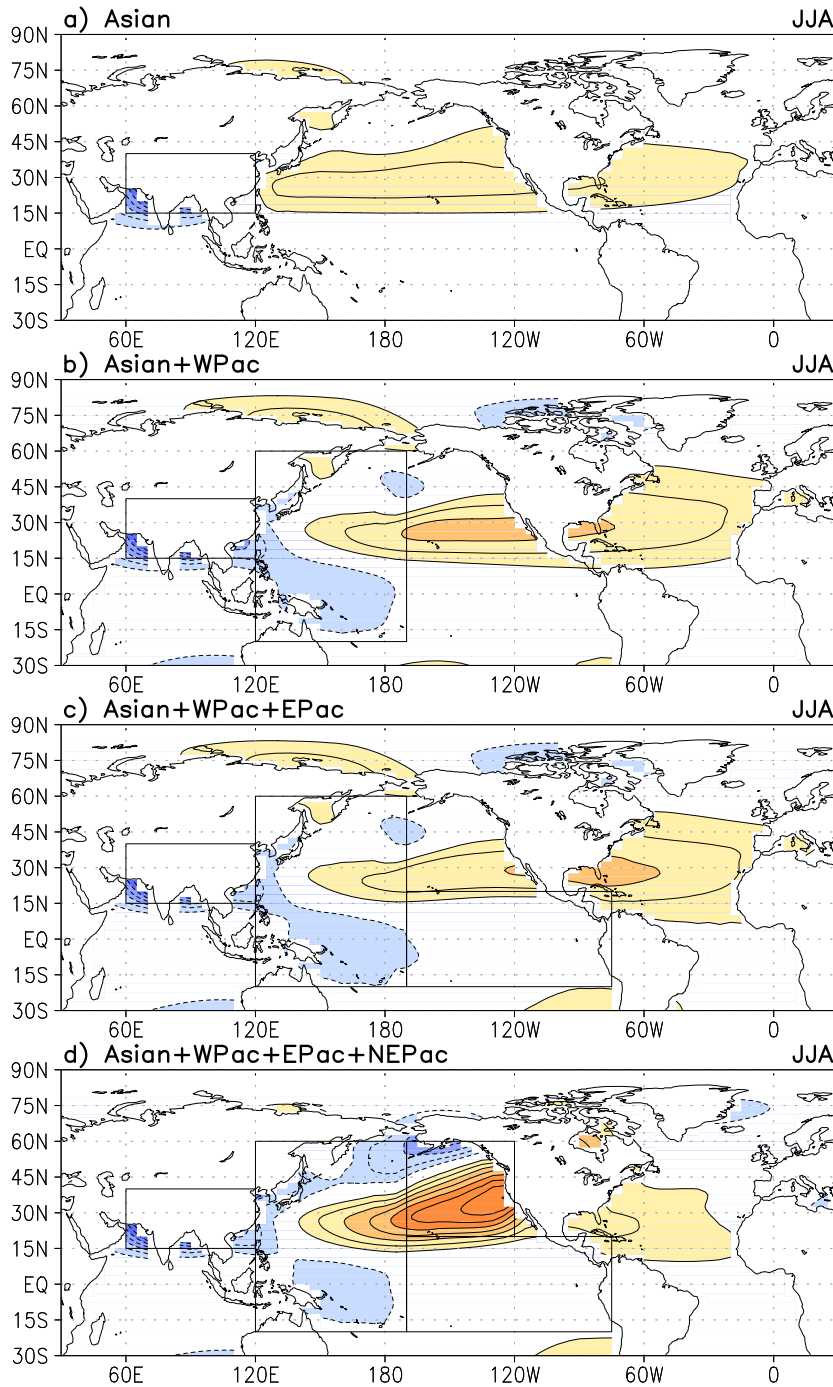


Figure 3.5: Different JJA regional (as indicated by the boxed area) diabatic heating and transients forced SLP* under a JJA basic state are superposed in increasing complexity. Panel *a* show the Asian box forced solution only, *b*: Asian + WPac, *c*: Asian + WPac + EPac, and *d*: Asian + WPac + EPac + NEPac. Contours are every 1 hPa.

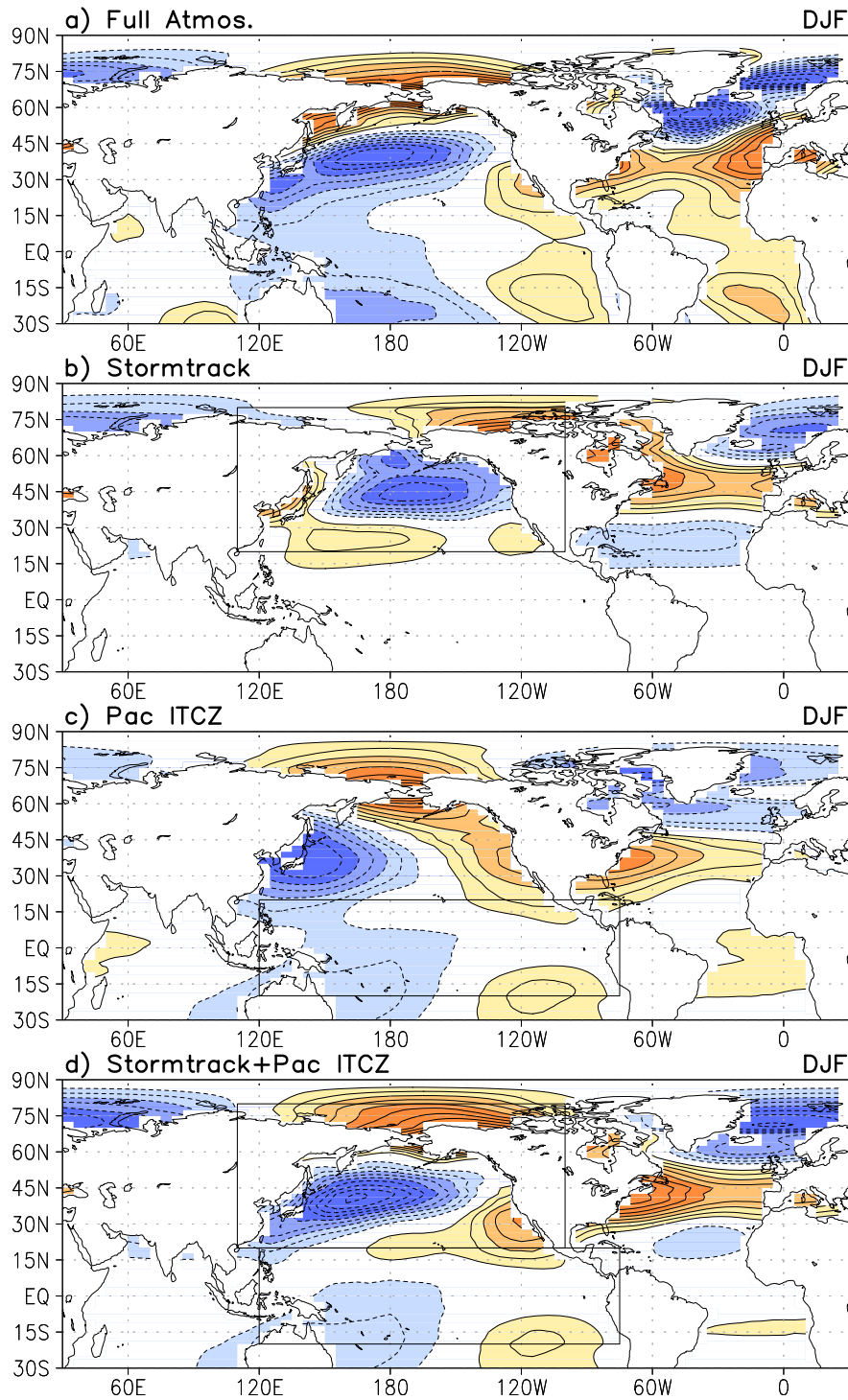


Figure 3.6: Same as in Figure 3.4, but it is for DJF basic state. The full atmospheric forced solution is shown in panel *a*. The regionally forced SLP* from the Stormtrack and Pac ITCZ box is shown in panel *b-d*. Contour intervals are 1 hPa.

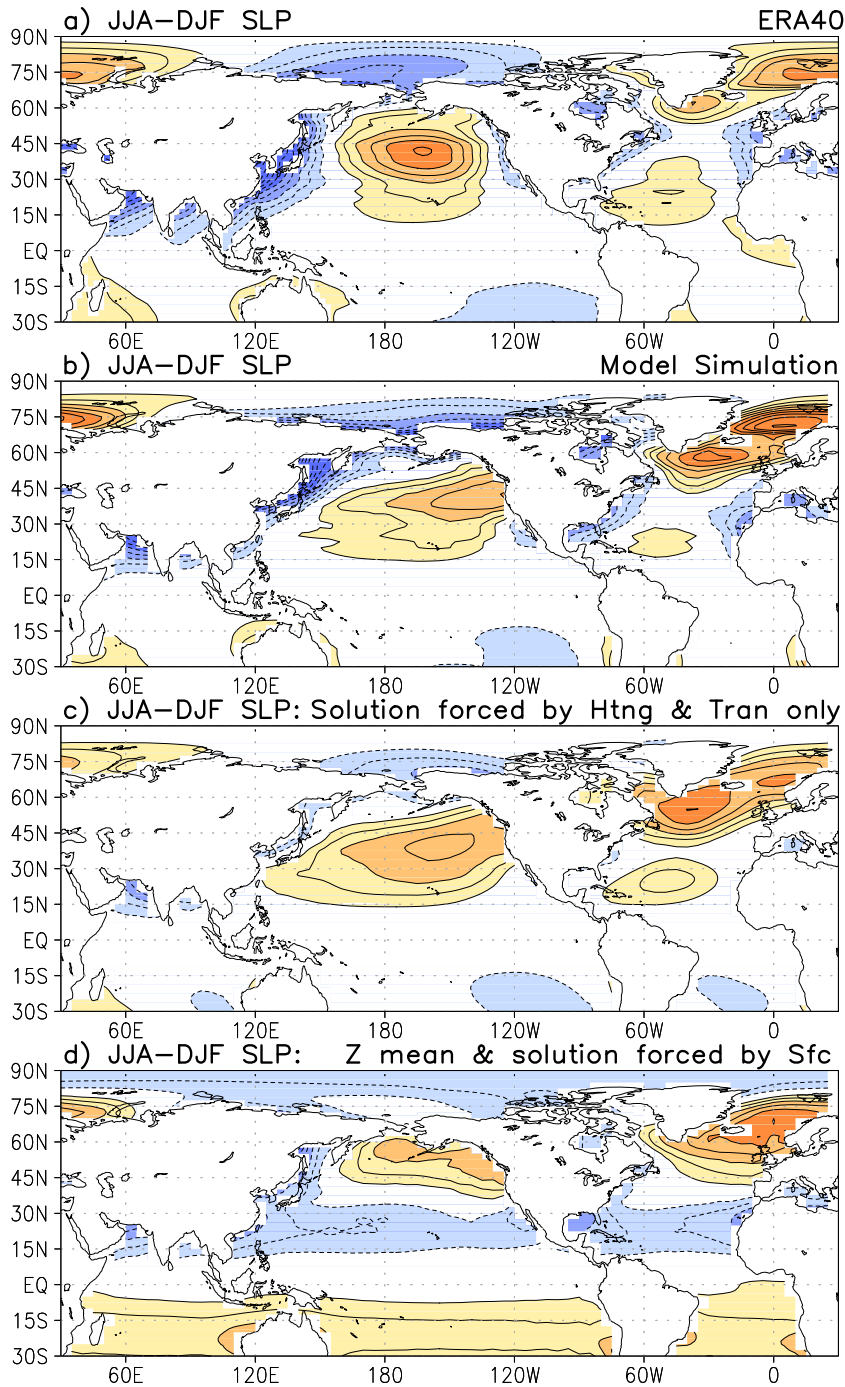


Figure 3.7: The above four panels are the JJA minus DJF in *a*: 1979-1998 ERA40 SLP* climatology, *b*: modeled SLP* difference due to atmospheric and surface forcings, *c*: atmospheric forcing forced JJA-DJF SLP* differences, and *d*: SLP difference due to surface forcing and prescribed zonal mean. Contour intervals are 2 hPa.

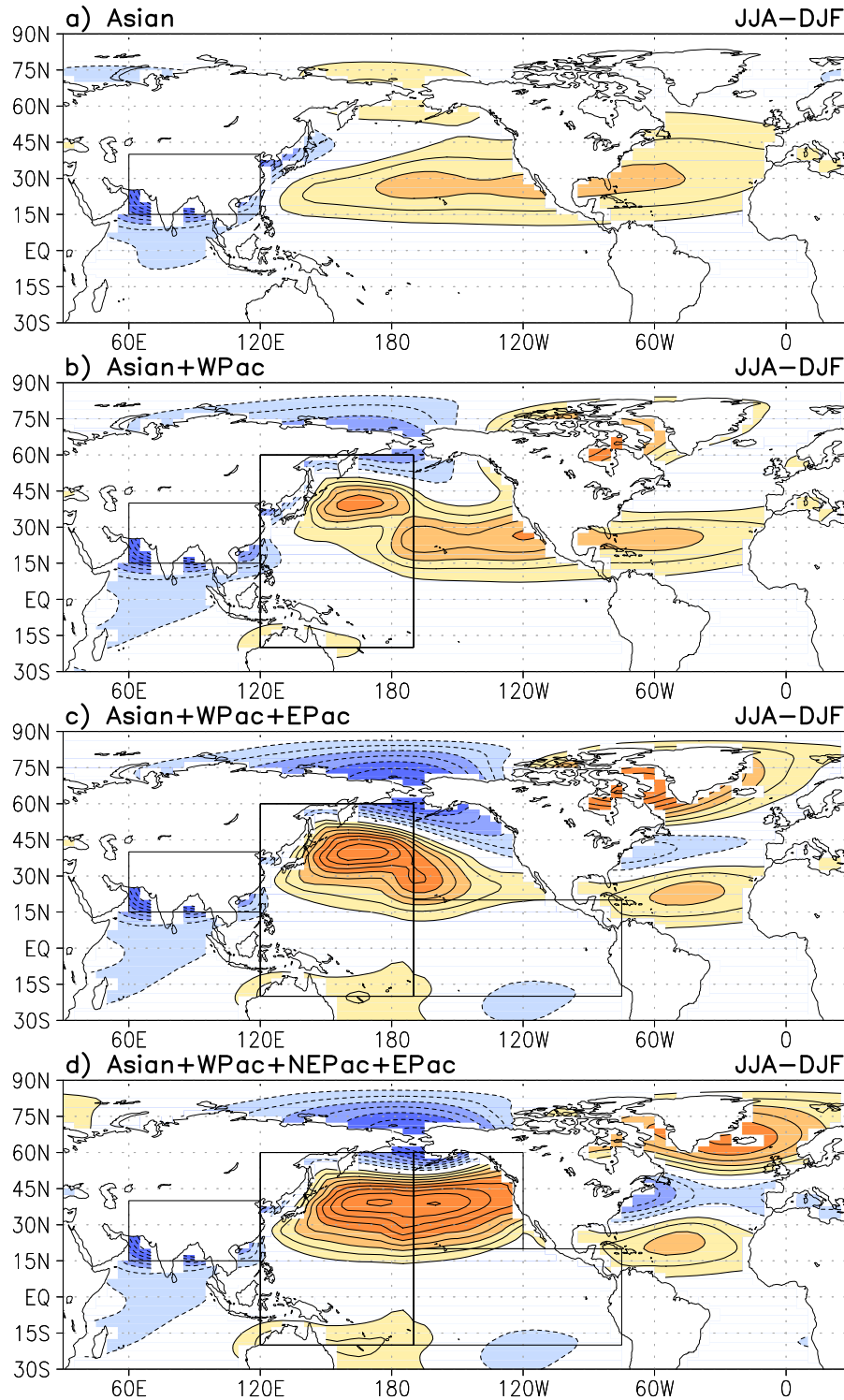


Figure 3.8: Similar to Figure 3.7, but the above panels are for modeled JJA-DJF differences that are forced by the atmospheric forcing within the boxed areas. Contour intervals are 1 hPa.

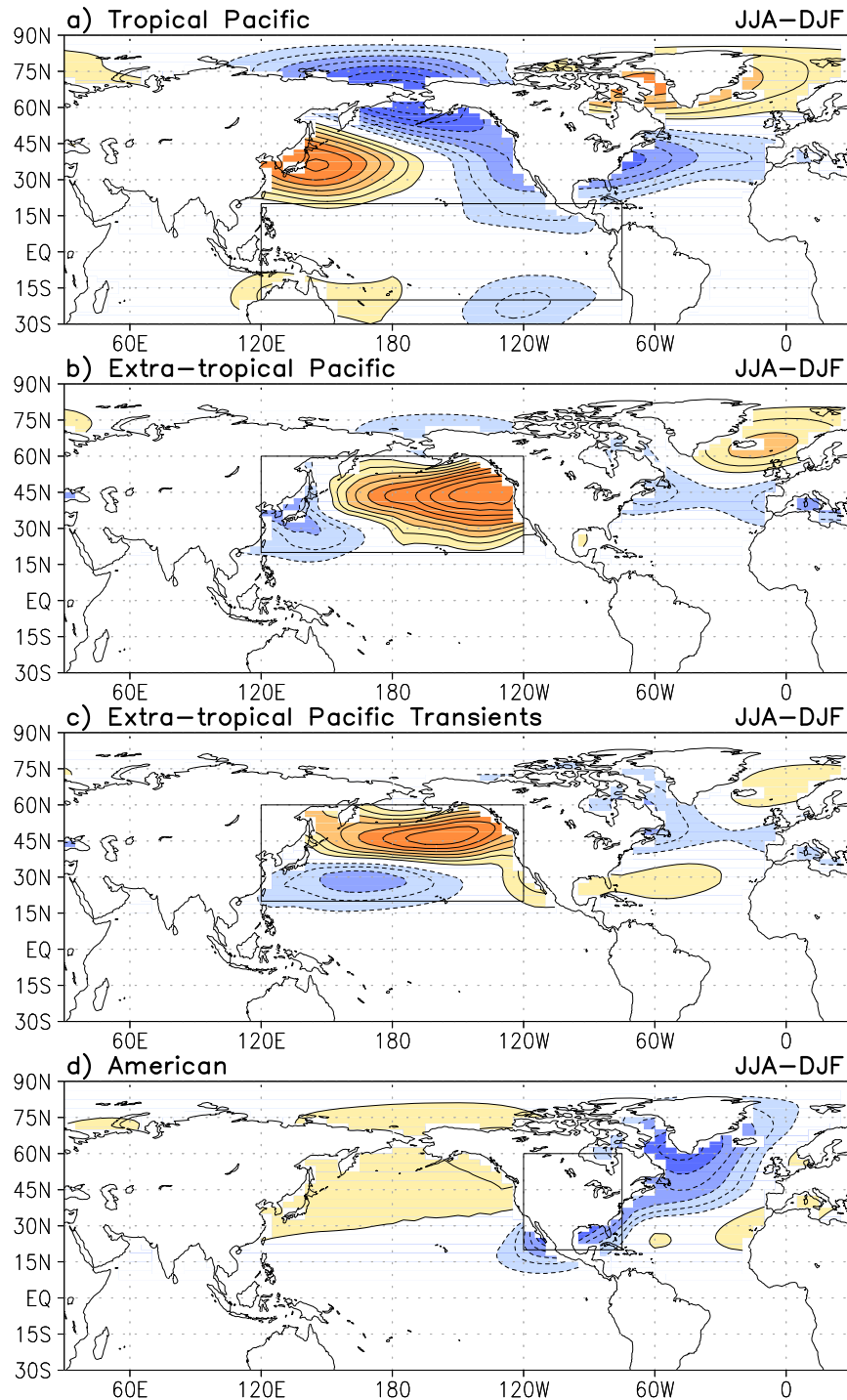


Figure 3.9: Similar to Figure 3.8, but different boxes are used. The boxes are *a*: box Pac ITCZ, *b*: extratropical Pacific (box WPac plus NEPac, 20°N-60°N only), *c*: same as in *b* but with only transient fluxes, and *d*: box American. Contour intervals are 1 hPa.

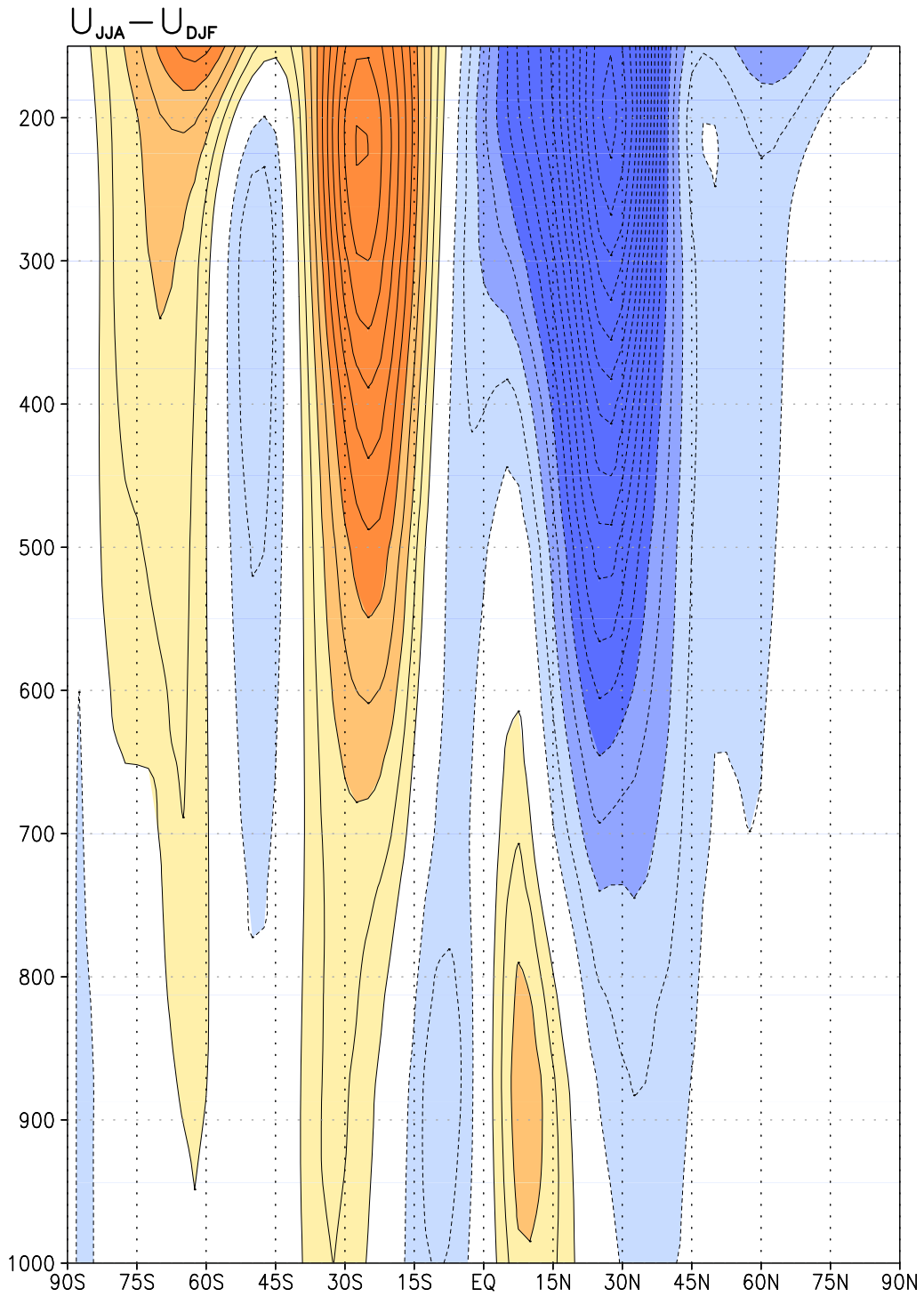


Figure 3.10: The vertical profile of 1979-1998 ERA-40 climatological JJA minus DJF zonal wind difference is shown above. Contour intervals are every 2 ms^{-1} .

Box	Definition
Topo	No Atmospheric Forcing
Asian	60°E-120°E, 15°N-40°N
WPac	120°E-170°W, 20°S-60°N
EPac	170°W-80°W, 20°S-20°N
NEPac	170°W-60°W, 20°N-60°N
American	120°W-75°W, 20°N-60°N
ET Pac	120°E-120°W, 20°N-60°N
Stormtrack	110°E-100°W, 20°N-80°N
Pac ITCZ	120°E-80°W, 20°S-20°N

Table 3.1: The above table shows the definition of the boxes that forcings are prescribed. All forcings are from 1979-1998 ERA-40 climatologies, and both diabatic heating and transients within the boxes are used.

Chapter 4:

Residue diagnosis of diabatic heating from ERA-40 and NCEP reanalyses: intercomparison with TRMM

4.1 Introduction

The earth's atmosphere is primarily heated from below by the sensible, latent, and radiative (longwave) heat fluxes originating at the land surface. Related flux-divergence and the water phase change leads to diabatic heating of the atmosphere. Atmospheric circulation arises in response to the horizontal and vertical variations of (latent, radiative, and sensible) heating forced temperature variations; and in turn, modulates diabatic heating itself, through impact on the heat fluxes. The diabatic heating distribution and the general circulation of the atmosphere are thus strongly linked. Diabatic heating is however an elusive quantity, observationally. The elusiveness stems from it being related to both local and advective changes, and that too of potential temperature; rather than ordinary temperature which can at least be measured. The diagnosis of potential temperature change moreover involves the vertical velocity, which is measurable, in principle, but not in practice on account of its extreme smallness at synoptic scales.

Diabatic heating is thus diagnosed from the atmospheric circulation (winds, temperature), usually through the thermodynamic equation (e.g., Holopainen and Fortelius 1986, Hoskins et al. 1989), where diabatic heating appears explicitly. The

residual estimation is however prone to errors in view of the uncertainties in diagnosis of the pressure vertical velocity (ω), especially, from uninitialized atmospheric data. Modern retrospective analysis (i.e., reanalysis) of global atmospheric circulation produced at NCEP (Kalnay et al. 1996) and, more recently at ECMWF (Uppala et al. 2005) with improved forecast models and data assimilation strategies, yield more consistent ω -estimates; dynamically, thermodynamically, and mass-balance wise; enhancing prospects of obtaining a refined distribution of diabatic heating for at least the recent decades.

A refined description of the heating structure is needed for improving the physical parameterizations in atmospheric models. Modeling of atmospheric convection, especially, partitioning between convective and stratiform processes remains a formidable challenge. The partitioning is as consequential for atmosphere-land-surface interactions in the subtropics as it is for atmosphere-ocean interaction in the deep Tropics. In both cases, the diabatic heating profile in the lower troposphere exerts profound influence on the low-level circulation, planetary boundary layer structure, and surface fluxes; albeit in different ways, given the different thermodynamic balance in the regions. The considerable influence of the heating profile on the upper troposphere circulation is well documented (e.g., Ting and Sardeshmukh 1993, Schumacher et al. 2004).

A refined description of the circulation-consistent heating vertical structure can, perhaps, spur development of convection algorithms, alleviating current model shortcomings such as lack of stratiform precipitation, and attendant over-production

of convective rain. The resulting bias in convective-stratiform precipitation-ratio can lead to bottom-heavy heating profiles in the Tropics (e.g., Houze 1997, Nigam et al. 2000) and spurious heating of the lower troposphere in the subtropics/mid-latitudes; which can lead to unwanted feedbacks, including precipitation recycling in the warm season.

Given the importance of the heating distribution in advancing understanding and modeling of the atmospheric general circulation, and the error prone residual estimation of heating, it is surprising that diabatic heating data is not part of the publicly accessible ECMWF reanalysis archives (ERA-15 or ERA-40). The field is, of course, generated during the reanalysis cycle, as part of the short-term bridging forecast, initiated from the reanalysis circulation. The [ERA-40 Atlas](#) (Kållberg et al. 2005) does display the heating obtained in this manner, both in column integrated and pressure-layer average formats. Diabatic heating generated during 6-hour forecasts initiated with NCEP reanalysis circulation has been available for sometime, both in total and partitioned forms from the NCAR data archives.

The diagnosed heating vertical structure cannot be easily validated as diabatic heating is not an observable quantity. But the correspondence between vertically-averaged heating and observed precipitation can provide an assessment of the residual diagnosis; at least, in the deep tropics where latent heating is dominant. Note, the correspondence is not assured in the heating fields diagnosed from the NCEP and ERA global reanalysis as the latter do not assimilate precipitation. Precipitation (diabatic heating) produced during the short-term bridging forecast of the reanalysis

cycle – the archived precipitation – is impacted only by circulation observations and the model’s physical parameterizations in these data sets. Not surprisingly, both NCEP and ERA precipitation often exhibit substantial departures from the observed distribution.¹⁷ Residually diagnosed heating – the focus of this paper – thus seems preferable to the one generated in the bridging forecasts, especially, if precipitation observations are not assimilated; the case, in current global reanalyses.¹⁸

The recent availability of the Tropical Rainfall Measuring Mission’s (TRMM) surface convective and stratiform rain rates, and related latent heating profiles based on cloud-resolving model analysis (Tao et al. 2001) raise prospects for validation of the tropical heating vertical structure in the tropics for both diagnosed reanalysis heating and TRMM profiles. Intercomparison of the profiles over continental and oceanic regions of intense precipitation in the tropics is discussed in detail in this chapter. TRMM profiles serve as a useful reference, but it is not necessarily the validation target. The TRMM profiles are still heavily based on cloud models, and such models are often of suspect. The comparisons, in fact, provide useful reading on the amplitude of the TRMM latent heating profiles, especially, in regions of adequate surface rainfall observations.

The data sets are briefly described in section two and the residual diagnosis of heating in section three. Heating intercomparisons follow in section four which focuses on the zonal and vertical averages, and the Hadley and Walker circulations

¹⁷ Sparse sampling of the atmospheric circulation (winds, temperature, humidity, etc.) in the Tropics, especially over oceanic regions also contributes to the precipitation departures, both directly and indirectly; the latter, by allowing the model biases and deficiencies to be more influential.

¹⁸ Precipitation has been additionally assimilated in the recent North American Regional Reanalysis (Mesinger et al. 2004).

and related heating distributions. Section five compares the evolution of vertically averaged heating against precipitation in regions where latent heating is dominant, to assess the reasonableness of ERA-40 and NCEP heating. Section six focuses on the heating vertical structure, especially intercomparisons with TRMM, in the ITCZ and four selected continental and oceanic regions of intense precipitation: Indian summer monsoon, Maritime Continent, South American continent, and the Pacific winter storm tracks. Concluding remarks follow in section seven.

4.2 Data sets

4.2.1 ERA-40

The ERA-40 reanalysis (Uppala et al. 2005) is ECMWF's state-of-the-art global reanalysis for the period 1957 to 2002. Being generated almost a decade after the NCEP reanalysis (Kalnay et al. 1996), it benefits from recent advances in data assimilation and physical parameterizations; and of course, more complete historical data sets.

The reanalysis combines model forecast fields, radiosonde and other in-situ data including aircraft and ship reports, and satellite data using a 3D-VAR data assimilation strategy. ERA-40 directly assimilates satellite sounder radiances. The ERA-40 assimilating model (T159, with 60 vertical levels) is the modified ECMWF Integrated Forecasting System that was used in ECMWF operations between June 2001 and January 2002. The assimilating model uses the Tiedtke (1989, 1993)

cumulus and large-scale precipitation parameterization schemes, and updated land-surface and PBL schemes. Additional details can be found at the [ERA-40 website](#).

Andersson et al. (2005) have shown that in the post-satellite-sounder period ERA-40 has a positive tropical moisture and precipitation bias, leading to hydrological imbalance; with the annual-mean global P-E being positive after 1973. Intercomparisons in this study also show the ERA-40 diagnosed heating to be excessive over the Maritime Continent.

4.2.2 ERA-15

ERA-15 is the predecessor of ERA-40, but for the period 1979-1993 (Gibson et al. 1997). The initialized reanalysis was produced from intermittent statistical (optimum interpolation) analysis with 6-hour cycling, one-dimensional variational physical retrieval of TIROS Operational Vertical Sounder cloud cleared radiances, and diabatic, non-linear normal mode initialization of 5 vertical modes, using a T106 resolution (~120 km) spectral model with 31 vertical hybrid levels. Other model features include a prognostic cloud scheme and a mass flux convection scheme (Tiedtke 1989). More details can be found on the [ERA-15 website](#).

The ERA-15 reanalysis exhibits some artificial trends, arising from assimilation of satellite data (Trenberth et al. 2001). The related problem was fixed prior to ERA-40's generation (Uppala et al. 2005). The ERA-15 data was obtained from NCAR where the 6-hourly fields are archived on a $2.5^{\circ} \times 2.5^{\circ}$ global grid and at

17 pressure levels.

4.2.3 NCEP Reanalysis

The NCEP reanalysis (Kalnay et al. 1996) is produced from spectral statistical interpolation using a T62 resolution (~210 km) global spectral model with 28 vertical sigma levels; the operational model in December 1994. The model uses a diagnostic scheme for clouds, and a simplified Arakawa-Schubert cumulus convection scheme (Pan and Wu 1994). A 3D-VAR data assimilation scheme is employed and satellite soundings rather than radiances are assimilated. The 6-hourly fields are available on a $2.5^{\circ} \times 2.5^{\circ}$ global grid and at 17 pressure levels from January 1958. The pressure-level gridded geopotential, winds, temperature, and vertical velocity (ω) fields are generated from the leading T36 spectral amplitudes.

The diabatic heating generated during a 6-hour model forecast starting from each time-step's reanalysis circulation is available, partitioned into 6 components: large scale condensation, deep convective, shallow convective, longwave and shortwave, and vertical diffusion heating rates. White and Saha (1996) document the vertical structure of the heating components and their variability during the 1982–93 period. However, in view of potential differences between the model produced and the reanalysis-consistent heating (Ebisuzaki 1996), diabatic heating was residually diagnosed from the NCEP reanalysis circulation by Yanai and Tomita (1998) and Nigam et al. (2000).

4.2.4 NOAA-CPC Merged Analysis of Precipitation

The NOAA Climate Prediction Center's merged analysis of monthly precipitation (Xie and Arkin 1997) is used to benchmark vertically-averaged latent heating over the oceanic regions. Merged precipitation (on a 2.5° grid) was generated by combining gauge observations and satellite estimates derived from the infra-red, outgoing longwave, and microwave scattering and emission based precipitation indices. The Xie-Arkin data set is short, beginning in January 1979, but global, and especially valuable over oceanic regions. The version used here (CMAP-2) is not based on any input from the NCEP reanalysis.

4.2.5 TRMM Precipitation

Two analyses of surface precipitation are used in this study: The first is the [3B43](#) analysis (on a 0.25° grid) which provides total monthly surface rainfall based on TRMM's Microwave Imager (TMI) and Precipitation Radar (PR), and ground station data. The second analysis ([3A12](#)) – an experimental one (on a 0.5° grid) – estimates monthly surface rainfall from the TMI only.

4.2.6 Station Precipitation

Precipitation from the Climate Research Unit's TS2.1 analysis of station data (Mitchell and Jones 2005) provides the monthly station precipitation estimate on a 0.5° grid over land regions. The recent 1.0° station precipitation analysis by the India Meteorological Department (Rajeevan et al. 2006, IMD rainfall) provides an additional rainfall estimate over the Indian subcontinent.

4.2.7 TRMM Precipitation Radar-based Latent Heating

TRMM latent heating comes from the Convective-Stratiform Heating (CSH) algorithm. The algorithm produces monthly latent heating profiles (up to 18 Km in the vertical) at 0.5° horizontal resolution, for the December 1997 onward period (Tao et al., 1993; Tao et al., 2001). The algorithm is based on surface convective and stratiform rain rates as well as the type and location of observed cloud systems, identified using the precipitation radar. A lookup table provides stored convective and stratiform latent heating profiles for various types of cloud systems in different geographic locations; these profiles are obtained from simulations with the Goddard Space Flight Center cumulus ensemble model. The TRMM latent heating profiles are specified in geometric height coordinates, from 500 m up to 18 Km. The corresponding pressure-level profiles are obtained by linearly interpolating the geometric-height heating rates to the geopotential heights of the ERA-40 pressure levels; with the 1000 hPa specification needing extrapolation.

4.3 Residual diagnosis of diabatic heating

The 3D diabatic heating is diagnosed as a residual in the thermodynamic equation (e.g., Hoskins et al. 1989; Nigam 1994) using the analyzed vertical velocity (ω):

$$\overline{\dot{Q}}(x, y, p, t) = \frac{\Delta T}{\Delta t} + \bar{\mathbf{v}} \cdot \nabla \bar{T} + \left(\frac{p}{p_0}\right)^\alpha \bar{\omega} \frac{\partial \bar{\theta}}{\partial p} + \left(\frac{p}{p_0}\right)^\alpha \left[\nabla \cdot \bar{\mathbf{v}}' \theta' + \frac{\partial (\bar{\omega}' \theta')}{\partial p} \right]$$

Here $\overline{\dot{Q}}(x, y, p, t)$ is the diagnosed monthly diabatic heating rate (in K/day), \mathbf{v} the horizontal wind vector, ω the pressure vertical velocity, and θ the potential temperature [$=T(p_0/p)^{R/C_p}$]. The over-bar denotes the monthly-mean and the prime denotes the deviation of the 6-hourly analysis from this mean (i.e., the transient component). The transient component thus represents both synoptic and low-frequency (but sub-monthly) fluctuations.

Heating diagnosis from the ERA-15 and NCEP reanalyses was reported in Nigam et al. (2000), where intercomparison of ENSO heating structure was the focus. The heating diagnosed using analyzed and the mass-balanced ω was very similar in the ERA-15 case. The ERA-40 diagnosis was thus undertaken with the archived ω , i.e., without any adjustments to this field. Except for the refined treatment of vector winds in the high polar latitudes, the diagnosis technique is identical to the earlier

ones.¹⁹

The ERA-40 heating is diagnosed at the resolution of its NCAR data archive, i.e., on a 2.5° global horizontal grid and 23 pressure levels ranging from 1000 to 1 hPa), for the 1957-2002 period. Heating intercomparisons, all for the 1979-93 common period, are on a 5° longitude by 2.5° latitude grid.

4.4 Heating intercomparisons

4.4.1 Zonal-mean

The integrated view – zonally and vertically – of the diabatic heating distribution is compared first, in Fig. 4.1. Shown is the full ERA-40 field (in black), along with its *departure* from NCEP and ERA-15 counterparts (in color). Both the January and July ERA-40 heating contain a tropical heating maximum, with the boreal summer maximum being particularly intense. In these maxima, resides the well-known Inter-Tropical Convergence Zone (ITCZ) – the ascending branch of the meridionally divergent Hadley Circulation. The ERA-40 departures are significant in both months but especially in July when they approach 50% of the full-field amplitude northward of the equator. The departures moreover mimic the full field structure (except in polar latitudes), indicating the diagnosed ERA-40 heating to be

¹⁹ The distinction between zonal and meridional wind is lost at the poles, where horizontal flow can only be meridional, dominated by the wave number-1 component. Zonal wind is thus set to zero and the meridional wind forced to be wave number-1 along the first off-polar grid row. In the earlier ERA-15 and NCEP heating diagnoses, the meridional wind was, incorrectly, set to zero instead, but with virtually no impact on heating estimates in the off- polar regions, as ascertained later.

notably strong, especially, in July when it is almost twice as large as NCEP heating.

The diagnoses are in greater accord in the winter subtropics, the Hadley Cell descent region. Diabatic cooling in this region – of radiative origin – is no less impressive, but again the ERA-40 fields are stronger in both hemispheres; and more equatorward focused as well. Further poleward, a secondary heating maximum is in evidence in the full fields, arising from the heat released along winter storm tracks. The ERA-40 and NCEP are in good agreement on this feature.

4.4.2 Zonal distribution

The heating distribution is, of course, far from being zonally uniform because of the presence of land-surface and SST variations, and orography. Surface inhomogeneities and their circulation influence organize heating, generating regional features such as the ITCZ, South Pacific Convergence Zone, Maritime Continent convection, Asian Monsoon heating, and the subtropical and eastern Pacific descent and cooling zones, among others. These heating features, in turn, exert profound impact on the atmospheric general circulation.

The January and July ERA-40 heating distributions are shown in Figs. 4.2 and 4.3, respectively; along with the deviations from other heating fields. The ERA-40 heating is substantially stronger over the Maritime Continent and the eastern Pacific and Atlantic ITCZs in winter, e.g., it is at least 50% larger than NCEP over the Maritime Continent. Consistent with stronger equatorial heating in most longitudes, ERA-40 exhibits stronger diabatic cooling in the off-equatorial latitudes, i.e., a

stronger Hadley Cell. The winter cooling over mid-latitude continents is however suppressed; notably, over North America. The Atlantic stormtrack also extends more northward (into the Davis Straits) in ERA-40; as evident from the difference map.

The July differences (Figs. 4.3b-c) exhibit some of the same biases, but with heightened amplitude in the deep tropics, especially in the central/eastern basins. The ERA-40 heating in these ITCZ sectors is almost twice as strong as NCEP's; with attendant off-equatorial cooling biases in the winter hemisphere. The heating bias over the Asian and American monsoon regions is weaker but of the opposite sign, e.g., the negative ERA-40 bias over the Indian subcontinent.

4.4.3 Hadley Circulation

The zonal-mean distribution of ERA-40 heating is shown in Fig. 4.4, along with differences from the NCEP structure. The meridionally divergent circulation, comprising of zonally averaged meridonal and vertical velocity, is also shown in the same panels, using vectors. The ERA-40 heating in the deep tropics is stronger, especially in July, as seen in the earlier plots. The departure from NCEP heating (right panels) – the ERA-40 excess – is confined to the region above the planetary boundary layer in the Northern Hemisphere (NH), where its distribution mimics the climatological heating profile. The ERA-40 Hadley cells are, of course, clearly and consistently stronger. The mid-latitude heating departures indicate ERA-40's stormtrack heating to be weaker in NH winter, but not at other times or in the other

hemisphere.

4.4.4 Walker Circulation

The October heating and divergent circulation is shown along the equator in the Pacific basin in Fig. 4.5. The divergent component of the zonal wind and negative- ω are plotted in the 5S-5N latitude band. The month of October is chosen as the SST contrast between the western and eastern basin is largest in this month; on account of the fully fledged SST cold-tongue in the eastern basin at this time. The divergent circulation is thus anticipated to be robust in this month. The ERA-40 plot shows one big clockwise cell over the Pacific – the Walker Circulation – with strong rising motion over the Maritime Continent and weak sinking across the central and eastern Pacific basin. Narrow counterclockwise cells are evident at both ends of this big cell: The west one arising from the east-west symmetry of the Maritime Continent outflow, and the east one from convection over equatorial South America, including Amazonia.

The ERA-40 Walker Circulation is stronger than NCEP's, as indicated by the clockwise cell in the western/central basin in the difference map. ERA-40's stronger divergent circulation is, of course, consistent with its previously noted heating strength over the Maritime Continent in both summer and winter. The related strengthening of low-level descent over the central and eastern basin must lead to a stronger trade inversion in ERA-40. The counterclockwise cell to the east is however

weaker in ERA-40, reflecting less intense convection over equatorial South America vis-à-vis NCEP reanalysis; as also in January (cf. Fig. 4.2b).

4.5 Tropical heating diagnosis: inference from precipitation

Diabatic heating obtained from the ERA-40 circulation is found to be stronger in the tropics in both January and July (cf. Figs. 4.2-3). As both global reanalyses are constrained by similar (if not the same) large-scale circulation observations, which of the two heating diagnoses should be considered more reasonable? The dynamical consistency of 3D diabatic heating and the large-scale circulation can be a basis for this choice, but the involved diagnostic modeling is not without its own caveats. Short of this exercise, a comparison of the heating structure and precipitation can be insightful, but only in regions where latent heating dominates, e.g., the monsoon region and the deep tropics. The CMAP-2 precipitation rate (mm/day) is converted into the vertically averaged heating rate (K/day) by multiplying the former by $(gL\rho_w 10^{-5})/[C_p(P_s-125)]$, where L is the latent heat of condensation (2.5×10^6 J/kg), g is gravity, ρ_w is the water density (10^3 kg/m³), C_p is the specific heat of air at constant pressure (1004 J/kg/K), and P_s is surface pressure in hPa.

The monsoon region intercomparison is shown first, in Fig. 4.6. A Hovmöller plot of vertically-averaged diabatic heating, additionally averaged across the eastern Indian subcontinent (80°E-100°E), is displayed at monthly resolution. The

comparison with precipitation is, of course, useful only in the rainy season.²⁰ More than amplitude, it is the monthly evolution of rainfall that provides discrimination between the competing heating diagnoses. From the perspective of northward migration of rainfall in the January-July period, the ERA-40 heating mimics CMAP rainfall evolution more closely than does NCEP; likewise for the monsoon retreat. The south-of-the-equator location of the convection center in the non-monsoon period is also more realistically captured in the ERA-40 based heating diagnosis. But the ERA-40 heating is a bit too strong, by ~ 0.5 mm/day ($\sim 15\%$) in the monsoon season, especially with respect to the CMAP-2 rainfall.

Heating evolution in the eastern tropical Pacific (140°W - 120°W) where heating diagnoses are far apart, especially in July (cf. Fig. 4.3b), is examined in Fig. 4.7. In this sector, the differences in diagnosed heating are not subtle and the choice of heating that is more in accord with observed precipitation (and large-scale circulation) is clear-cut; the ERA-40 based diagnosis. The CMAP-2 representation of the eastern Pacific ITCZ, including its northward summer migration and a hint of double-ITCZ structure in March-April, is mirrored in the ERA-40 heating structure. The heating amplitude however appears to be marginally excessive, as in the Indian monsoon sector.

²⁰ Precipitation, by virtue of being positive definite, is of little corroborative value in other seasons (and regions) when (where) radiative cooling is dominant; as in winter over the Indian subcontinent.

4.6 Heating vertical structure: intercomparison with TRMM profiles

The vertical distribution of heating is closely examined in the 1999-2001 period, when TRMM latent heating profiles are available as reference. The heating vertical structure is of some consequence in the tropics as circulation is sensitively dependent on the vertical gradient of heating (Q): The horizontal divergence ($-\partial\omega/\partial p$) is proportional to $\partial Q/\partial p$ in the Tropics, linking the divergent circulation directly, and the rotational circulation indirectly (through vortex stretching), with the vertical heating gradient. The heating vertical structure, to an extent, also reveals the convective-stratiform mix of precipitation, given the rather different characteristic heating profiles associated with the two convection processes (Houze 1997).

4.6.1 ITCZ heating

The heating vertical structure across boreal winter's ITCZ is examined first, in Fig.4.8. The latent heating estimate from the TRMM-*CSH* algorithm is shown along with NCEP-model latent heating (generated from 6-hour forecasts initialized by the reanalysis circulation) in the left panels. Residual diabatic heating from the ERA-40 reanalysis, which includes radiative and sensible components as well, is displayed in the top right panel, while its NCEP counterpart from model forecasts is in the bottom right one. The NCEP-model latent heating compares favorably with the TRMM estimate in the middle troposphere, with maximum heating ($\sim 3\text{K/day}$) at 400-500 hPa. Notable differences are however present at both upper and lower levels: The NCEP-

model latent (and total) heating, and even more, the diagnosed ERA-40 heating extend too far up in the vertical, to the tropopause; at variance with the TRMM-*CSH* structure. At lower levels, the NCEP-model latent heating contains a secondary maximum ($\sim 1.5\text{K/day}$) in the central and eastern basin, while there is no hint of such feature in TRMM heating.

A comparison of NCEP-model's latent and total diabatic heating suggests the presence of pervasive radiative cooling ($\sim 1\text{K/day}$), which lowers the heating maximum in the western basin (to $\sim 2\text{K/day}$), and leads to net cooling of the troposphere in the central/eastern basin; consistent with Johnson and Ciesielski's (2000) analysis of radiative cooling. The total model heating also does not contain the low-level structure present in latent heating, indicating offsets by the near-surface sensible heating and lower-troposphere radiative cooling. The ERA-40 residual heating differs from the NCEP-model total heating, principally, in the strength and vertical extent of the western basin heating maximum, with the ERA-40 one being stronger (by $\sim 1\text{K/day}$).

4.6.2 Regional heating profiles

The heating vertical structure is closely compared in Fig. 4.9 by plotting the vertical profiles in four regions (two continental, one maritime land, and one oceanic): Indian summer monsoon ($80^{\circ}\text{E}-90^{\circ}\text{E}$, $20^{\circ}\text{N}-25^{\circ}\text{N}$); South American convection ($55^{\circ}\text{W}-40^{\circ}\text{W}$, $20^{\circ}\text{S}-\text{EQ}$); Maritime Continent ($130^{\circ}\text{E}-155^{\circ}\text{E}$, $10^{\circ}\text{S}-\text{EQ}$);

and winter storm tracks over the Pacific (145°E - 175°E , 32.5°N - 35°N). The first region is marked on Fig. 4.3 while the other three are outlined in Fig. 4.2. Since local maxima in the ERA-40 heating field are a basis for the choice of regions, there is potential for an implicit bias towards the ERA-40 profile being the strongest in the following intercomparisons. In addition to TRMM and the diagnosed ERA-40 and NCEP profiles, the NCEP-model latent and total diabatic heating profiles are also shown. Note, TRMM provides a valuable reference but not, necessarily, the validation target in the tropical plots as it is itself produced, in part, from a model, albeit a cloud-resolving one; which is no less immune to parameterization deficiencies.

4.6.3 Indian Summer Monsoon

The Indian summer monsoon heating profiles are plotted in Fig. 4.9a. The diagnosed heating profiles (black and green) exhibit remarkable agreement. The TRMM-*CSH* latent heating profile (red) is broadly similar but weaker than diagnosed heating everywhere, especially in the lower troposphere and near the tropopause. Some of the difference could be attributed to the implicit inclusion of sensible and radiative heating in the diagnosed profiles, except that the TRMM-*CSH* profile is weaker. One normally expects total diabatic heating (e.g., residual heating) to be smaller than latent heating in the middle and upper troposphere in view of radiative cooling of the region (negative radiative heating). Such cooling is evident, for example, in the difference of NCEP-model's latent (thin dashed red) and total (thin

dashed green) heating profiles; a difference, in line with Johnson and Ciesielski's (2000) radiative cooling estimate. The intercomparisons indicate TRMM-*CSH* heating to be an underestimate (by up to 2K/day in the lower troposphere!) and/or the residual ERA-40 and NCEP heating to be overestimates.

The aforementioned discrepancy is serious enough to merit further analysis. For instance, is there independent data that can help assess the competing heating diagnoses? Although, assessment of the vertical structure is challenging, weighing in on the heating amplitude, especially, of vertically integrated heating, is not. In the deep tropics, where latent heating dominates, the heating integral should equal the heat released in vapor condensation (at the rate of surface precipitation). The integral constraint is powerful but only where surface precipitation is well measured. The summer monsoon rainfall region over the Indian subcontinent may be one such region, having sufficient station data (e.g., Rajeevan et al. 2006).

The vertically integrated heating is converted into precipitation units (mm/day) to facilitate comparison with various station and satellite-based surface precipitation estimates in Table 4.1. The estimates range from 5.86 mm/day (TRMM-*CSH*) to 12.90 mm/day (NCEP-model latent), with the ERA-40 and NCEP diagnosed heating based precipitation close to the upper end of the range (~12.2 mm/day); IMD rainfall is 12.5 mm/day, for reference. The large range results not from differences in the maximum heating rate (3.5-4.5K/day) but from the spread in upper and lower troposphere heating rates. The overlap of the diagnosed heating profiles is quite reassuring in this regard, but the lack of internal consistency between

the TRMM-*CSH* model based precipitation (5.86 mm/day) and the constraining TRMM precipitation retrievals – *3B43* (10.92 mm/day) and the experimental *3A12* (7.57 mm/day) – is worrisome. Station precipitation analyses over this part of the subcontinent are unfortunately not in accord either; with CRU (8.22) and IMD (12.50) estimates being ~50% apart. The 1979-2001 CRU and IMD summer rainfall climatologies do not exhibit such discrepancy, though.

The spread in station and satellite analyses notwithstanding, our assessment indicates the TRMM-*CSH* based precipitation estimate to be an outlier – on the low side – at least over this Indian subcontinent region. The conclusion is supported by TRMM’s own precipitation retrievals and station observations. It is presently unclear if the underestimation results from *CSH*-heating profile’s shape or weak amplitude (or both).

4.6.4 Maritime Continent

The heating vertical structure over the western end of the South Pacific Convergence Zone (SPCZ, cf. Fig. 4.2a) is examined in the top right panel of Fig. 4.9. Heating profiles are displayed in January when convection is most intense in this region (and over northern Australia, peak-phase of the Australian monsoon). The profiles are in remarkable agreement except for the ERA-40 one which is much too strong in the middle and lower troposphere. The Table-4.1 precipitation intercomparison supports this assessment: Satellite-based estimates are in the 7-9

mm/day range, i.e., just shy of the CRU station precipitation (9.18 mm/day). The precipitation rate implied by the residual ERA-40 heating profile, on the other hand, is 11.22 mm/day, i.e., about 25% larger. The diagnosed ERA-40 heating thus seems excessive and indicative of an overly strong divergent circulation in the deep tropics in ERA-40 reanalysis (see also Figs. 4.4a-b).

4.6.5 South American continent

Heating profiles over the major continental convection center in austral summer – eastern tropical South America – are shown in the bottom left panel of Fig. 4.9. One finds interesting parallels with the boreal summer continental convection case (Indian monsoon) examined earlier: Remarkable similarity of the ERA-40 and NCEP diagnosed heating profiles, with both being larger than TRMM-*CSH* heating at every level, but especially in the lower troposphere. The station and satellite precipitation analysis are in good agreement here, all being in the 6.79-7.52 mm/day range. The implied precipitation rate from the ERA-40 heating diagnosis also comes in at 7.70 mm/day. Against this backdrop of rare accord among observational estimates, the TRMM-*CSH* based precipitation rate (3.31 mm/day) stands out as; an outlier, on the low side (by up to 50%), much as in the Indian summer monsoon case.

4.6.6 Pacific winter stormtracks

Heating profiles in an oceanic mid-latitude region where winter precipitation is of stratiform origin are shown in Fig. 4.9d. The region stands out for exhibiting remarkable agreement not only amongst the diagnosed heating profiles but also between them and the NCEP-model total heating. The latter agreement, in particular, gives credence to the NCEP-model latent heating distribution, making it a reasonable target for the TRMM-*CSH* latent heating profile. The availability and credibility of NCEP's latent heating offers unique opportunities for assessing TRMM-*CSH* latent heating in the subtropics and mid-latitudes where surface precipitation cannot be used for evaluation of competing heating diagnoses; in view of substantial sensible and radiative heating contributions to total diabatic heating here. The very large difference (~100%) between the TRMM-*CSH* and NCEP-model latent heating is thus quite disconcerting.

4.7 Concluding remarks

Diabatic heating is a very influential but elusive quantity. It exerts a profound influence on the atmospheric general circulation, which in turn modulates the heating distribution. The heating vertical structure, in particular, is of some consequence for atmosphere-ocean interaction in the tropics and atmosphere-land-surface interactions in the subtropics. Diabatic heating is generated, principally, from the latent heat release during atmospheric convection. Modeling of convection, especially,

partitioning between convective and stratiform processes remains a formidable challenge, compromising diabatic heating estimates from atmospheric models (e.g., Nigam et al. 2000). Refined estimates of 3D heating presented here are based on consistency with the large-scale circulation, and should facilitate improvements in convection parameterizations.

Diabatic heating, interestingly, is not part of the publicly accessible ERA-40 data archive, despite its wide use in climate diagnostics. The diabatic heating generated during the reanalysis cycle, as part of the short-term bridging forecast, would be useful even though its consistency with the large-scale reanalysis circulation is not assured, given the influence of the physical parameterization schemes during the bridging forecast period. For these and other reasons, diabatic heating is residually diagnosed from the ERA-40 circulation and compared with heating distributions obtained similarly from the NCEP and ERA-15 reanalyses, and with the TRMM-*CSH* heating.

The present study is also motivated by the need to confront TRMM's diagnosis of latent heating structure, based on *local* retrievals of surface convective and stratiform rain rates and *local* convective and stratiform heating profiles from the Goddard cumulus ensemble model, with the heating vertical structure based on *large-scale* circulation (assimilated in reanalysis); evaluating both in the process.

It is found:

- ERA-40 residual heating in the tropics to be stronger than NCEP's (and ERA-

15), especially, in July when its zonal-vertical average is twice as large. The bias relative to NCEP is strongest over the Maritime Continent in January and over the eastern basins and Africa in July; and reflected in the vigor of the divergent Hadley and Walker circulations, and in enhanced diabatic cooling of the off-equatorial descent regions.

- Another notable bias relative to NCEP is the suppressed winter cooling of the mid-latitude continents in the ERA-40 residual heating, by $\sim 0.5\text{K/day}$.
- Comparison of seasonal precipitation and vertically-averaged heating evolutions shows ERA-40 heating to be much more realistic than NCEP's over the eastern tropical Pacific, albeit a bit excessive.

The ERA-40 and NCEP residual heating profiles are finally compared with the TRMM-*CSH* latent heating profile and NCEP-model heating profiles in four regions of heavy precipitation: Indian summer monsoon, South American convection, Maritime Continent, and winter storm tracks over the north Pacific. Intercomparison of precipitation estimates from heating-profile integrals, and station and satellite analyses during the overlapping data period (1999-2001) provides a basis for assessment of the heating products (cf. Table-4.1); assuming confidence in the station precipitation data sets. It is found:

- TRMM-*CSH* latent heating to be generally weak, by as much as a factor of 2; a low-side outlier among 9 precipitation estimates in three of the four analyzed regions.
- Vertical integral of the *CSH* latent heating profile in the tropics to be

inconsistent with the TRMM rainfall retrievals constraining the *CSH* algorithm (e.g., the *3B43* analysis).

More regionally and specifically, it is found:

- Monsoon heating profiles over eastern India to be remarkably similar in the ERA-40 and NCEP residual diagnoses, with vertically integrated heating of ~ 12 mm/day. The TRMM profile is weak at all levels, with a ~ 6 mm/day integral. Station analyses, unfortunately, have large spread: ~ 8 mm/day (CRU) and ~ 12 mm/day (IMD); with CMAP-2 in between (~ 10.5 mm/day). The station-satellite spread notwithstanding, TRMM-*CSH* heating is strongly underestimated, and the ERA-40 and NCEP residual heating fairly accurate here.
- The Maritime Continent heating profile in NCEP's residual diagnosis and TRMM-*CSH* heating to be quite similar, with vertical integrals of ~ 5 mm/day. The ERA-40 residual heating is almost twice as strong here, with an integral of ~ 11 mm/day. Comparison with CRU and CMAP-2 rainfall (both ~ 9 mm/day) however shows ERA-40 heating to be excessive and TRMM-*CSH* heating to be too weak.
- Diagnosed heating profiles over eastern tropical South America to be in remarkable agreement, much as over eastern India. The implied rainfall (~ 8 mm/day) is moreover in agreement with the station-satellite rainfall estimates (~ 7 mm/day). Against this backdrop of rare accord, the TRMM-*CSH* heating integral stands out, at 3.3 mm/day, i.e., 50% smaller; with the profile amplitude,

rather than shape, being the cause of the discrepancy.

The TRMM-*CSH* algorithm clearly needs to be evaluated more thoroughly, across more regions and seasons. The evaluation must include close intercomparisons with 3D diabatic heating diagnosed from the *large-scale* circulation (the component assimilated in current global reanalysis); and new station precipitation data over the oceans, e.g., the TOGA-TAO array rainfall measurements in the eastern tropical Pacific.

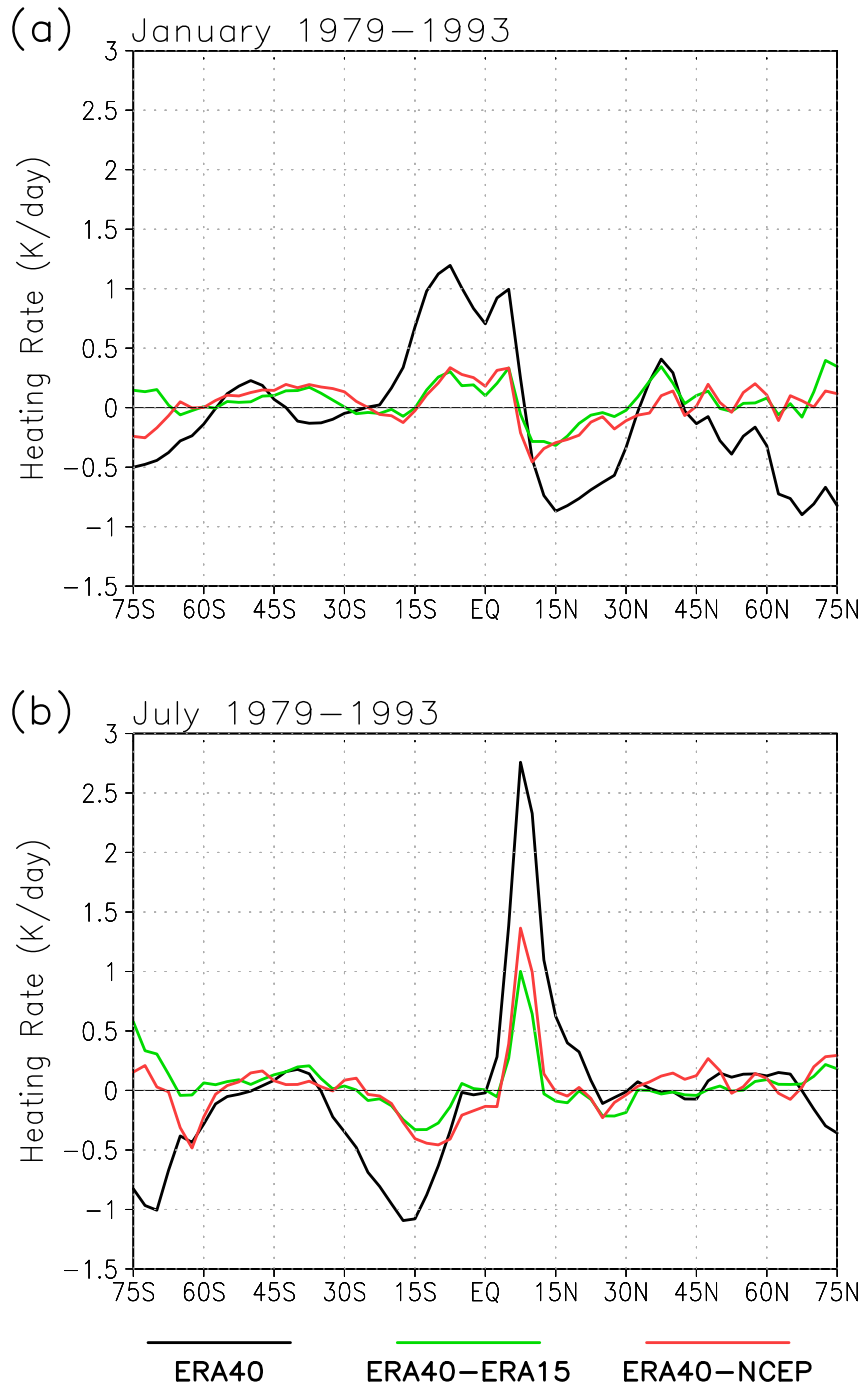


Figure 4.1: Zonally and vertically averaged ERA-40 diabatic heating in January (top) and July (bottom) in the 1979-1993 period climatology. Heating is residually diagnosed and the surface-to-125 hPa vertical average is mass-weighted. ERA-40's departure from the NCEP (red) and ERA-15 (green) diagnosed heating is also shown.

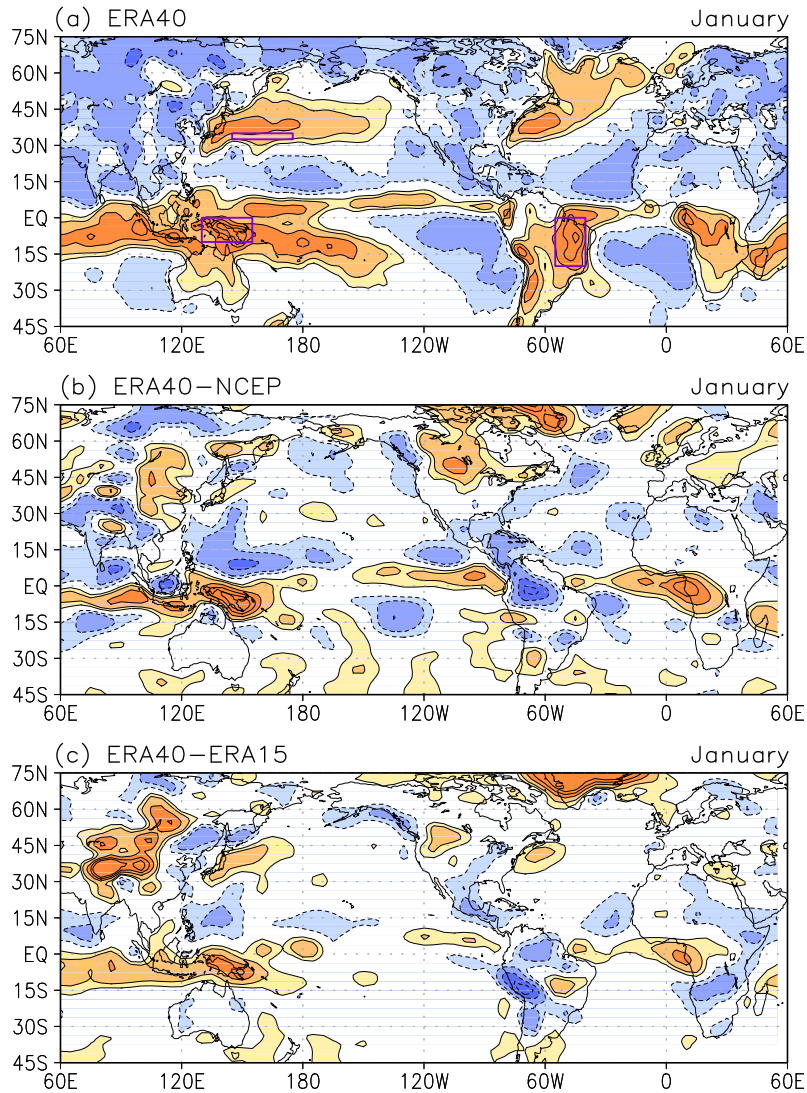


Figure 4.2: Vertically-averaged ERA-40 diabatic heating in January in the 1979-1993 period climatology (top panel). Heating is residually diagnosed and the surface-to-125 hPa vertical average is mass-weighted. ERA-40's departure from the NCEP and ERA-15 diagnosed heating are shown in the middle and bottom panels, respectively. The ERA-40 heating (top panel) is shown using the ± 0.5 , ± 1.0 , ± 2.0 , ± 3.0 , and ± 4.0 K/day contours, while its *departure* is contoured at *half* these levels. Red (blue) color indicates the diabatic heating (cooling) region. The zero-contour is omitted in all panels.

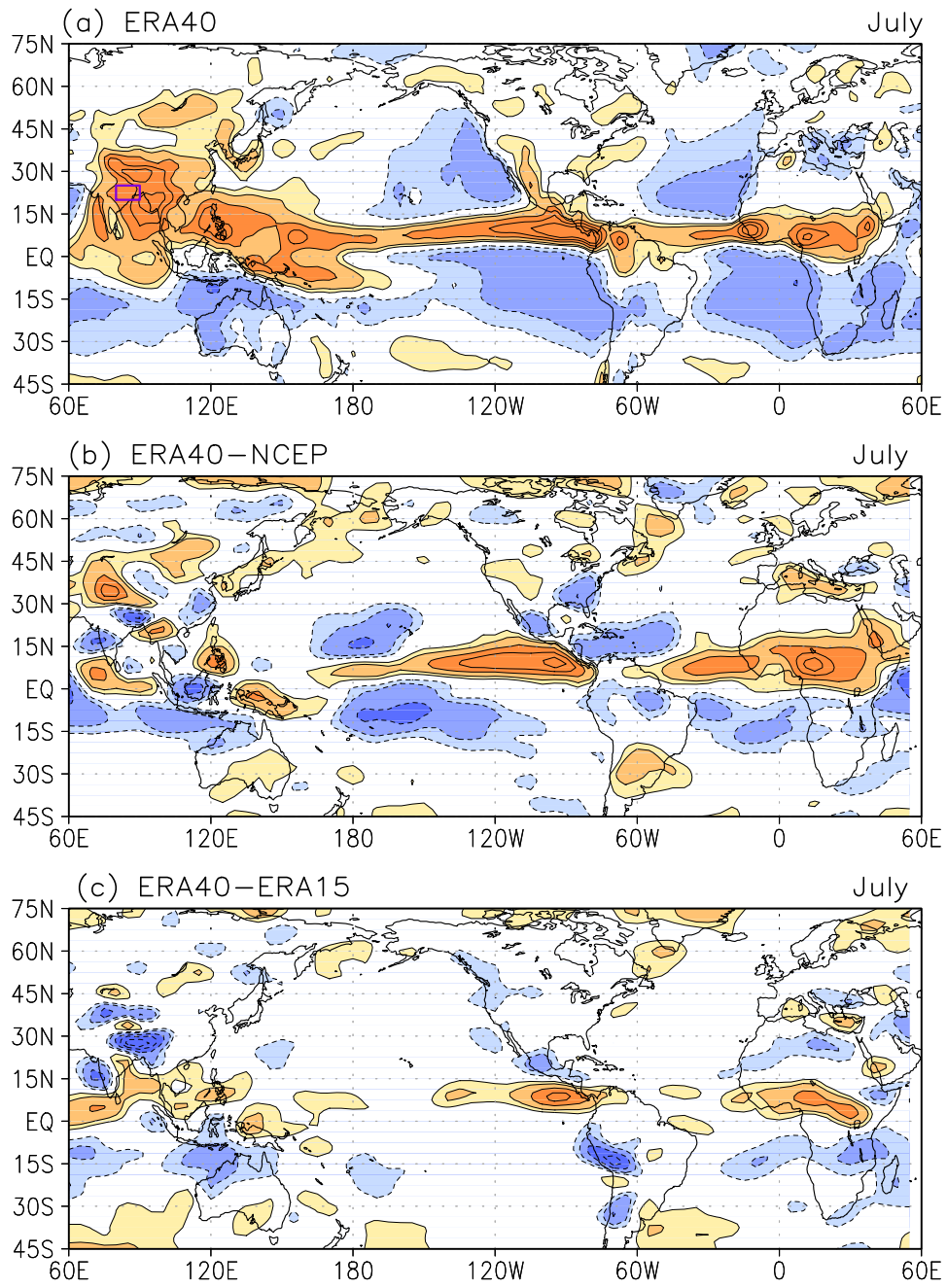


Figure 4.3: As in Figure 4.2, but for July.

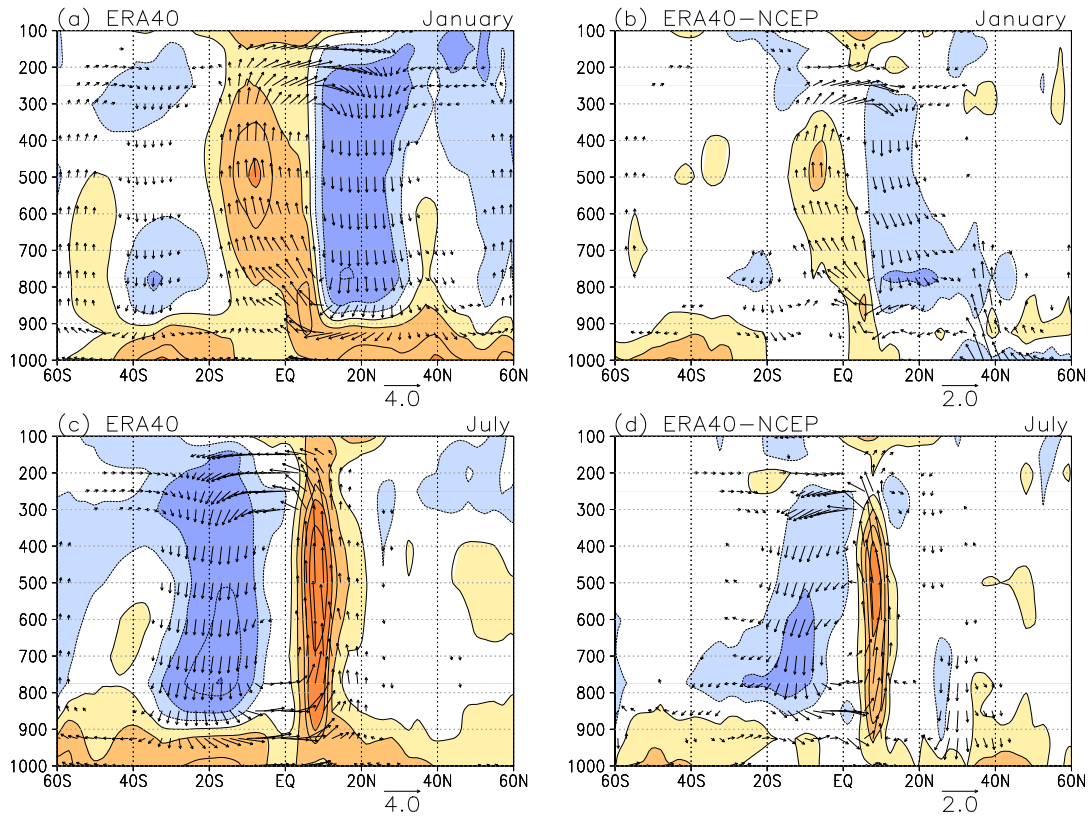


Figure 4.4: Zonally-averaged diabatic heating and the Hadley Circulation in the ERA-40 reanalysis in January (panel *a*) and July (panel *c*), based on the 1979-1993 period climatology. The ERA-40 departures from the corresponding NCEP fields are shown in the right panels. Residual diabatic heating is contoured and shaded at the ± 0.25 , ± 0.75 , ± 1.5 , ± 2.0 , and ± 3.0 K/day levels. Red (blue) color indicates the heating (cooling) region. The Hadley Circulation [zonal-mean v (m/s) and $-\omega$ (Pa/min)] is displayed using vectors with the indicated scale; vectors smaller than 10% of the scale are not plotted. Note, vector-scale for departures is half that of the full fields.

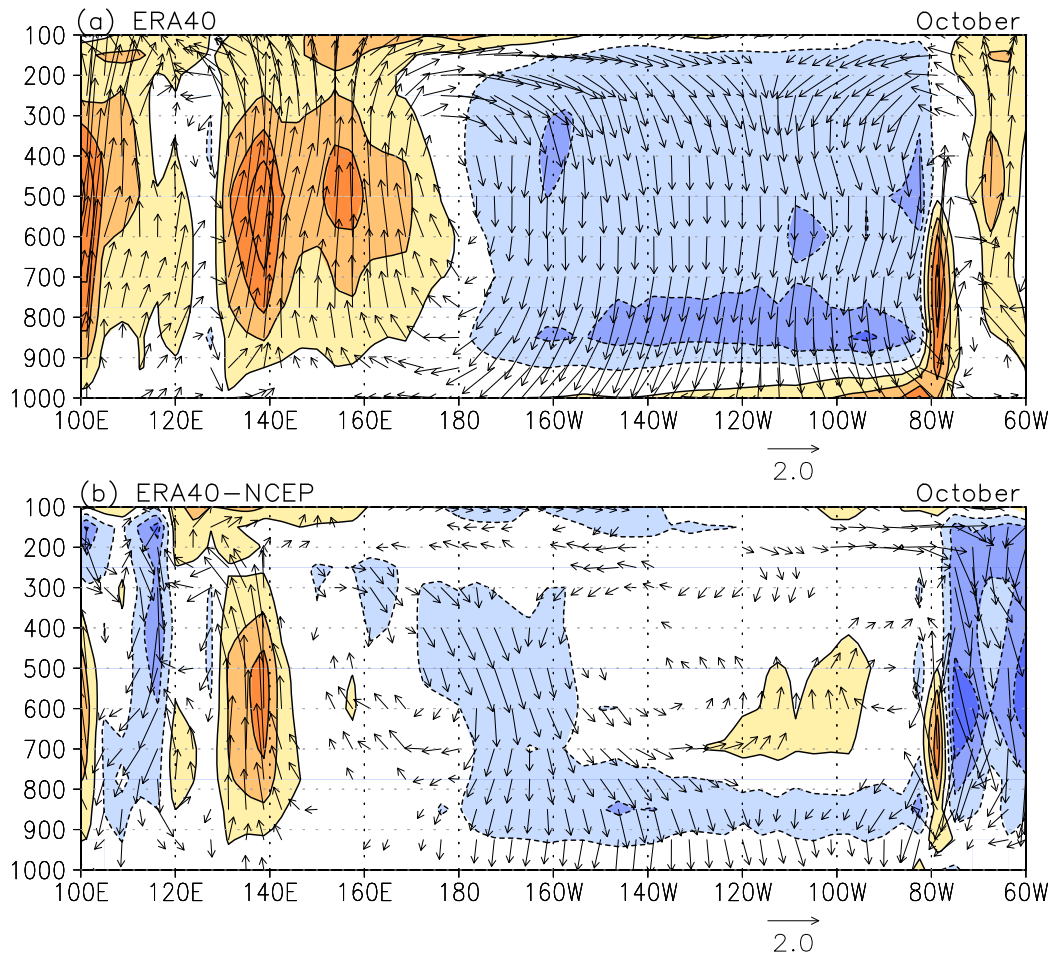


Figure 4.5: Diabatic heating and the Walker Circulation in the ERA-40 reanalysis in October, based on the 1979-1993 period climatology. The 5S-5N latitudinal average is plotted in the calendar month of heightened zonal SST-contrast, i.e., when the SST cold-tongue is fully fledged. ERA-40 departures from the corresponding NCEP fields are shown in the bottom panel. Residual diabatic heating is contoured and shaded at the for ± 0.5 , ± 1.5 , ± 2.5 , ± 3.5 , and ± 4.5 K/day levels. Red (blue) color indicates the heating (cooling) region, as before. The Walker Circulation [divergent zonal wind (m/s) and $-\omega$ (Pa/min)] is displayed using vectors with the indicated scale; vectors smaller than 20% of the scale are not plotted.

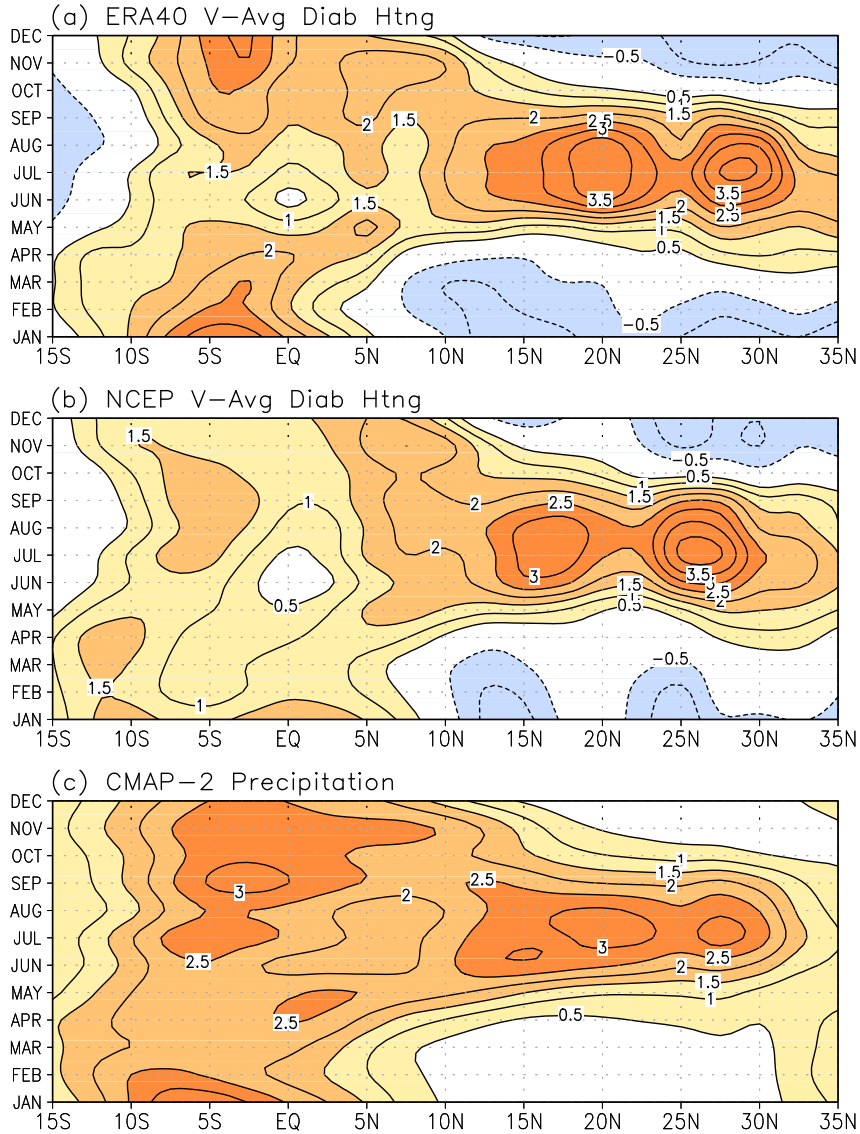


Figure 4.6: Seasonal evolution of diabatic heating and precipitation in the Indian subcontinent sector (80E-100E), in the 1979-2002 climatology: Heating is residually diagnosed from global reanalyses and the mass-weighted surface-to-125 hPa vertical average is shown in panels (a) ERA-40, and (b) NCEP. Panel c displays CMAP-2 precipitation, after its conversion into latent heating units. The contour interval and shading threshold is 0.5 K/day and the zero-contour is omitted in all panels. Note, negative contours are present in upper panels as radiative (and sensible) heating is included there, on account of residual estimation.

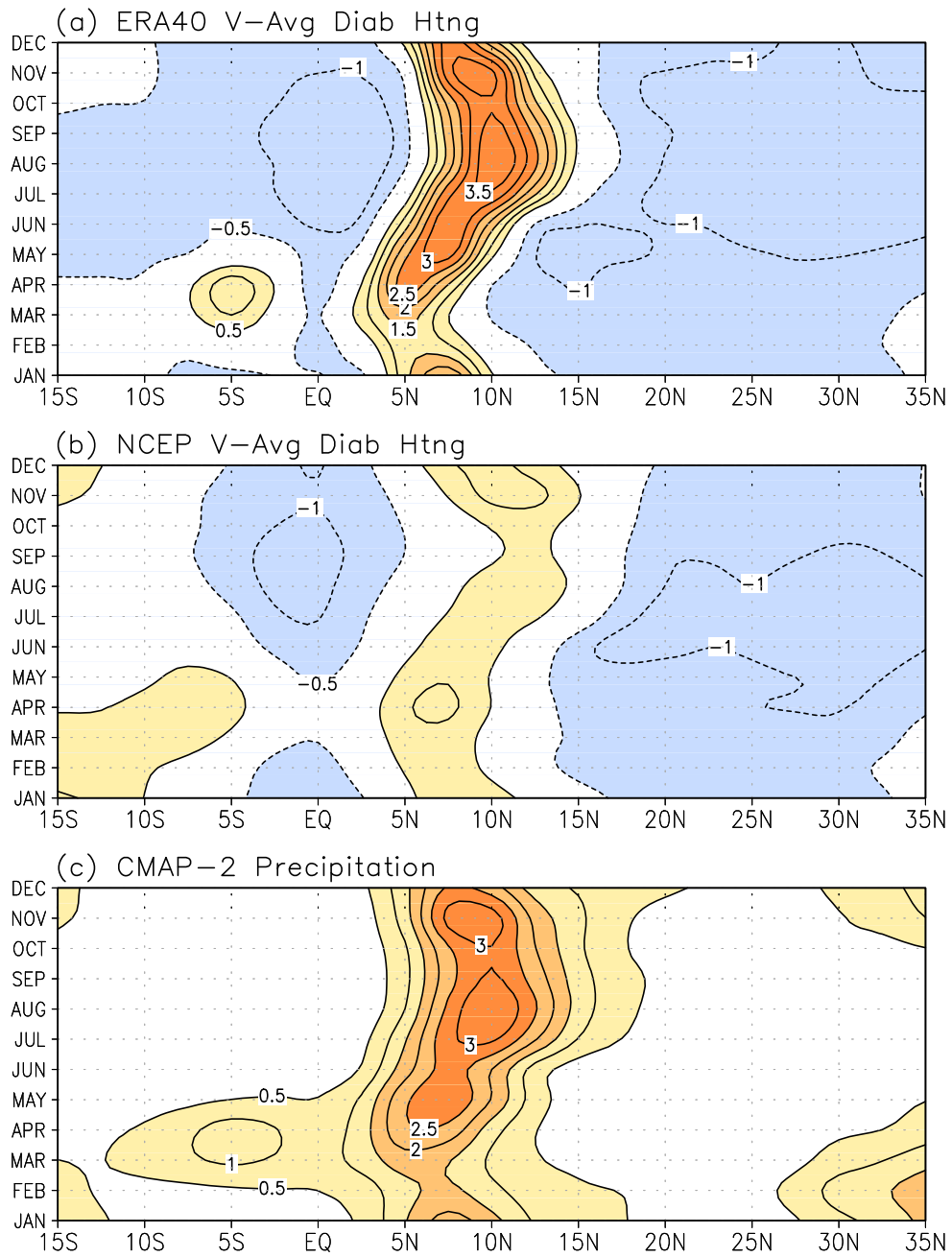


Figure 4.7: As in Figure 4.6 but for the eastern Pacific sector (140W-120W).

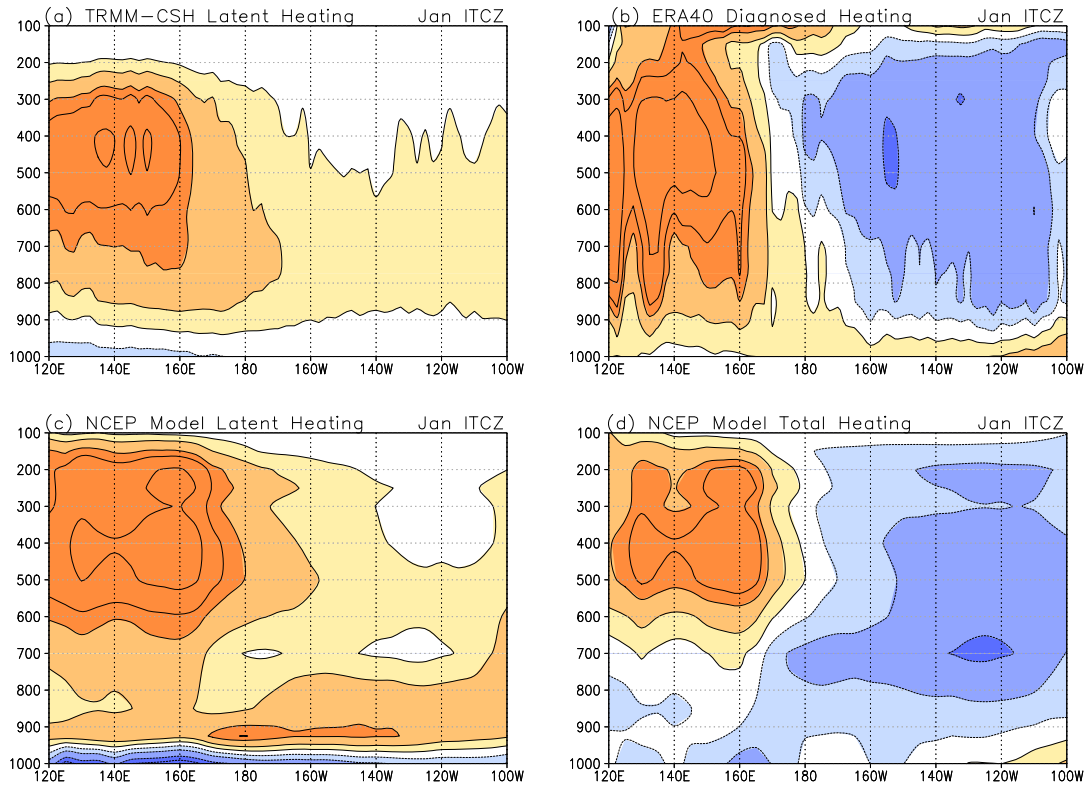


Figure 4.8: Heating vertical structure in the Inter-Tropical Convergence Zone, based on 3-year climatology (1999-2001); the overlapping data period. The EQ-5N latitudinal average in January is displayed, with latent heating in the left panels and total diabatic heating in the right ones: (a) TRMM-CSH latent heating, (b) ERA-40 diabatic heating (diagnosed), (c) NCEP latent heating (model), (d) NCEP diabatic heating (model). Heating is contoured and shaded at ± 0.25 , ± 0.75 , ± 1.5 , ± 2.0 , and ± 3.0 K/day levels, with the zero-contour omitted, as before. Red (blue) color indicates the heating (cooling) region.

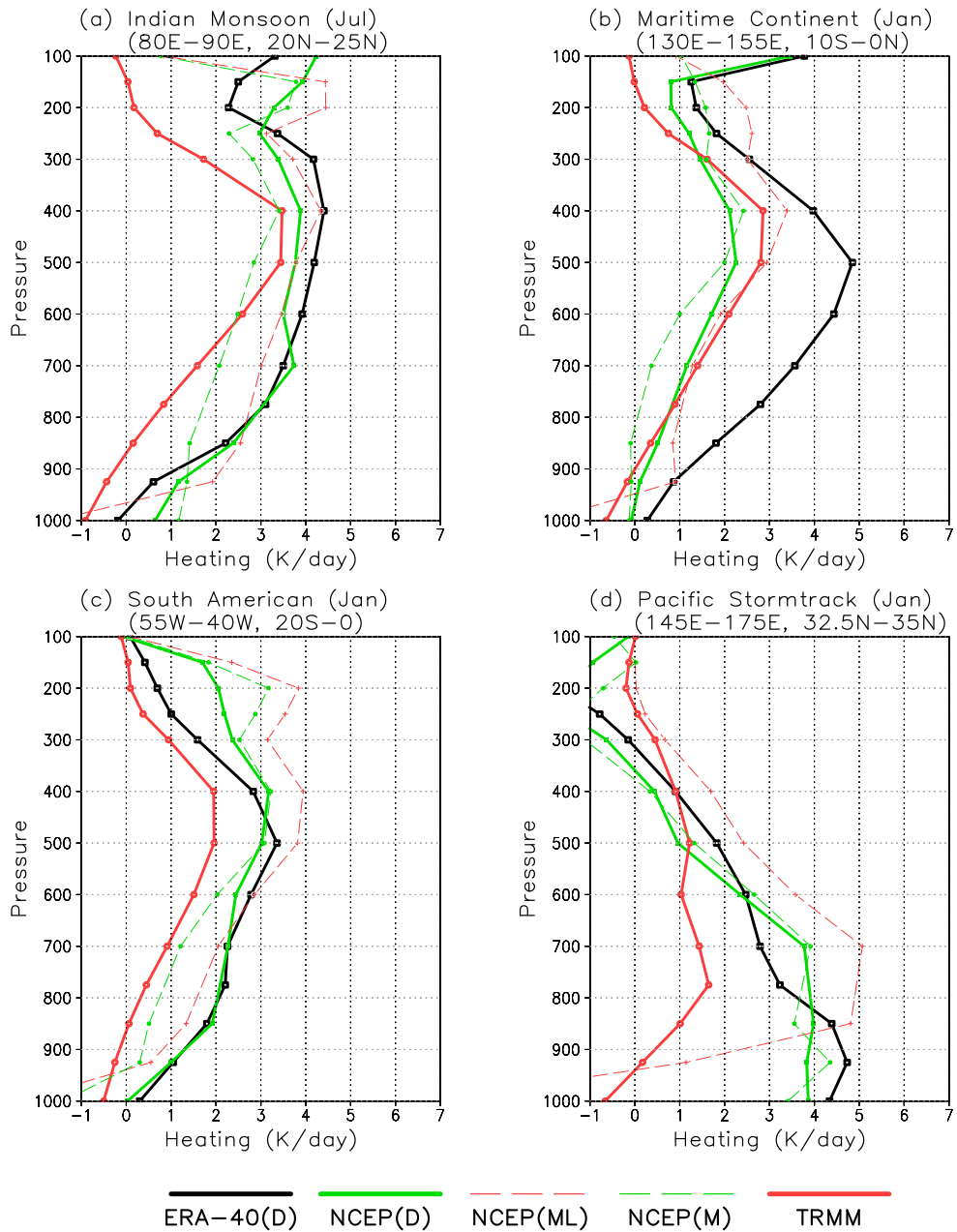


Figure 4.9: Diabatic heating profiles in selected region, marked in figures 2-3: (a) Indian summer monsoon (July, land box); (b) Maritime Continent (January, land box); (c) South American continent (January, land box); and (d) Pacific winter storm tracks (January, oceanic box). Five profiles are shown in each case: Diagnosed ERA-40 (thick black) and NCEP (thick green) heating; NCEP model latent (thin red dashed) and total diabatic (thin green dashed) heating; and the TRMM-CSH latent heating profile (thick red).

	<i>Diagnosed Total Diabatic Heating</i>		<i>Influenced by model and/or satellite data</i>						<i>Land Stations</i>	
	ERA-40	NCEP	TRMM CSH	NCEP Model Total	NCEP Model Latent	CMAP V2	TRMM 3B43	TRMM 3A12	CRU	IMD
IND 80-90E 20-25N	12.3	12.2	5.86	9.47	12.9	10.7	10.9	7.57	8.22	12.5
Mari. Cont. 130-155E 10S-EQ	11.2	4.84	5.15	4.14	7.74	9.17	8.09	7.10	9.18	X
S. Amer. 55-40W 20S-EQ	7.70	8.69	3.31	7.45	10.1	6.79	6.83	6.98	7.52	X
Pac. STrack 145-175E 32.5-35N	7.69	6.97	2.88	7.40	8.33	5.58	6.37	5.01	X	X

Table 4.1: Estimated Precipitation in four geographical regions. Estimates (mm/day) are obtained from (a) the vertical integral of diagnosed heating profiles, (b) cloud-ensemble simulations and global model forecasts, (c) satellite observations, and (d) station data. The smallest estimate for each region is indicated in red.

Chapter 5:

Conclusions

The objective of this piece of thesis research is to gain further understanding to the North Pacific sea-level pressure seasonal evolution. This is done by both analyzing ERA-40 climatologies and linear diagnostic model simulations. The two key North Pacific SLP issues that are raised and attempted to answer are:

- There is a disagreement between the seasonal evolutions of the North Pacific and Atlantic subtropical SLP anti-cyclone and the zonal-mean meridional divergent circulation.
- Observed North Pacific and Atlantic SLP seasonal cycles are largest in the mid-latitudes poleward beyond the Tropic of Cancer.

The above two questions evolves around the seasonal forcing of stationary waves and the general circulation by climatological diabatic heating and transient fluxes. The forcing mechanisms are diagnosed using a linear diagnostic model. The ERA-40 diabatic heating is diagnosed to force the diagnostic model, and is also intercompared with other independent estimates of diabatic and latent heating.

5.1 Key findings

5.1.1 Findings in the observed subtropical anti-cyclone seasonality (chapter two)

Chapter two focuses on the ERA-40 climatological subtropical high seasonalities in both Northern and Southern Hemispheres. The analysis has yielded the following key findings:

- The largest ERA-40 North Pacific and Atlantic SLP seasonality is found in the mid-latitudes and sub-polar latitudes with SLP reaches maximum in the boreal summer.
- The subtropical North Pacific and Atlantic SLP seasonality is relatively small, and SLP tends to peak in the boreal spring. That is inconsistent with both the zonal mean Hadley Cell and continental monsoon seasonal cycles.
- The Southern Hemisphere subtropical anti-cyclones mature in late austral winter, and develop toward the tropics; that is unlike the North Pacific/Atlantic highs, which develop poleward. The close seasonal timing of the Northern and Southern Hemisphere subtropical SLP highs maturation are not consistent with zonal mean Hadley Cell dynamics.
- The continental monsoon seasonal cycle plays a key role in the Northern Hemisphere zonal-mean SLP seasonal cycle with intense SLP lows over the monsoon regions.

The results question the accuracy of the traditional zonal moist ascent description to the ITCZ. The boreal summer Northern Hemisphere Hadley ascent is dominated by zonal asymmetric forcings and waves. The zonal interpretation of the Northern Hemisphere ITCZ ascent is questioned independently in Dima and Wallace (2003). Privé and Plumb (2007) have shown that asymmetric continental heat source

distorts the classical zonal ITCZ model. Our analysis shows that Northern Hemisphere stationary eddies play an important role in the zonal-mean ITCZ forcing.

Results in chapter two also call into question that the Pacific and Bermuda/Azores Highs development is driven by deep latent heating. The large SLP seasonality in the mid-latitudes is often associated with the growth and decay of the winter stormtracks. Due to the complexity of the stationary waves forcing, models are needed to ascertain and diagnose the forcing mechanisms. That forms the motivation for chapter three.

5.1.2 Findings in the North Pacific SLP modeling (chapter three)

Chapter three diagnoses the mechanisms that are behind the observed SLP seasonality. This is done by using a linear diagnostic model, which is prescribed with ERA-40 zonal means and asymmetric forcings. The current modeling literature argues that continental monsoon heating is the primary mechanism in PH development, which contradicts with the evidences that are presented in chapter two.

The diagnostic linear model seasonal cycle is comparable with the observations. Previous similar studies focus on mature phase features. Chapter three's key difference with similar studies is the focus on seasonal change rather than mature features.

The key chapter three findings are:

- As consistent with the literature, the JJA Asian/Pacific Monsoon forcing leads

to a downstream SLP ridge. The American heat source forces an upstream SLP ridge to the northwest, but the overall American response is weak compare to the Asian/Pacific Monsoon forced downstream response.

- JJA East Pacific forcing serves as an important cancellation to the Asian/Pacific Monsoon forced subtropical ridge.
- The mid-latitude and subtropical Northeast Pacific diabatic cooling is found to be a major contributor (exceeding the contribution from the Asian/Pacific Monsoon) to mid-latitude JJA North Pacific SLP development.
- The winter Pacific stormtrack forces a SLP low over the mid-latitudes. During the annual seasonal cycle, the mid-latitudes changes from a winter stormtrack regime to a summer radiative cooling regime. Such forcing changes lead to an increase of extra-tropical SLP from boreal winter to summer – the dominant mode of the modeled annual North Pacific SLP seasonality.
- Pacific ITCZ influence to the extra-tropical North Pacific SLP is limited to the boreal winter; the Pacific ITCZ footprint to the North Pacific SLP seasonality is the reduced influence during the boreal summer. Such reduction of influence is consistent with increased zonal-mean upper troposphere easterlies.

The zonal-mean basic state assumption is a questionable representation of the large-scale tropical winds during JJA. It is not possible here to ascertain the role of the Tropical Westerly Duct in PH forcing. The reasonable agreement between the modeled and ERA-40 North Pacific climatologies implies the discrepancy due to the Tropical Westerly Duct is possibly small.

The presented results downplay both the downstream and upstream monsoon forcings to Northern Pacific SLP seasonality. However, they may still be important in triggering cloud-radiative feedbacks. It is shown clearly that extra-tropical (radiative) cooling is important in forcing the North Pacific SLP seasonality. The model used here is time-independent, and cannot be used to investigate any feedback mechanisms.

5.1.3 Findings in the diabatic heating intercomparison (chapter four)

The ERA-40 diabatic heating (and transient) diagnoses are required to complete the modeling diagnosis in chapter three. The ERA-40 dataset is, of course, one of the state-of-the-art products of its kind, and an independent examination of its thermodynamics and large-scale circulation is of great interest. A major challenge itself is a proper definition of a “control” to compare with; in practice, the best available other comparisons are other remote sensing and reanalyses data, which are just as controversial as ERA-40 itself.

The major findings in chapter four are:

- The ERA-40 Hadley and Walker Circulations are too intense. The zonal-mean vertical integrated JJA ERA-40 ITCZ diabatic heating is nearly twice of NCEP Reanalysis. The stronger ERA-40 ITCZ is compensated with enhanced zonal-mean cooling in the winter subtropics.
- The deep heating and ascent over the Maritime Continent is too strong compare to all other compared independent estimates.

- Despite of the excessive ERA-40 ITCZ diabatic heating, ERA-40 captures the East Pacific Warm Pool/ITCZ diabatic heating seasonal cycle significantly better than the NCEP Reanalysis.
- TRMM CSH tropical latent heat appears to be too weak, and shows significant differences even with other TRMM products. Most TRMM CSH errors appears to be caused by insufficient upper and lower tropospheric latent heating in deep convective zones, and inability to handle shallow latent heating.

The differences between ERA-15 and ERA-40 are discerning as ERA-40 is supposed to be the successor to ERA-15. The numerous updates from ERA-15 to ERA-40 are significant enough to significantly strengthen the Hadley Cell (as much as doubling the vertical integrated ITCZ heating) – one of the most important features in the general circulation.

TRMM latent heating diagnoses is an ongoing project (Tao et al. 2006, Tao et al. 2007). The lower troposphere latent heating differences are not of surprise; CSH algorithm requires net surface precipitation to produce latent heating. Shallow convection is often associated with non- or weakly precipitation clouds, which the CSH algorithm is not designed to handle. Upper troposphere latent heating tends to be associated with stratiform precipitation bands in deep convective clouds (Houze 1997). Is the stratiform heating and precipitation being underestimated by CSH? The publicly available CSH latent heating data does not provide the division between stratiform and convective latent heating.

5.2 Final Words

This piece of research has touched on subjects beyond boreal summer subtropical SLP ridge forcing. Seasonal cycles of the Hadley Cell and mid-latitudes, the thermodynamics of reanalyses, and the remote sensing of latent heating are all touched here. All covered topics are fundamental questions to the general circulation. The diabatic heating estimation is a historical difficult topic in atmospheric science. Unlike diabatic heating, it is more a surprise that subtropical anticyclones – one of the most prominent climatological features – have been overlooked for such a long time.

This research is not possible without the assistance of the superior guidance and support from the University of Maryland Department of Atmospheric and Oceanic Sciences faculty members, staffs, and graduate students. I personally thank you for reading this, and I hope this thesis is a step forward for the Earth System Sciences.

Bibliography

- Andersson, E., and Coauthors, 2005: Assimilation and modeling of the atmospheric hydrological cycle in the ECMWF forecasting system. *Bull. Amer. Meteor. Soc.*, **86**, 387-402.
- Bergeron, T., 1930: Richlinien einer dynamischen klimatologie. *Met. Zeit.*, **47**, 246-262.
- Bjerknes, J., 1935: La circulation atmosphérique dans les latitudes sous-tropicales. *Scientia*, **57**, 114-123.
- Bjerknes, V., 1937: Application of Line Integral Theorems to Hydrodynamics of Terrestrial and Cosmic Vortices. *Astrophysica Norvegica*, **2**.
- Charney, J. G., and A. Eliassen, 1949: A numerical method for predicting the perturbations of the middle latitude westerlies. *Tellus*, **1**, 38-54.
- Chan, S., and S. Nigam, 2008: Residue diagnosis of diabatic heating from ERA-40 and NCEP reanalyses: intercomparison with TRMM. *J. Climate*, submitted.
- Chen, P., M. P. Hoerling, and R. M. Dole, 2001: The Origin of the Subtropical Anticyclones. *J. Atmos. Sci.*, **58**, 1827-1835.
- Dima, I. M., and J. M. Wallace, 2003: On the seasonality of the Hadley Cell. *J. Atmos. Sci.*, **60**, 1522-1527.
- Ebisuzaki, W., 1996: Consistency of the diabatic heating in the NMC/NCAR Reanalysis. *Proceeding for 20th Climate Diagnostic Workshop* (ref#: PB96-168646), 232-234.
- Gibson, J. K., P. Kållberg, S. Uppala, A. Hernandez, A. Nomura, and E. Serrano, 1997: ERA-15 Description. ERA-15 Project Report Series, No. 1, 84 pp.
- Held, I. M., and A. Y. Hou, 1980: Nonlinear Axially Symmetric Circulations in a Nearly Inviscid Atmosphere. *J. Atmos. Sci.*, **37**, 515-533.
- Holopainen, E. and C. Fortelius, 1986: Accuracy of estimates of atmospheric large-scale energy flux divergence. *Mon. Wea. Rev.*, **114**, 1910-1921.
- Hoskins, B. J., 1996: On the Existence and Strength of the Summer Subtropical Anticyclones. *Bull. Amer. Meteor. Soc.*, **77**, 1287-1291.
- ___, and D. J. Karoly, 1981: The Steady Linear Response of a Spherical Atmosphere to Thermal and Orographic Forcing. *J. Atmos. Sci.*, **38**, 1179-1196.

- ___, and P. D. Sardeshmukh, 1987: Transient eddies and the seasonal mean rotational flow. *J. Atmos. Sci.*, **44**, 328-338.
- ___, and P. J. Valdes, 1990: On the Existence of Storm-Tracks. *J. Atmos. Sci.*, **47**, 1854-1864.
- ___, and___, 2002: New perspectives on Northern Hemisphere winter storm tracks. *J. Atmos. Sci.*, **59**, 1041-1061.
- ___, and___, 2005: A new perspective on Southern Hemisphere storm tracks. *J. Climate*, **18**, 4108-4129.
- ___, H. H. Hsu, I. N. James, M. Masutani, P. D. Sardeshmukh, and G. H. White, 1989: Diagnostics of the global atmospheric circulation based on ECMWF analyses 1979-1989. WCRP-27; WMO/TD-No. 326, 217pp.
- Houze, R. A., 1997: Stratiform precipitation in regions of convection: A meteorological paradox. *Bull. Amer. Meteor. Soc.*, **78**, 2179-2196.
- James, I. N., 1995: *Introduction to Circulating Atmospheres*. Cambridge University Press, 422 pp.
- Johnson R. H., and P. E. Ciesielski, 2000: Rainfall and radiative heating rates from TOGA COARE atmospheric budgets. *J. Atmos. Sci.*, **57**, 1497-1514.
- Källberg, P., and Coauthors, 2005: ERA-40 Atlas. ERA-40 Project Report Series No. 19. 191pp. http://www.ecmwf.int/research/era/ERA-40_Atlas/docs/index.html
- Kalnay, E., and Coauthors, 1996: The NCEP/NCAR 40-Year Reanalysis Project. *Bull. Amer. Meteor. Soc.*, **77**, 437-471.
- Karoly, D. J., and B. J. Hoskins, 1982: Three dimensional propagation of planetary wave. *J. Meteor. Soc. Japan.*, **60**, 109-123,
- Klein, S. A., 1997: Synoptic variability of low-cloud properties and meteorological parameters in the subtropical trade wind boundary layer. *J. Climate*, **10**, 2018-2039.
- Krishnamurti, T. N., and H. N. Bhalme, 1976: Oscillations of a monsoon system. Part I. Observational aspects. *J. Atmos. Sci.*, **33**, 1937-1954.
- Lahey, J. I., R. A. Bryson, E. W. Wahl, 1958: *Atlas of Five-day Normal Sea-level Pressure Charts for the Northern Hemisphere*. University of Wisconsin Press, 75 pp.

- Lamb, H. H., and A. I. Johnson, 1959: Investigations of long series of observations and circulation changes in January. *Geografiska Annaler*, **41**, 104-134.
- Lindzen, R. S., and A. V. Hou, 1988: Hadley Circulations for Zonally Averaged Heating Centered off the Equator. *J. Atmos. Sci.*, **45**, 2486-2522.
- Liu, Y., G. Wu, and R. Ren, 2004: Relationship between the Subtropical Anticyclone and Diabatic Heating. *J. Clim.*, **17**, 682-698.
- Mesinger, F., and Coauthors, 2006: North American Regional Reanalysis. *Bull. Amer. Meteor. Soc.*, **87**, 343-360.
- Mitchell, T. D, and P. D. Jones, 2005: An improved method of constructing database of monthly climate observations and associated high-resolution grids. *Int. J. Climatol.*, **25**, 693-712.
- Miyasaka, T., and H. Nakamura, 2005: Structure and formation mechanisms of the northern hemisphere summertime subtropical highs. *J. Climate*, **18**, 5046-5065.
- Nigam, S., 1983: On the Structure and Forcing of Tropospheric Stationary Waves. Ph.D. dissertation, Princeton University, 203 pp.
- ___, 1994: On the dynamical basis for the Asian summer monsoon rainfall—El Niño relationship. *J. Climate*, **7**, 1750-1771.
- ___, 1997: The annual warm to cold phase transition in eastern equatorial Pacific: Diagnosis of the role of stratus cloud-top cooling. *J. Climate*, **10**, 2447-2467.
- ___, and R. S. Lindzen, 1989: The sensitivity of stationary waves to variations in the basic state zone flow. *J. Atmos. Sci.*, **12**, 1746-1768.
- ___, and A. Ruiz-Barradas, 2006: Seasonal hydroclimate variability over North America in global and regional reanalyses and AMIP simulations: Varied Representation. *J. Climate*, **19**, 815-837.
- ___, and S. Chan, 2008: On the summertime strengthening of the Northern Hemisphere Pacific sea-level pressure anticyclone. *J. Climate*, submitted.
- ___, C. Chung, and E. DeWeaver, 2000: ENSO diabatic heating in ECMWF and NCEP reanalyses, and NCAR CCM3 simulation. *J. Climate*, **13**, 3152-3171.
- Norris, J. R., 1998: Low Cloud Type over the Ocean from Surface Observations. Part II: Geographical and Seasonal Variations. *J. Climate*, **11**, 383-403.
- Oort, A. H., and J. J. Yienger, 1996: Observed interannual variability in the Hadley Circulation and its connection with ENSO. *J. Climate*, **9**, 2751-2767.

- Pan, H.-L., W. S. Wu, 1994: Implementing a mass flux convective parameterization package for the NMC medium-range forecast model. *Tenth Conf. on Numerical Weather Prediction*, Portland, Oregon, Amer. Meteor. Soc., 96-98.
- Petterssen, S., 1940: *Weather analysis and forecasting; a textbook on synoptic meteorology*. McGraw-Hill, 505 pp.
- Pierrehumbert, R. T., 1995: Thermostats, radiator fins, and local runaway greenhouse. *J. Atmos. Sci.*, **52**, 1784-1806.
- Plumb, R. A., and A. Y. Hou, 1992: The response of a zonally symmetric atmosphere to subtropical thermal forcing: Threshold behavior. *J. Atmos. Sci.*, **49**, 1790-1799.
- Privé, N. C., and R. A. Plumb, 2007: Monsoon dynamics with interactive forcing. Part II: impact of eddies and asymmetric geometries. *J. Atmos. Sci.*, **64**, 1431-1442.
- Rajeevan, M., J. Bhate, J. D. Kale and B. Lal, 2006: A high resolution daily gridded rainfall data for Indian region: Analysis of break and active monsoon spells, *Current Sci.*, 91(3) 296-306.
- Rodwell, M. J., and B. J. Hoskins, 1996: Monsoons and the Dynamics of Deserts. *Quart. J. Roy. Meteor. Soc.*, **122**, 1385-1404.
- ___, and ___, 2001: Subtropical Anticyclones and Summer Monsoons. *J. Climate*, **14**, 3192-3211.
- Sardeshmukh, P. D., 1993: The baroclinic χ problem and its application to the diagnosis of atmospheric heating rates. *J. Atmos. Sci.*, **50**, 1099-1112.
- Schubert, W. H., J. S. Wakefield, E. J. Steiner, and S. K. Cox, 1979: Marine stratocumulus convection. Part I: Governing equations and horizontally homogenous solutions. *J. Atmos. Sci.*, **36**, 1286-1307.
- Schumacher, C., R. A. Houze, and I. Kraucunas, 2004: The tropical dynamical response to latent heating estimates derived from TRMM precipitation radar. *J. Atmos. Sci.*, **61**, 1341-1358.
- Seager, R., R. Murtugudde, N. Naik, A. Clement, N. Gordon, and J. Miller, 2003: Air-Sea Interaction and the Seasonal Cycle of the Subtropical Anticyclones. *J. Climate*, **16**, 1948-1966.

- Smagorinsky, J., 1953: The dynamical influence of large-scale heat sources and sinks on the quasi-stationary mean motions of the atmosphere. *Quart. J. Roy. Meteor. Soc.*, **79**, 342-366.
- Tao, W-K., S. Lang, J. Simpson, R. Adler, 1993: Retrieval algorithms for estimating the vertical profiles of latent heat release: Their applications for TRMM. *J. Meteor. Soc. Japan*, **71**, 685-700.
- _____, and R. H. Houze, and E. A. Smith, 2007: The forth TRMM latent heating workshop. *Bull. Amer. Meteor. Soc.*, **88**, 1255-1259.
- _____, and Coauthors, 2001: Retrieved vertical profiles of latent heat release using TRMM rainfall products for February 1998. *J. Appl. Meteor.*, **40**, 957-982.
- _____, and Coauthors, 2006: Retrieval of latent heating from TRMM measurements. *Bull. Amer. Meteor. Soc.*, **87**, 1555-1572.
- Tiedtke, M., 1989: A comprehensive mass flux scheme for cumulus parameterization models. *Mon. Wea. Rev.*, **117**, 1779-1800.
- _____, 1993: Representation of clouds in large-scale models. *Mon. Wea. Rev.*, **121**, 3040-3061.
- Ting, M., 1994: Maintenance of Northern Summer Stationary Waves in a GCM. *J. Atmos. Sci.*, **51**, 3286-3308.
- _____, and P. D. Sardeshmukh, 1993: Factors determining the extratropical responses to equatorial diabatic heating anomalies. *J. Atmos. Sci.*, **50**, 907-918.
- Trenberth, K. E., D. P. Stepaniak, J. W. Hurrell, and M. Fiorino, 2001: Quality of Reanalyses in the Tropics. *J. Climate*, **14**, 1499-1510.
- Uppala, S., and Coauthors, 2005: The ERA-40 Re-Analysis. *Quart. J. Roy. Meteor. Soc.*, **131**, 2961-3012.
- Valdes, P. J., and B. J. Hoskins, 1989: Linear Stationary Wave Simulations of the Time mean Climatological Flow. *J. Atmos. Sci.*, **46**, 2509-2527.
- Walker, G. T. and E. W. Bliss, 1932: World weather V. *Mem. Roy. Meteorol. Soc.*, **4**, 53-84.
- Webster, P. J., and J. R. Holton, 1982: Cross-equatorial response to a middle-latitude forcing in a zonally varying basic state. *J. Atmos. Sci.*, **39**, 722-733.
- White, G., and S. Saha, 1996: Three dimensional diabatic heating fields from the NCEP/NCAR reanalysis. *Proceeding for 20th Climate Diagnostic Workshop* (PB96-168646), 284-287.

- Xie, P., and P. Arkin, 1996: Analyses of global monthly precipitation using gauge observations, satellite estimates, and numerical model predictions. *J. Climate*, **9**, 840–858.
- Yanai, M., and T. Tomita, 1998: Seasonal and interannual variability of atmospheric heat sources and moisture sinks as determined from NCEP-NCAR Reanalysis. *J. Climate*, **11**, 463-482.